



# Phenotypic Characterization with Software Development for Analysis of the Visual System in Animal Models of Neurodevelopmental Diseases

**RAFAELA BALTAREJO DOS SANTOS JORGE**

Outubro de 2021

# **Phenotypic Characterization with Software Development for Neurophysiological Analysis of the Visual System in Animal Models of Neurodevelopmental Diseases**

**Rafaela Baltarejo dos Santos Jorge**

Biomedical Engineer from Instituto Superior de Engenharia do Porto

“Dissertation presented at the Instituto Superior de Engenharia do Porto to obtain a  
Master's degree in Biomedical Engineering”

Advisers: João Martins (Post-Doc at CIBIT, ICNAS)  
Luís Coelho (Professor at ISEP)

March 2021



*“The difference between a successful person and others is not a lack of strength, not a lack of knowledge, but rather a lack in will.”*

A. Branson Alcott



## Acknowledgments

I would like to thank the Instituto Superior de Engenharia do Porto for all the training received, all the teachers with whom I interacted during my academic path and who contributed to my personal development. To the engineer Luís Coelho, for all the help provided for the accomplishment of the project as well as for the elaboration of this report. To engineer Carlos Ramos, for the opportunity to develop this subject.

I am thankful to the Coimbra Institute for Biomedical Imaging and Translational Research (CIBIT), for providing me the conditions to carry out this work. To João Martins, responsible for my orientation, for all the guidance and attention given throughout the project. To Joana Gonçalves for all the support provided in the laboratory meetings. To professor Miguel Castelo-Branco for all the work developed to support the theme of this thesis.

I thank my parents and grandparents for all the support they always gave me, for always being always by my side and for giving me the opportunity to pursue my education.

To everyone who directly or indirectly took part in my development.

To all, my sincere appreciation.



## Resumo

A neurofibromatose tipo 1 (NF1) é uma perturbação do desenvolvimento neurológico com implicações cognitivas adultas. Provoca anomalias do sistema nervoso central e afeta 1 em 3000 indivíduos em todo o mundo. Contudo, pouco se sabe sobre os efeitos no sistema visual e como estes podem estar associados a défices cognitivos e preveem a sua progressão. Neste trabalho, avalia-se as potenciais alterações na fisiologia da retina num modelo genético de murgalho de NF1, utilizando uma técnica neurofisiológica não invasiva, o eletroretinograma (ERG), para determinar o seu potencial diagnóstico. Como um indicador fiável da função da retina em resposta à luz, o ERG tem a capacidade de ajudar a nossa interpretação da fisiopatologia das perturbações do neurodesenvolvimento e neurodegenerativas.

Os principais objetivos desta tese são a caracterização fenotípica do sistema visual num modelo animal de NF1 e o desenvolvimento de ferramentas informáticas (MATLAB e Phyton) para processamento de sinais, análise de forma de onda, extração de características, e classificação. Verificou-se que os parâmetros ERG relacionados principalmente com a atividade oscilatória inibitória revelam alterações subtis dependentes do sexo. Para vários potenciais oscilatórios, machos e fêmeas exibem alterações opostas associadas ao genótipo mutante. Além disso, as características do ERG foram utilizadas para formar um classificador de aprendizagem de máquina baseado nos aglomerados significativos encontrados para algumas interações entre indivíduos, um classificador que se destina a ser capaz de receber um sinal e devolver o provável diagnóstico.

**Palavras-chave:** Autismo; Neurofibromatose tipo 1; Eletrocardiograma; Onda-a; Onda-b; Potenciais Oscilatórios; Análise Estatística; Aprendizagem de Máquina





## **Abstract**

Neurofibromatosis type 1 (NF1) is a neurodevelopmental disorder with adult cognitive implications. It causes central nervous system anomalies and affects 1 in 3000 individuals worldwide. However, little is known about the effects on the visual system circuitry and how these may be associated with cognitive deficits and predicts its progression. In this work, it was evaluated the potential alterations in retinal physiology in a genetic mouse model of NF1, using a non-invasive neurophysiological technique, the electroretinogram (ERG), to ascertain its diagnostic potential. As a reliable indicator of retinal function in response to light, the ERG has the ability to aid our interpretation of the pathophysiology of neurodevelopmental and neurodegenerative disorders.

The main objectives of this thesis are the phenotypic characterization of the visual system in an animal model of NF1 and the development of computer tools (MATLAB and Python) for signal processing, waveform analysis, feature extraction, and classification. This work found that ERG parameters mainly related to inhibitory oscillatory activity reveal subtle sex-dependent alterations. For various oscillatory potentials males and females exhibit opposite changes associated with the transgenic background. Furthermore, the ERG features were used to form a machine learning classifier based on the significant clusters found for some interactions between individuals, a classifier that is meant to be able to receive a signal and return the likely diagnosis.

**Keywords:** Autism; Neurofibromatosis type 1; Electrocardiogram; a-Wave; b-Wave; Oscillatory Potentials; Statistical Analysis; Machine Learning



# Contents

ACKNOWLEDGMENTS.....	III
RESUMO.....	V
ABSTRACT.....	VII
FIGURES LIST.....	XI
TABLE LIST .....	XIII
ABBREVIATIONS.....	XV
1. INTRODUCTION .....	3
1.1. MOTIVATION AND OBJECTIVES.....	3
1.2. DISSERTATION STRUCTURE .....	3
2. THEORETICAL FOUNDATIONS .....	7
2.1. HUMAN EYE .....	7
2.1.1. <i>Retina</i> .....	9
2.2. AUTISM.....	10
2.2.1. <i>Neurofibromatosis type 1</i> .....	11
2.3. AUTISM OPTICAL MANIFESTATIONS .....	13
2.3.1. <i>Neurofibromatosis type 1</i> .....	15
2.4. ELECTRORETINOGRAM .....	16
2.4.1. <i>Full-Field ERG</i> .....	18
2.4.2. <i>Pattern ERG</i> .....	19
2.4.3. <i>Multifocal ERG</i> .....	19
2.4.4. <i>Focal Flash ERG</i> .....	20
2.4.5. <i>Applications of Electroretinography</i> .....	20
2.5. SIGNAL PROCESSING.....	21
2.5.1. <i>Digital Filters</i> .....	21
2.6. STATISTICAL ANALYSIS.....	22
2.6.1. <i>Statistical Analysis Software</i> .....	24
2.6.2. <i>Analysis of Linear and Logistic Regression</i> .....	24
2.6.3. <i>Correlation Analysis</i> .....	25
2.6.4. <i>Categorical Data Analysis</i> .....	25
2.6.5. <i>Survival Analysis</i> .....	26
2.6.6. <i>Parametric and Nonparametric Two-Sample and Multisample Comparisons</i> .....	26
2.7. MACHINE LEARNING .....	32
2.7.1. <i>Classification Algorithms</i> .....	33
3. STATE OF THE ART .....	37

3.1.	ANIMAL MODELS.....	37
3.2.	ELECTRORETINOGRAM APPLIED TO THE STUDY OF AUTISM.....	38
3.3.	ERG PROCESSING AND POINTS OF INTEREST DETECTION.....	39
3.4.	STATISTICAL ANALYSIS.....	43
3.4.1.	<i>T-test</i> .....	44
3.4.2.	<i>Two-Way ANOVA</i> .....	44
3.5.	CLASSIFICATION ALGORITHM.....	45
3.5.1.	<i>Random Forest</i> .....	47
4.	MATERIALS AND METHODS .....	53
4.1.	THE PROBLEM.....	<b>ERRO! MARCADOR NÃO DEFINIDO.</b>
4.2.	ANIMALS .....	55
4.3.	LIGHT STIMULATION .....	55
4.4.	ERG RECORDINGS .....	56
4.5.	DATABASE.....	56
4.6.	THE SOLUTION – ELECTRORETINOGRAM .....	59
4.7.	THE SOLUTION – STATISTIC ANALYSIS.....	61
4.8.	THE SOLUTION – CLASSIFICATION ALGORITHM .....	61
5.	RESULTS.....	65
5.1.	ELECTRORETINOGRAM PROCESSING AND POINTS DETECTION .....	65
5.2.	STATISTICAL ANALYSIS.....	71
5.2.1.	<i>T-test – Genotype</i> .....	72
5.2.2.	<i>T-test – Sex</i> .....	73
5.2.3.	<i>Two-Way ANOVA</i> .....	74
5.3.	CLASSIFICATION ALGORITHM.....	93
6.	CONCLUSIONS .....	99
6.1.	CONCLUSION .....	99
6.2.	FUTURE WORK .....	101
	ATTACHMENTS .....	120

## Figures List

Figure 2.1 -Anatomy of the human eye [4]. .....	7
Figure 2.2 - ERG waveform [57]......	17
Figure 2.3 - Diagram of retina showing origin of ERG components [57]......	18
Figure 2.4 - Normally distributed data compared with skewed data. Left panel: Visual inspection of the data reveals them to be normally distributed [80]......	23
Figure 3.1 - Block diagram of the electroretinography used in [147]. .....	39
Figure 3.2 - FA of a composite ERG, averaged from 40 subjects, showing the 3 typical frequency components that contribute to the ERG (~30Hz: a- and b-waves contribution, black arrow; ~75 Hz and ~150Hz: oscillatory potentials (OPs) contribution, gray arrows) [151]. .....	40
Figure 3.3 - ERG Data Collection Block Diagram used in [156]......	41
Figure 3.4 - ERG Components Decomposition Process of [156]......	42
Figure 3.5 - Statistical tests utilized by the articles surveyed by [80]. A bar chart is shown with the breakdown of test type, total number encountered, and percentage of total. The graph shows all tests (not all articles). .....	43
Figure 4.1 - Analysis Interface of RETI-port. ....	54
Figure 4.2 - Filters applied by equalizer in RETI-port. a) the extraction of the b- wave peak with low-pass filter with cutoff frequency at 47.5 Hz. b) for the extraction of oscillatory potentials with a high-pass filter for frequencies above 60 Hz. ....	60
Figure 4.3 - Pipeline used in the signal processing and points detection. ....	60
Figure 4.4 - Comparison between some scikit-learn algorithms by [173]......	62
Figure 5.1 - Original ERGs, all the 16 channels recorded with infrared light and 7 other light intensities, for both eyes, in MATLAB. ....	66
Figure 5.2 - Points detected after filters were applied in MATLAB. ....	67
Figure 5.3 - Original ERGs, all the 16 channels recorded with infrared light and 7 other light intensities, for both eyes, in Python. ....	68
Figure 5.4 - Points detected after filters were applied in Python. a) a-wave detected in the original signal. b) b-wave detected after low-pass filter. c) Oscillatory Potentials detected after high-pass filter. ....	69
Figure 5.5 - Scatter plot of oscillatory potentials. ....	71
Figure 5.6 - Boxplot of a and b wave, comparing sex and genotype.....	74

Figure 5.7 - Boxplot of the first and second oscillatory potentials, comparing sex and genotype.....	75
Figure 5.8 - Boxplot of the third and fourth oscillatory potentials, comparing sex and genotype.....	75
Figure 5.9 - Interaction plot for the a-wave amplitude.....	77
Figure 5.10 - Interaction plot for the a-wave latency. ....	79
Figure 5.11 - Interaction plot for b-wave amplitude.....	80
Figure 5.12 - Interaction plot for b-wave latency. ....	82
Figure 5.13 - Interaction plot for the first oscillatory potential amplitude. ....	83
Figure 5.14 - Interaction plot for the first oscillatory potential latency.....	84
Figure 5.15 - Interaction plot for the second oscillatory potential amplitude. ...	86
Figure 5.16 - Interaction plot for the second oscillatory potential latency.....	87
Figure 5.17 - Interaction plot for the third oscillatory potential amplitude. ....	88
Figure 5.18 - Interaction plot for the third oscillatory potential latency. ....	90
Figure 5.19 - Interaction plot for the fourth oscillatory potential amplitude.....	91
Figure 5.20 - Interaction plot for the fourth oscillatory potential latency. ....	92
Figure 5.21 - Decision Trees number exploration. ....	94
Figure 5.22 - Results of the application of the algorithm. ....	94

## Table List

Table 2.1 - Symptoms and Incidence of NF1 (Adapted from [28]). .....	12
Table 5.1 - Estimation of the window in milliseconds (latencies) where the waves appear according to the intensity of the luminous flash. ....	66
Table 5.2 - Mean values obtained for each feature in study for WT and NF1... ..	70
Table 5.3 - T-test table for Genotype.....	72
Table 5.4 - T-test table for Sex. ....	73
Table 5.5 - ANOVA table for the a-wave amplitude.....	76
Table 5.6 - Tukey's table for the a-wave amplitude.....	78
Table 5.7 - ANOVA table for the a-wave latency. ....	78
Table 5.8 - Tukey's table for the a-wave latency. ....	79
Table 5.9 - ANOVA table for b-wave amplitude. ....	79
Table 5.10 - Tukey's table for b-wave amplitude. ....	80
Table 5.11 - ANOVA table for b-wave latency.....	81
Table 5.12 - Tukey's table for b-wave latency.....	82
Table 5.13 - ANOVA table for the first oscillatory potential amplitude.....	83
Table 5.14 - Tukey's table for the first oscillatory potential amplitude.....	84
Table 5.15 - ANOVA table for the first oscillatory potential latency. ....	84
Table 5.16 - Tukey's table for the first oscillatory potential latency. ....	85
Table 5.17 ANOVA table for the second oscillatory potential amplitude. ....	85
Table 5.18 - Tukey's table for the second oscillatory potential amplitude. ....	86
Table 5.19 - ANOVA table for the second oscillatory potential latency.....	87
Table 5.20 - Tukey's table for the second oscillatory potential latency.....	88
Table 5.21 - ANOVA table for the third oscillatory potential amplitude.....	88
Table 5.22 - Tukey's table for the third oscillatory potential amplitude.....	89
Table 5.23 - ANOVA table for the third oscillatory potential latency. ....	89
Table 5.24 - Tukey's table for the third oscillatory potential latency. ....	90
Table 5.25 - ANOVA table for the fourth oscillatory potential amplitude.....	90
Table 5.26 - Tukey's table for the fourth oscillatory potential amplitude. ....	91
Table 5.27 - ANOVA table for the fourth oscillatory potential latency.....	92
Table 5.28 - Tukey's table for the fourth oscillatory potential latency.....	93
Table 5.29 - Confusion Matrix of predictions. ....	95
Table 5.30 - Classification Report of the Algorithm. ....	95



Table 6.1 - Differential parameters found in the statistical analyses.....	100
--	-----

## **Abbreviations**

ASD	–	Autism Spectrum Disorder
ADHD	–	Attention Deficit Hyperactivity Disorder
NF1	–	Neurofibromatosis Type 1
WT	–	Wild-Type
CNS	–	Central Nervous System
MRI	–	Magnetic Resonance Imaging
BTBR	–	Model of idiopathic autism
dLGN	–	Dorsal Lateral Geniculate Nucleus
RAH	–	Retinal Astrocytic Hamartomas
RNFL	–	Retinal Nerve Fiber Layer
ERG	–	Electroretinogram
VEP	–	Visually Evoked Potential
OP	–	Oscillatory Potential
ERP	–	Early Receptor Potential
ffERG	–	Full-Field Electroretinogram
mfERG	–	Multifocal Electroretinogram
fERG	–	Focal Electroretinogram
LA-ERG	–	Light-Adapted Electroretinogram
DA-ERG	–	Dark-Adapted Electroretinogram
ISCEV	–	International Society for Clinical Electrophysiology of Vision
LED	–	Light-Emitting Diode
FIR	–	Finite Impulse Response
IIR	–	Infinite Impulse Response
ROC	–	Receiver Operating Characteristic

ANOVA – Analysis Of Variance

PPF – Percent Point Function

CDF – Cumulative Distribution Function

RF – Random Forest

HCN – Hyperpolarization-activated Cyclic Nucleotide-gated

AC – Alternating Current

FFT – Fast Fourier Transform

DTW – Dynamic Time Warping

EMS – Expected Mean Squares

SVM – Support Vector Machines

AUC – Area Under the ROC Curve

## CHAPTER 1 – INTRODUCTION



# **1. Introduction**

## **1.1.Motivation and Objectives**

According to WHO [1]- World Health Organization, One in 160 children has an autism spectrum disorder worldwide, which is a neurodevelopmental disorder marked by social interaction deficiencies as well as limited activities and atypical sensory responses [2]. This type of disease presents optic manifestations, which make possible to distinguish an autistic individual in several visual examinations [3], such as those treated in the subject of the current thesis.

Therefore, one of the objectives of this research is to describe the visual system in an animal model of NF1, in order to differentiate the form of Autism from healthy people. The main goal of this paper is to develop computer tools for automated analysis of electroretinogram (ERG) component analysis and the study of their behavior in the different models with statistical analysis to preform to the ERGs components. It is also critical to determine the ability of ERG components to predict previously reported cognitive deficits.

## **1.2.Dissertation Structure**

This dissertation is divided into six chapters. This first chapter introduces the main objectives of the work and the respective motivation. The structure of the dissertation is also presented here.

Chapter 2 is the literature review on the main themes of this work. An approach is made to the human eye and retina, objects of study of the techniques. Autism and respective strain concerned, neurofibromatosis type 1, is defined. It is described and characterized the technique used in the study of autism strain in the human visual system, the electroretinogram and its applications. The subject of signal processing is addressed with the aim of characterizing the digital filters applied in the development of the subject, as well as the concepts and definitions relating to statistical analysis and the respective tests applied to the data. Finally, the subject of machine leaning and the algorithm used in this work is addressed.

The third chapter consists in the exposition and analysis of some literature studies already done relating the techniques in question and the disease.

In the fourth section, the materials and methods chosen to de development of the theme and define the problem are described and justified.

Chapter five, Development, presents de solution chosen to the existing problem and describes the procedure followed.

The sixth section presents the results obtained with the solution found and developed, which includes the signal processing, point identification, return of information from the signal and from each component, development of various graphics and images to aid in data comprehension, statistical analysis and respective tests results and the semi-automatic method created for characterization and provable diagnosis.

Finally, chapter 7 presents the main conclusions of this work and gives some suggestions for future work.

## CHAPTER 2 – THEORETICAL FOUNDATIONS





## 2. Theoretical Foundations

The purpose of chapter 2 is to present the theoretical development necessary for the project. This chapter has the intention of defining and characterizing the concepts that the subject of the current dissertation includes.

### 2.1.Human Eye

Our eyes never stay still and are always moving to sense differences in the world. As a result, research into eye activity is critical in vision science. Eye movement due to external stimulus is a significant research field for scientists because external stimuli are called environmental changes. Face movement can actually be studied in response to a variety of external stimuli, including visual, auditory, and olfactory stimuli. Over the years, psychologists have used a number of methods to research eye activity in response to external stimulus [4].

The eyes are crucial to our daily lives because visibility provides us with about 70% of the input we get from our environment. They are situated within the upper face's eye sockets, which are two cavities [5].

The human eye has several constituents in its structure as shown in Figure 2.1.

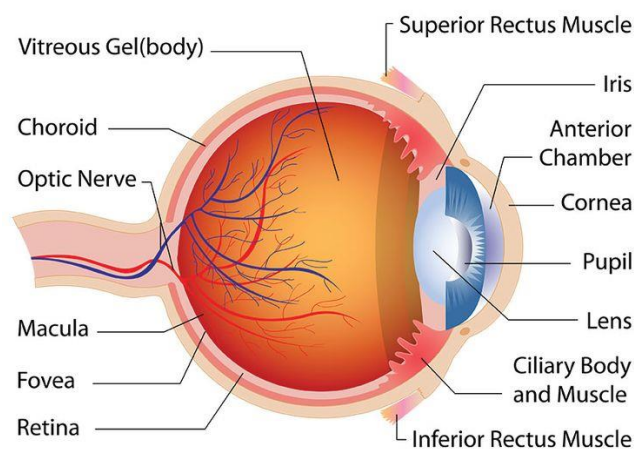


Figure 2.1 -Anatomy of the human eye [4].

Cornea is the eye's outer layer, which is kept wet by the tear fluid that coats it. The cornea behaves similarly to a window in that it is disk-shaped, translucent, and allows light to reach the eye. It also protects the eyes from harmful environmental influences including soil, pollen, and surface injuries. It has a high natural resistance. Its curvature has optical properties and is crucial in allowing us to see clearly.

Sclera prevents the retina from damage by being thicker and heavier than the cornea. It protects the whole eye, with two exceptions: the cornea is included in the center, and the optic nerve fibers are located in the rear.

Pupils are the black spots in the human eye's middle. It adjusts to the strength of incident light by reacting to it. The scale of our pupils will also be affected by our emotional state [6].

Iris is a colored ring that circles the pupil and monitors the amount of light entering the eye in the same manner that an aperture does. It means that the pupil shrinks in a bright setting, allowing a smaller volume of light to pass through [7]. The iris is also responsible for the color of our eyes and has a distinct shape in each of us.

Chambers of the eye (camerae bulbi) are aqueous fluid-filled spaces in the anterior section. It includes the anterior and posterior chambers. The posterior chamber (not shown) is a small structure between the iris and ciliary. The fluid includes nutrients for the lens and cornea, supplies oxygen, and aids in the battle against pathogens. The aqueous fluid in the eye chambers often has another purpose: it assists in the eye's form maintenance.

The crystalline lens of the eye absorbs light that passes through the pupil and forms a sharp image on the retina. It is pliable and can change shape with the help of the ciliary muscle to focus on both distant and close objects [6]. The picture is reversed by the lens and projected on the retina from back to front. When the vision is viewed later by the brain, it is just reversed back to the correct direction [8].

The ciliary body and beam body (corpus ciliare) are essential for vision because they create aqueous fluid and house the ciliary muscle (musculus ciliaris). By adapting the lens, it's possible to focus on things both near and far apart.

The corpus vitreous is the largest portion of the eye which, as the name indicates, represents the body of the eye. It's translucent and made up of 98% water, 2% sodium hyaluronate, and collagen fibers [6].

The retina absorbs light and color sensations before transmitting them to the brain via the optic nerve. In other words, the retina serves as a medium, converting incoming light into a form that can be processed by the brain. Cones and rods make up these sensory cells. They are located in more high concentrations nowhere else in the eye except in the macula, or middle of the retina: 95 percent of all sensory cells are clustered in an area of around 5 square millimeters [9].

Between the sclera and the retina, the choroid extends to the ciliary body and the iris. It guarantees that nutrients are delivered to the retina's receptors, maintains a stable retinal temperature, and aids in accommodation.

The optic nerve (nervus opticus) is in charge of sending data from the eye to the brain. It has over a million nerve fibers (axons) and is about half a centimeter thick until exiting the retina via the papilla.

The fovea is a tiny component of our optical structure that plays an important role in our vision. It is found in the middle of the retina and is packed with sensory cells that enable us to see in color and as plainly as possible throughout the day [6].

### **2.1.1. Retina**

The retina of the human eye converts light into an electrical signal, making it the component responsible for the transition from the sensory to the nervous systems [10].

The light wave must travel through multiple layers of neurons before contacting the photoreceptors (detailed in Figure 3), and the central fovea and the blind spot are the two locations where this does not happen, since the signal is captured directly by photoreceptors or there are no photoreceptors, respectively. The region where the optic nerve and blood vessels enter, as well as the absence of photoreceptors, is known as the blind spot. The information is then sent to the ganglion cell axons, which are in charge of forming the optic nerve transporting action potentials to the brain [11].

The cones, which are responsible for catching colors and helping us to see with greater clarity, and the rods, which, while being more numerous, have less resolution and form images in low light environments. The central fovea is made up entirely of cones, and since light signals do not have to travel through several layers before reaching the

photoreceptors, it is the region that generates the clearest images and is the most commonly used in functional ophthalmic evaluations [9].

The human retina has 120 million rods and 6 million cones with just 1.2 million retinal ganglion cells, implying a high degree of neuron convergence. The cone pathways have less overall convergence than rod pathways, reaching the ratio of cone to retinal ganglion cells of about 1 to 1 in the fovea. This also explains why the resolution of the images produced by the cones is much higher than that generated by the rods. Since the light signals received by the rods are too small, this phenomenon aids in the production of action potentials [12].

Phototransduction is a phenomenon that happens in photoreceptors that turns light into an electrical signal that is then transmitted to the brain. The release of glutamate, a neurotransmitter responsible for the transfer of information from photoreceptors to bipolar and retinal ganglion cells, is decreased in rods when light hits the photoreceptor. The mechanism is identical in cones, but the pigment responsible for fading is distinct. There are only three types of cones in humans based on light wavelength their pigment is most sensitive: red or L (long-wavelength, ~560 nm), green or M (middle-wavelength, ~530 nm), and blue or S (short-wavelength, ~420 nm) [13]. Contrarily to primates, rodents do not have the red or L-cone. While the majority of visual input is sent to the visual cortex, a small amount, specifically 20% of it, is sent to the superior colliculi, which enable eye motor control, such as tracking moving objects [11].

## **2.2. Autism**

Autism spectrum disorder (ASD) is a neurodevelopmental disorder marked by social interaction deficiencies as well as limited activities and atypical sensory responses [2]. Although the cause of ASD is unclear in the majority of cases, genetic and environmental factors are thought to play a role in the phenotype by modulating synaptic connectivity [14] and controlling neurotransmitters and their transcription factors [15], [16]. While several genetic alterations have been related to ASD, the majority of cases have yet to be found. Alterations in sensory input processing, which are necessary for a thorough and accurate understanding of the social environment, could provide clues. As behavioral responses depend on the perception and integration of sensory information, effective sensory processing is crucial to higher-level cognition. Changes in sensory

processing pathways at any level can cause behavioral changes, with potentially debilitating effects on social competence [17]. Inefficient sensory integration has been widely documented in ASD research, and atypical sensory perception has recently been identified as a potentially significant cause of ASD symptoms [18], [19]. Extreme sensitivity to certain auditory sounds or textures, as well as altered pain levels, are examples of such behavioral indicators [20].

The Light-Adapted Electrocardiogram is a possible marker for neurodevelopmental disorders like ASD in children, according to a broad, multicenter review. This method can assist drug exploration that targets CNS production of signaling pathways common to the CNS and retina by providing a reproducible, noninvasive, and robust measure of CNS operation [21].

### **2.2.1. Neurofibromatosis type 1**

Neurofibromatosis is a monogenetic neurocutaneous condition marked by a proclivity for tumor development that may be benign or malignant [22]. Other clinical characteristics vary depending on the type of neurofibromatosis being studied. There are two types of neurofibromatosis: type 1, which is the most prevalent and is also known as classic neurofibromatosis, and type 2, which varies in the position of the mutation, and may appear on chromosome 17 or 22, respectively [23].

The type of neurofibromatosis analyzed in this paper is type 1, which is classified as a neurodevelopmental disorder because patients with this syndrome have cognitive impairments and CNS abnormalities [24]. Neurofibromatosis is an autosomal dominant disease caused by mutations in the NF1 gene, which codes for the neurofibromin protein [25]. Neurofibromin is a key regulator of a signaling pathway which controls cell growth and differentiation and is also involved in learning and memory processes. When developed properly, neurofibromin functions as an inhibitor of the above-mentioned pathway. This protein also functions as a GABAergic neurotransmitter modulator, according to previous reports [26].

Neurofibromatosis type 1 (NF1) is the most prevalent condition that causes anomalies in the CNS, affecting 1 in 3500 people worldwide, it affects people of all ethnicities and has no sex preference [27].

NF1 is a multisystemic disorder that manifests itself in a variety of ways through the human body's processes. It affects the central and peripheral nervous systems, as well as the skin, bones, blood vessels, endocrine system, and endocrine system. It is normal for neurological complications to occur in infancy, with cognitive impairments being the most common and, as a result, the ones that cause the most anxiety for patients suffering from this disorder [24]. Cognitive impairments are responsible for a large amount of academic and behavioral issues. The most frequent cutaneous and neuronal signs of patients with this mutation are Cafe'-au-lait stains, Lisch nodules, and cutaneous neurofibromas, which are present in almost 100% of patients (Table 2.1) [28].

Table 2.1 - Symptoms and Incidence of NF1 (Adapted from [28]).

Symptoms	Percentage of Incidence
Cafe'-au-lait spots	94-100%
Lisch nodules	22-96%
Cutaneous neurofibromas	14 -95%
Freckles on the lower arm or groin	67%
Impairment of Learning	30–65% (Kids)
Short Stature	25–35%
Plexiform Neurofibromas	~ 25%
Optic Gliomas	20 %
Headache	~ 20%
Scoliosis	12–20%
Mental Retardation	4-8%
Epilepsy	3–5%
Intracranial Tumors	1–2%
Hydrocephalus	2%
Pseudotorsis	3%
Sphenoidal Wing Dysplasia	< 1%
Renal Artery Stenosis	1–2%
Pheochromocytoma	< 1%

Lisch nodules and cutaneous neurofibromas have a wide range of incidence percentages, owing to the fact that these are the symptoms that develop over time and become more common as the patient ages, peaking at 20 and 30 years of age, respectively [28].

The clinical evolution of patients is used to make a diagnosis of this disease [24]. The clinical features found in most NF1 patients are the development of café-au-lait spots, optic gliomas and pseudarthrosis; these symptoms manifest within the first ten years of life, allowing the diagnosis to be made during this period [25]. If a person shows some of these symptoms, NF1 should be recognized as a possible diagnosis, and formal diagnostic guidelines have been developed [29].

The features mentioned above are detected using a variety of methods. Ultraviolet light may be used to correctly count the spots that individuals have on their skin, such as café-au-lait spots, since others may not be noticeable. There are several molecular genetic tests which could be used to detect the presence of this mutation before injuries arise, although they are rarely needed. Magnetic resonance imaging (MRI) can be used to assess whether plexiform neurofibromas have reached the end of their growth cycle [29].

### **2.3. Autism Optical Manifestations**

Vision is determinant of many behavioral responses and plays an important role in correct perception of social environments. A person's atypical visual processing can cause them to overlook essential social signals like eye contact and variations in facial expression or skin pigmentation, which can have a detrimental impact on their ability to learn and develop social skills [30], [31]. ASD patients also have atypical visual phenotypes [32], and several studies have shown that ASD patients prefer intricate descriptions of a visual scene (“local details”) over a contextual understanding of the picture as a whole (“global structure”). These phenotypes are thought to be caused by changes in neural processing of spatial vision or a relatively increased response to information with high spatial frequencies [33]. Outcomes from patient trials have been mixed, and there is still a lot of discussion. Establishing a reliable animal model for studying ASD-related alterations in visual processing might reveal the nature and underlying mechanisms of altered visual function observed in these patients [3], [34], [35].



Contrast sensitivity was measured across a spectrum of spatial frequencies in a human sample for both luminance and texture-defined vertically oriented sinewave gratings. According to the results, autistic people are more vulnerable to luminance-defined, high spatial frequency gratings [36]. In another study, children with ASD were found to be deficient in many aspects of facial image recognition, but they performed better when matching faces using high rather than low spatial frequency information [37]. Visual evoked potentials were used in another study to demonstrate that adults with ASD had improved fine-form processing but poorer face form processing due to a lack of incorporation of various local high spatial frequency information in the fusiform gyrus [38]. These results suggest that localized perception in ASD is triggered, at least in part, by improvements in early spatial response processes that favor precise spatial information processing, which may lead to atypical social awareness and interaction.

However, these findings are not universal, and the literature's mixed results have prompted much discussion. Although some studies have reported 'super vision' in ASD patients, later studies have generally accepted the notion that visual acuity in this population is normal [39]–[41]. Furthermore, no difference in contrast sensitivity was observed between ASD and control groups in other studies [42], [43]. The wide range of visual phenotypes identified in the literature may be due to the fact that ASD is a continuum disorder, with symptoms ranging in severity and presentation. Furthermore, because of large differences in research techniques, sample sizes, availability of high-functioning subjects, cooperativeness during visual testing, and social and communication problems, measuring visual function (including spatial acuity and contrast sensitivity) in this demographic, especially in children, has been challenging [32], [33].

The study of oscillatory potential indicates that improvements in post-photoreceptor retinal circuitry could be a compensatory occurrence for decreased photoreceptor input, which could lead, at least in part, to the improved visual functions found in the BTBR mice. This mouse model of autism has been shown to have disturbed sensory circuitry in the brain, with altered structural shape and reduced synaptic pruning in the dorsal lateral geniculate nucleus (dLGN), a central component in the visual pathway, while not specifically linked to the transmission of Optokinetic-associated stimuli [20].

Neuroimaging trials on people with ASD can help researchers figure out what's behind their atypical vision. Brainstem hypoplasia has been identified in any case of autism that has been studied to date, independent of age [44]. As previously stated, the optokinetic response is controlled by the accessory optic system, which relays information to the motor system through midbrain (brainstem) nuclei. Although deformation of the dLGN has been observed [45] in BTBR mice, it has yet to be determined if structural defects exist along the accessory optic system. There have been several reports on treatments for alleviating vision difficulties in people with ASD, and the findings have been mixed. Understanding vision changes may lead to new approaches to address the needs of people with autism and, as a result, reduce the disorder's symptoms [46].

### **2.3.1. Neurofibromatosis type 1**

Little is known about the possible retinal effects in NF1 patients, especially at the level of retinal circuitry. So far, clinical studies have mainly found structural changes associated with the presence with optic gliomas [47].

Palpebral plexiform neurofibroma is generally monolateral, affects the upper eyelid commonly, and arises after 2 years of life; it has a proclivity for growing and causing asymmetric ptosis with palpebral edge distortion [48].

Lisch nodules, a kind of iris hamartoma in NF1, are uncommon before the age of two, and may be seen rarely before the age of six, but their prevalence, quantity, and size in individual instances rise dramatically as they become older [49].

Glaucoma was found in 23 % of NF1 patients with orbital–facial involvement (such as plexiform palpebral neurofibroma) in recent research. This study revealed slight ocular enlargement in oculofacial NF1, even in eyes with normotensive intraocular pressure. Even in eyes with normotensive intraocular pressure, our investigation indicated mild ocular enlargement in oculofacial NF1; indeed, it has been postulated that megalophthalmous may be present in NF1 regardless of ocular hypertension [50].

The thickness of the choroidal and individual retinal layers was measured in individuals with NF1 and the mean choroidal thickness was shown to be reduced. When NF1 patients were compared to healthy control participants, the thickness of the neuroepithelium, photoreceptor-retinal pigment epithelium, and outer nuclear layer were

all decreased. It led to the hypothesis that retinal thinning might be caused by abnormal choroidal circulation caused by the presence of nodules [51].

Topcu-Yilmaz and colleagues, 2014 [52], assessed the macular volume and retinal nerve fiber layer thickness and found that within NF1 patients only those with optic glioma presented thinning of retinal nerve fiber layer and decrease macular volume.

## **2.4. Electrophoretinogram**

The electrophoretinogram (ERG) can be used to probe and quantify complex retinal signaling channels, which are an open model of neuronal integration in the brain [10]. In dark- and light-adapted settings, the ERG tracks the difference in voltage created by the retina over time in response to fleeting bursts of light [53], [54]. When dark-adapted or in low light conditions, rod photoreceptors synapse with rod ON-bipolar cells and horizontal cells drives the signal path; when light-adapted in bright light, cone photoreceptors synapse with both ON- and OFF— cone bipolar cells and horizontal cells drive the signal path. The ERG waveform reflects each cell type proportional contributions: the first negative a-wave indicates photoreceptor hyperpolarization to light, while the next positive b-wave indicates depolarizing bipolar cells.

When an amphibian eye was exposed to light in 1865, Holmgren observed electrical potentials [55]. By 1908, three waves of ERG had been identified: a, b, and c. Ragnar Granit published several experiments on cat retinas in 1933, modifying anesthetic levels to separate various components that lead to the ERG [56]. He discovered that the a-wave comes from retinal photoreceptors, the b-wave comes from the mid-retina (bipolar cells), and the c-wave comes from the retinal pigment epithelium. Ragnar Granit received the Nobel Prize in Physiology or Medicine in 1967 for this work.

Electrophoretinograms were first used in clinical practice in the 1950s, but the mainstream use of clinical ERGs and visually evoked potentials (VEPs) correlates with the advent of averaging computers in the 1960s. Electrophoretinograms and visually evoked potentials have advanced in complexity in tandem with advancements in computing technology, with multifocal ERGs and multifocal VEPs approaching present levels of sophistication.

A biphasic waveform recordable at the cornea is elicited by a burst of light, close to the one seen in Figure 2.2. The a- and b-waves are the most often measured components. The first strong negative variable is the a-wave, which is replaced by the b-wave, which is positive and normally has a greater amplitude than the a-wave [57].

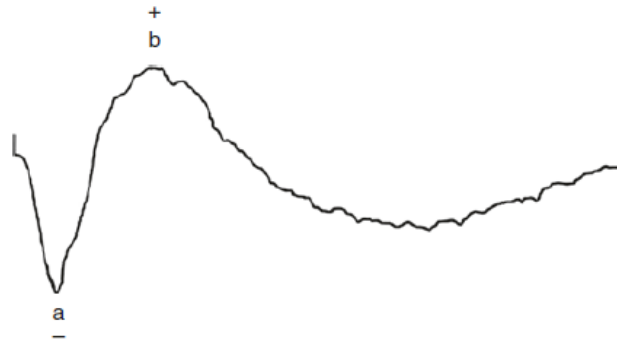


Figure 2.2 - ERG waveform [57].

In a clinical exam, the amplitude of the a-wave is determined from the mean baseline to the negative trough, and the amplitude of the b-wave is measured from the trough of the a-wave to the peak of the b-wave. The time from flash onset to the trough of the a-wave and the time from flash onset to the peak of the b-wave are quantified. These times or latencies are referred to as "implicit times" in electroretinography jargon. The positive pole of the amplifier is usually placed on the cornea of the eye and is shown as upward in ERG; the negative pole is normally placed on the head and is shown as downward in ERG.

The a-wave, also known as the "late receptor potential," reflects the general functional fitness of the photoreceptors in the outer retina (Figure 3). The b-wave, on the other hand, represents the fitness of the retinal inner layers, such as ON bipolar cells and Müller cells [58], and is influenced by the activity of all constituents of the mid-retina, horizontal, amacrine, and other forms of bipolar cells. The c-wave, which originates in the pigment epithelium [59], [60], and the d-wave, which shows activation of the OFF bipolar cells [61], [62], are two other waveforms that are periodically reported clinically. Oscillatory potentials (OPs), which were first identified by Cobb and Morton on the ascending limb of b-waves, appear alongside a-, b-, and c-waves (1954). Extracellular currents in the feedback loop between bipolar cells, amacrine cells, and ganglion cells can be connected to OPs [63], [64].

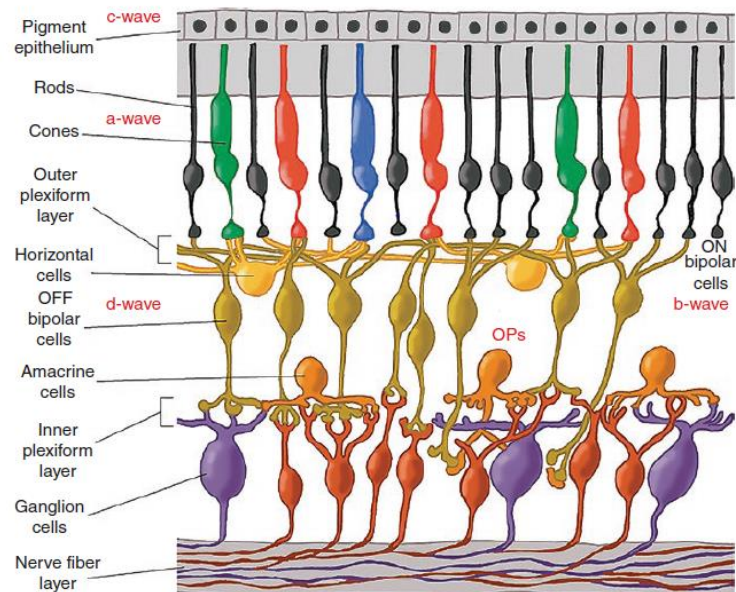


Figure 2.3 - Diagram of retina showing origin of ERG components [57].

The early receptor potential (ERP) is a small biphasic portion preceding the a-wave that occurs in the first 2 ms after a bright flash and reflects the photoreceptor outer segments' earliest chemical responses to light. In human, cones account for roughly 70% of the overall contribution. The ERP has a latency of under 60 microseconds. ERPs are better reported with a nonmetal electrode, such as a cotton wick, owing to photovoltaic effects. The ERP is difficult to report and is only used in therapeutic environments [57].

#### 2.4.1. Full-Field ERG

Full-field ERGs (ffERGs) are generated in dark-adapted and light-adapted environments using full-field flash stimulus. Between procedures, the testing sequence and flash triggers differ. Rod and cone function can be distinguished using the colors of flashes and the rate of stimulus. The ffERG is the most effective tool for measuring retinal dysfunction in the retina [65].

Context light, trigger hue, and flash intensity are all better regulated with the Ganzfeld. With the aid of a computer, the ERG can be recorded after a single flash or average responses to multiple flashes using a strobe lamp, LED flash, or Ganzfeld flash stimulus.

Dark-adapted rod-driven cconotopic and mixed flash ERGs: Proposed protocols allow for dark adaptation for at least 20 minutes before recording ERGs, with some

laboratories going as far as 30 minutes. Rod activity is measured using dim pulses of light after dark adaptation. The International Society for Clinical Electrophysiology of Vision (ISCEV) basic white-flash protocol [66] is the most widely used protocol. Bright white flashes in the dark-adapted condition produce the large-amplitude ERGs characterized by large-amplitude a-wave appearing at short implicit time followed by a large-amplitude b-wave with OPs on the ascending limb. For assessing rod and cone roles, the light intensity is varied so that dim flash ERGs are driven by rods and bright white flash ERGs demonstrate mixed rod-cone responses [67].

**Light-Adapted Cone-Driven ERG:** After 10 minutes of light adaptation, light-adapted ERG responses are reported with a background illumination of 30 cdm<sup>-2</sup>. Cone feature is assessed using single photopic bright white flash ERGs and 30 Hz flicker, as well as the x portion of the scotopic dim red flash ERG [68].

#### **2.4.2. Pattern ERG**

The pattern electroretinogram measures the retinal response to a pattern reversal stimulus, which is used to determine retinal ganglion cell activity. PERG is used in the diagnosis of glaucoma, optic neuropathies, and ganglion cell disorders in patients. It has a small amplitude, normally less than 10  $\mu$ V, with a small initial negative component with a latency of around 35 ms, a much larger positive component peaking about 50 ms, and a large negative component peaking about 95 ms. Macular function is reflected in the P50 component, and retinal ganglion cell function is mirrored in the N95 component [69].

#### **2.4.3. Multifocal ERG**

The recording is a mass potential representing the wellbeing of the entire retina and may not be susceptible to changes in small parts of the retina, which is a disadvantage of the conventional global, full-field ERG. The full-field ERG is normally common until 20% or more of the retina is affected by illness. The ERG of a person with macular degeneration, expanded blind spot or other small central scotomas may appear normal. The multifocal ERG is the most notable breakthrough of ERGs in the last 25 years. Erich Sutter modified the binary m-sequences mathematical sequences to create applications that can remove hundreds of focal ERGs from a single electrical signal channel. This

system can measure ERG function in a number of small areas of the retina. The ERG responses from hundreds of retinal areas can be recorded in a limited amount of time using this system [70].

### **2.4.4. Focal Flash ERG**

The focal ERG (fERG) is a test that evaluates the activity of a single small area of the retina, usually the foveal or macular region. Different stimulus frequencies are used, as well as different stimulus field sizes ranging from  $3^\circ$  to  $18^\circ$ . Focal ERGs, in combination with mfERGs, can be used to assess macular function in patients with age-related macular degeneration. fERG assesses only one region, while multifocal ERGs generate a map of up to  $60^\circ$  of central visual field [71].

### **2.4.5. Applications of Electroretinography**

ERG recording is noninvasive and can help with the diagnosis of retinal disorder in the clinic. The multifocal methodology has expanded the usefulness of electrodiagnostic research through helping physicians to objectively define local functional conditions and equate them with subjective measurements including perimetry as well as systemic measures offered by current imaging techniques. The ISCEV's criteria and recommendations provide valuable knowledge for clinical research. The ERG can be used to investigate normal retinal activity in both humans and animals [72]. The rod and cone processes can be analyzed independently, and specific stages of processing can be measured, using the right stimuli. ERGs can also be used for noninvasive, in vivo assessment of retinal activity in physiologically intact mammals thanks to a greater understanding of their origins. The rodent ERG is similar to human ERG and the main components such as a-wave, b-wave, and OPs are readily observable in both rats and mice. This can be a valuable supplement to functional knowledge gained from single cell studies. As retinas in humans and animal models degenerate and change their circuitries as a result of acquired disease and genetic mutations, the ERG is useful for noninvasively monitoring the improvement of retinal function and the deterioration of retinal function. The ERG shows potential as a translatable technique that can be used as a practical

outcome measure in animal models and clinical trials, particularly as new therapies for blindness disease become available [73].

## **2.5.Signal Processing**

The acquisition and processing of physiological signals is of essential importance in the diagnosis of certain pathologies.

The signal is a function of a set of independent variables. The signal itself carries some kind of information available for observation. As far as processing is concerned, to process means operating in some way on the signal to extract some useful information. In many cases this processing will be a non-destructive "transformation" of the of the given data signal, however, sometimes important processing turn out to be irreversible and therefore destructive [74].

Our world is full of signals, some of these signals are natural, but most signals are man-made. Some signals are necessary, such as speech, some are pleasant, like music while many are undesirable or unnecessary in a given situation. In an engineering context, signals are carriers of information, both useful and undesired. Therefore, extracting or changing the useful information from a mix of undesirable information is the simplest form of signal processing. Generally, signal processing is an operation designed to extract, enhance, store, and transmit useful information [75].

### **2.5.1. Digital Filters**

Analog signal analysis needs specific care since its capture is coupled with a variety of contaminants, such as noise. In this regard, the employment of filters allows for the treatment of data to enable the discussion of the information that has been eliminated, as well as to improve the accuracy of the signal's diagnosis. Depending on the criteria used for categorization, filters can be divided into numerous categories. Finite impulse response (FIR) and infinite impulse response (IIR) filters are the two major types of digital filters. [76].

IIR (Infinite Impulse Response) filters allow us to generate a theoretically infinite number of output pulses from a single input value. The output of the IIR filter is known



to be dependent on the preceding input and output samples. Because IIR filters don't have a linear phase characteristic, they can only be utilized in applications where signal linearity isn't essential. Because IIR filters include zeros and poles, if the zeros and poles are outside the unit circle, the filter might become unstable [77].

We get a limited number of return pulses by utilizing FIR filters. The output no longer depends on past output samples, but simply on previous input samples. It allows to obtain a linear phase characteristic with a FIR because the sequence of coefficients may be made symmetric around the center coefficient. Because FIR filters are meant to have a linear phase characteristic, they should be utilized in applications that demand it. By making the coefficient sequence symmetric around the center coefficient, we may achieve a linear phase characteristic. This indicates that the first and last coefficients are the same, and the second and third coefficients are the same, and so on. The issue with FIR filters is that they use more memory than IIR filters since they are not recursive and hence require more coefficients. This fact also causes a delay in calculation [78].

### **2.6.Statistical Analysis**

The discipline of gathering data and identifying patterns and trends is known as statistical analysis [79]. After data collection, regardless of research design, the initial step should be description rather than comparison. Following the acquisition of data, each variable in the data set should be visually evaluated, investigated, and summarized in line with the predetermined analytical strategy established before data collection began. In addition to giving written explanations of events, steps may include:

- Reviewing data for typos and missing values;
- Computing each continuous variable's measures of central tendency (e.g., mean, median, and mode) and dispersion (e.g., range, interquartile range);
- To visually examine for normality and probable outliers by plotting continuous variables as scatter plots, histograms, box-and-whisker plots, or violin plots;
- Calculating the proportion of data in each category and tabulating categorical variables [80].

Using a histogram to visualize continuous data helps the researcher to assess if the variables are regularly distributed, which can help define the type of hypothesis testing to be undertaken. Notably, non-normally distributed data, such as the right-skewed example in Figure 2.4, may frequently be changed to a normal gaussian distribution using logarithmic or square root transformations [81]. Because differences among normally distributed variables may be analyzed using parametric hypothesis tests, and differences among nonnormally distributed variables are best assessed with nonparametric tests, determining normality is an important part of the data exploration process [82]. In addition to visual inspection, statistical tests of normality, such as the D'Agostino K-squared test, the Kolmogorov-Smirnov test, and the Shapiro-Wilk test are available, which test the data against the null hypothesis that they are normally distributed. Each of these tests has different performance characteristics, and none is particularly powerful for small sample sizes. They may not reject the null hypothesis of normality, even for data that deviate significantly from the gaussian distribution. For small sample sizes, it is recommended that nonparametric tests be used even if the data appear normally distributed on formal testing. It should be noted that when sample sizes are exceptionally large, formal testing may reject the null hypothesis of normality, even for trivial deviations that have little to no effect on the conclusions drawn from parametric hypothesis tests. Therefore, for most medical data sets, visual inspection for normality is sufficient [83].

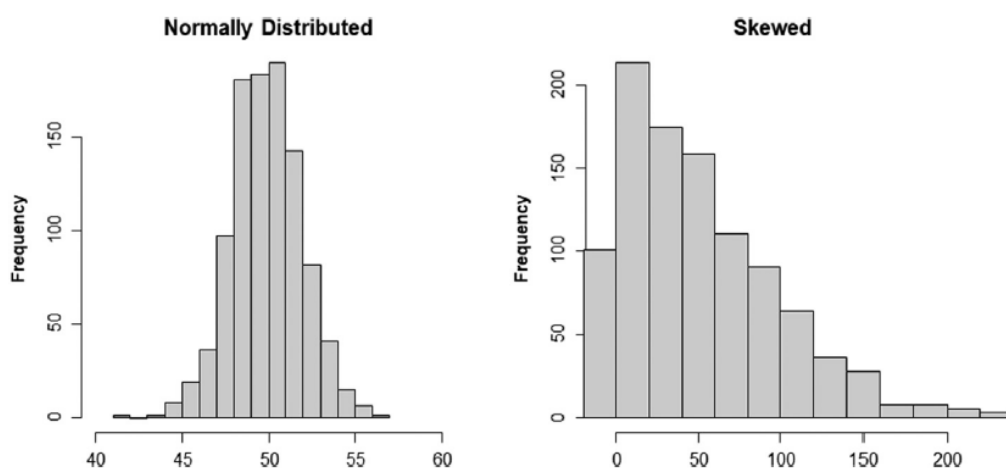


Figure 2.4 - Normally distributed data compared with skewed data. Left panel: Visual inspection of the data reveals them to be normally distributed [80].

### **2.6.1. Statistical Analysis Software**

Data collection and analysis can begin once a research topic, study design, and statistical analysis methodology have been determined. It is necessary to be familiar with one or more frequently used data management systems and statistical software programs. Although beginners may find free web-based analysis tools like MedCalc and OpenEpi useful, intermediate users will likely prefer Excel, which not only allows for data entry, storage, and filtering, but also provides a graphical user interface for graphical data exploration, descriptive and comparative statistics, and correlation and regression analysis through the Analysis ToolPak. GraphPad Prism, Minitab, SPSS, and PSPP are some more graphical user interface-based choices that are easily available. Most researchers, on the other hand, will want to learn to program in a robust statistical programming environment like R, Stata, SAS, or Anaconda/Python [84].

### **2.6.2. Analysis of Linear and Logistic Regression**

The main method for identifying the behavior of a dependent outcome variable in respect to one or more independent predictor factors is regression analysis. A classic example in research is determining the influence of one or more continuous or categorical independent (predictor) variables on a continuous dependent variable of interest using linear regression. While logistic regression is similar to linear regression, it contains a binary dependent variable [85].

Linear and logistic regression, like other statistical models, involve assumptions about data distribution that should be evaluated before the model is built. The connection between predictor and outcome variables is assumed to be linear in linear regression. It also presupposes homoscedasticity and normally distributed input variables. Linearity is also assumed in logistic regression. Both techniques also imply that independent variables have little or no collinearity.

Determining the amount of predictor variables that can be included in a multivariate regression model is a crucial step in regression modeling. Making the decision to include predictor variables in a regression model in the first place is a distinct challenge. To acquire unadjusted results, one need first construct univariate regression models for each possible predictor variable. Then, while developing multivariate models,

predictor variables should ideally be chosen in a sensible, hypothesis-driven way based on disease pathophysiology knowledge [86].

### **2.6.3. Correlation Analysis**

In the same way that regression investigates the statistical connection between two variables, correlation analysis does the same [87].

It is not commonly used for prediction, since it does not presume a causal link, unlike regression. Its goal is to determine and quantify the degree of connection or relatedness between two variables, which is expressed as a correlation coefficient. Multiple forms of correlation analysis exist, much like other statistical approaches, and the best method relies on the nature of the data in question [88].

### **2.6.4. Categorical Data Analysis**

In pathology, binary categorical and multilayer categorical data are frequently encountered. For analysis, these data are frequently presented in tabular form. Conducting two-sample or multisample comparisons using categorical variables is typically of interest, just as it is with numeric data.

Data tabulation is also used to assess the accuracy of diagnostic tests. Sensitivity and specificity, or the likelihood that a test result will be positive or negative depending on whether the illness is present or absent, are intrinsic to a diagnostic test and are not affected by disease prevalence.

A receiver operating characteristic (ROC) curve, which also offers a visual evaluation of diagnostic test accuracy, can be used to investigate the relationship between a diagnostic test's sensitivity and specificity. Positive and negative predictive values, on the other hand, rely on the prevalence of the disease in the population being tested, as do the likelihood that the disease is present or absent when the test is positive or negative, respectively. These prevalence-dependent values are extremely useful, yet they are frequently neglected in pathology research [89].

### **2.6.5. Survival Analysis**

The term "survival analysis" refers to a group of statistical methods for analyzing time-to-event data. Overall survival, cancer-specific survival, and progression-free survival are all examples of pathology. A continuous variable and a binary variable combine to provide time-to-event data [90]. The period is computed from diagnosis to death date for participants who have died, and the event is represented in the data set by the numeral 1. The time interval is estimated for living participants from the date of diagnosis to the last known date when they were alive or known to be progression-free.

These factors may be combined and fed into a survival function, which calculates the likelihood that the subject will live (or not) for a certain period of time. The two variables (time and status) may be used to create a Kaplan-Meier survival curve, which is a nonparametric function that shows % survival on the y axis and time on the x axis. The curve drops down each time an event occurs, forming a ladder-like line. Tick marks are used to signify censored topics [91].

Many sorts of investigations in pathology include findings that must be explained and appraised but do not really include statistical comparisons. Descriptive statistics approaches allow summarize a dataset using frequency, central tendency, dispersion or variance, and position or rank [92]. Inferential statistics, on the other hand, uses hypothesis testing to generalize findings from a smaller data set to a larger population. More crucially, the nature of the observations typically determines the statistical description that is required, and an analytic strategy should ideally be pre-specified before commencing descriptive research, just as it would be for a randomized trial [93].

### **2.6.6. Parametric and Nonparametric Two-Sample and Multisample Comparisons**

Statistical tests are necessary after a comparison is introduced to an experiment to establish whether observed differences are likely to represent true differences. The use of statistical hypothesis testing to generalize findings from a sample to the wider population from which the sample was obtained is one of the approaches of inferential statistics. The type of data to be compared determines the comparative test to use. The difference between numeric and categorical variables is crucial. Numeric variables can be defined using discrete values or a continuous range of values.

A parametric statistical test can be used to determine if a numeric-dependent variable differs between two or more groups if it is normally distributed [94]. Post hoc testing can be used to examine the significance of an individual effect size in multisample tests, whether parametric or nonparametric [95]. However, studies are seldom sufficiently powered for decisive post hoc testing, which is a caution. Post hoc testing results should be viewed as exploratory in nature and should preferably be subjected to independent evaluation in a different experiment. Furthermore, if their original hypothesis was not confirmed by their experiment, researchers should not utilize post hoc testing to dredge subgroups. Nonparametric tests should be employed at least as often as parametric tests, if not more often, in pathology since sample sizes are frequently small [96]. For data with a skewed distribution or in the form of a discrete or ranking scale, nonparametric tests are utilized. These tests offer the benefit of letting go of preconceptions regarding data distribution. They function by giving rankings to data and comparing the ranks without taking into consideration the sample size difference.

Extreme outlier values can readily sway parametric tests, such as t-tests. Nonparametric tests, on the other hand, are unaffected by outliers since the rank scheme between the results remains fixed. It's worth reiterating that a nonparametric test could be used on normally distributed data, and while this would limit the power of the test to find differences, substantial differences would still be discovered [97].

Student's t test (t test) and analysis of variance (ANOVA) are statistical procedures for comparing means between groups in hypothesis testing. The testing variable (dependent variable) should be on a continuous scale and roughly regularly distributed for these approaches. The mean is the typical measure for a normally distributed continuous variable, and parametric techniques are statistical methods used to compare the means. The median is a typical measure for nonnormal continuous variables, and in this case, nonparametric approaches are used to compare the groups. Most parametric tests have a nonparametric counterpart [83], [98].

The Student's t test (also known as the T-test) is used to compare the means of two groups with no need for multiple comparisons because a single P value is observed, whereas the ANOVA is used to compare the means of three or more groups with no need for multiple comparisons because a single P value is observed [99]. In an ANOVA, the first variable receives a shared P value. A significant P value in an ANOVA test implies that the mean difference between at least one pair was statistically significant [100].

### **Hypothesis testing steps**

Building hypotheses: Just like other tests, there are two types of hypotheses: null and alternative hypotheses. The alternative hypothesis asserts that there is a statistically significant difference between the means, whereas the null hypothesis maintains that there is no such difference.

Test statistics computation: The first step in these tests is to compute test statistics (also known as calculated value) (called t value in student's t test and F value in ANOVA test). It is determined by entering data (from the samples) into a statistical test algorithm. The computed t value in a student's t test is the ratio of mean difference to standard error, whereas the generated F value in an ANOVA test is the ratio of variability between groups to variability of observations within groups.

Value tabulated: The appropriate tabular value of the T test or F test is determined based on the degree of freedom of the provided observations and the desired level of confidence (typically at two-sided test, which is more powerful than one-sided test).

Null hypothesis and comparison of calculated and tabulated values: If the calculated value is larger than the tabulated value, reject the null hypothesis, which claims that the groups' means are statistically equal. As the sample size grows, the degree of freedom rises as well. Higher degrees of freedom have a lower tabulated value for a given level of confidence. When a result, as the sample size grows, the significance level grows as well (i.e., P value is decreasing) [83], [98], [101].

#### **2.6.6.1. T-Test**

It's one of the most used statistical methods for determining if a difference in mean between two groups is statistically significant. The null hypothesis claimed that both means are statistically equal, but the alternative hypothesis stated that both means are statistically distinct from one another [98], [101].

The test is performed by comparing the means of two samples to see if they are substantially different. It accomplishes this by computing the standard error of the difference in means, which may be used to determine how probable a difference exists if the two samples have the same mean (the null hypothesis). By comparing the t statistic

obtained by the test to crucial values from the t-distribution, the t statistic may be understood. With the percent point function (PPF), the critical value may be determined using degrees of freedom and a significance level. In a two-tailed test, the statistic value might be interpreted to suggest that if the null hypothesis is rejected, it could be because the first mean is less or bigger than the second mean. To do so, we may compute the test statistic's absolute value and compare it to the positive (right tailed) critical value, as shown below:

- If  $|t\text{-statistic}|$  is equal to the critical value, accept the null hypothesis of equal means.
- If  $|t\text{-statistic}|$  is not equal to the critical value, reject the null hypothesis of equal means.

To compute a p-value, we may use the cumulative distribution function (CDF) of the t-distribution to extract the cumulative probability of witnessing the absolute value of the t-statistic. The p-value can then be compared to a pre-determined significance threshold ( $\alpha$ ), such as 0.05, to see if the null hypothesis can be dismissed:

- If  $p > \alpha$ , accept the null hypothesis that the means are identical.
- If  $p \leq \alpha$ , the null hypothesis that the means are equal is rejected.

The test assumes that both samples were selected from a Gaussian distribution when working with their means. The test also implies that the samples are of the same variance and size, albeit there are remedies if these assumptions are not met [102].

### **One-sample t test**

The one sample t test is a statistical process for determining if a sample's mean value is statistically the same as or different from the mean value of the parent population from which the sample was chosen. The mean, standard deviation (SD), sample size (Test variable), and population mean, or hypothetical mean value (Test value) are all utilized to perform this test. The sample must be a continuous variable with a normal distribution. When the sample size is smaller than 30, a one-sample t test is employed. When the sample size is equal to or more than 30, one sample z test is preferred over one sample t test, albeit population SD must be known for one sample z test. If the population SD is



unknown, a one-sample t test with any sample size can be employed. The tabulated value in one sample Z test is z value (instead of t value in one sample t test) [103], [104].

### **Independent samples t test**

The independent t test, also known as the unpaired t test, is an inferential statistical test that examines if two unrelated (independent) groups have statistically significant differences in their means. A continuous normally distributed variable (Test variable) and a categorical variable with two categories (Grouping variable) are utilized to perform this test. To determine the significance level, the mean, SD, and number of observations of groups 1 and 2 would be utilized. In this procedure, the first significance level of Levene's test is calculated, and if it is insignificant ( $P > 0.05$ ), equal variances are assumed between the groups; if it is significant ( $P \leq 0.05$ ), unequal variances are assumed between the groups, and the appropriate P value for independent samples t test is selected [104], [105].

### **Paired samples t test**

The dependent samples t test, also known as the paired samples t test, is used to see if the difference in means between two paired observations is statistically significant. The same participants are assessed at two separate time points or observed using two different ways in this test. Pair variables (pre and post observations of the same individuals) are employed in this test, and the paired variables should be continuous and regularly distributed. The sample size (i.e., the number of pairs) and the mean and SD of the paired differences would be used to compute the significance level [104], [106].

#### **2.6.6.2. ANOVA**

The ANOVA or F test is a statistical technique for comparing the means of three or more groups. It's significant P value implies that the mean difference in at least one pair is statistically significant. Post hoc tests (many comparisons) are performed to determine the specific pairs. There are several types of ANOVA tests, each with its own set of objectives. One-way ANOVA and one-way repeated measures ANOVA are the two primary forms of ANOVA. The first method is used for independent observations, while the second method is used for dependent observations. When just one categorical

independent variable is used, it is referred to as one-way ANOVA, however when two categorical independent variables are used, it is referred to as two-way ANOVA [107], [108].

### **ANOVA Assumptions**

- The residuals (experimental error) are distributed about regularly (Shapiro-Wilks test or histogram)
- Homoscedasticity or Homogeneity of Variances (variances are equal between treatment groups) (Levene's or Bartlett's Test)
- The observations are sampled in a random order (no relation in observations between the groups and within the groups)
- The dependent variable must be a continuous variable. If the dependent variable is ordinal or rank, the assumptions of normality and homogeneity of variances are more likely to be violated.

After an ANOVA has been shown to be significant, post hoc tests (pairwise multiple comparisons) are utilized to find the significant pair(s). Before doing a posthoc test (in between subject variables), one should make sure the variances in the groups are homogeneous (Levene's test). If the variances are homogenous ( $P \geq 0.05$ ), one of several post hoc tests can be chosen: least significant difference (LSD), Bonferroni, Tukey's, and other multiple comparison procedures. If the variances are not homogenous ( $P < 0.05$ ), choose from Games-Howell, Tamhane's T2, and other multiple comparison methods [109], [110].

### **One-way ANOVA**

The one-way ANOVA is an extension of the independent samples t test (which compares the means of two independent groups, whereas the one-way ANOVA compares the means of three or more separate groups). This test's significant P value relates to the multiple comparisons test used to find the significant pair (s). One continuous dependent variable and one categorical independent variable, each with at least three categories, are utilized in this test [111].

## **Two-way ANOVA**

The two-way ANOVA is an extension of the one-way ANOVA (only one independent variable is used in one-way ANOVA, whereas two independent variables are used in two-way ANOVA). The basic goal of a two-way ANOVA is to determine if two independent variables on a dependent variable have any association. Two categorical independent variables and a continuous dependent variable (roughly normally distributed) are utilized in this test [112].

## **2.7.Machine learning**

Machine learning is one of the hottest fields in computer science, with a wide range of applications. It is the process of automatically detecting meaningful patterns in data. The goal of machine learning technologies is to provide algorithms the capacity to learn and adapt [113].

As a consequence of the expansion of smart and nano technology, there has been considerable improvement in data mining and machine learning, which has sparked interest in discovering hidden patterns in data to derive value. The combination of statistics, machine learning, information theory, and computers has resulted in a robust discipline with a strong mathematical foundation and a set of extremely powerful tools. Machine learning algorithms are classified into a taxonomy based on the algorithm's expected output. The function that translates inputs to desired outputs is generated through supervised learning. Machine learning algorithms have gotten increasingly sophisticated as a result of unprecedented data production [114].

A learning problem, in general, takes a set of  $n$  samples of data and then attempts to predict unknown data attributes. A sample is considered to include numerous qualities or features if it contains more than one number, such as a multi-dimensional entry.

There are a few types of learning problems:

- Supervised learning, in which the data has extra characteristics that we wish to forecast.
  - Classification: samples are divided into two or more classes, and we want to learn how to predict the class of unlabeled data using data that has previously been labeled. Another approach to think of

classification is as a discrete kind of supervised learning in which one is given a restricted number of categories and is asked to classify each of the  $n$  samples with the proper category or class.

- Regression: the job is called regression if the intended output consists of one or more continuous variables.
- Unsupervised learning: the training data is made up of a series of  $x$  input vectors with no matching target values. The goal of such problems may be to find groups of similar examples within the data, which is known as clustering, or to determine the distribution of data within the input space, which is known as density estimation, or to project data from a high-dimensional space down to two or three dimensions for visualization, which is known as projection [115].

### **2.7.1. Classification Algorithms**

The act of classifying thoughts and things involves identifying, comprehending, and arranging them into predetermined groups or "sub-populations." Machine learning systems classify future datasets into categories using pre-categorized training datasets and a range of techniques.

In machine learning, classification algorithms utilize input training data to predict whether following data will fall into one of the established categories.

In a nutshell, classification is a type of "pattern recognition" in which classification algorithms are applied to training data in order to detect the same pattern in subsequent data sets [116].

Linear Classifiers, Logistic Regression, Nave Bayes Classifier, Perceptron, Support Vector Machine; Quadratic Classifiers, K-Means Clustering, Boosting, Decision Tree, Random Forest (RF); Neural networks, Bayesian Networks, and so on are among the supervised machine learning algorithms that deal with classification [114].

#### **2.7.1.1. Random Forest**

RF is a well-known and effective ensemble supervised classification algorithm. RF has been successfully used to several machine learning applications, including those

in bioinformatics and medical imaging, due to its superior accuracy and resilience, as well as some capacity to give insights via ranking of its features. RF is made up of a "forest" of classifiers, each of which is formed using the bagging method with no pruning, resulting in a "forest" of classifiers voting for a certain class. Two parameters, the number of trees in the forest and the number of randomly selected features/variables used to assess at each tree node, as well as a training database containing ground-truth class labels, must be given in order to train an RF. The voting threshold or cutoff (percentage of trees in the forest required to vote for a specific class) may also be adjusted using RF, which is used to compute recall, accuracy, and f-score. Out of Bag Error (OOB) is the accuracy estimate built into the RF method and all of its software implementations, and it estimates the average misclassification ratio of samples not utilized for RF training [116].

There are several advantages to employing it such as:

- There are several trees and each tree is trained on a portion of data, the RF technique is not biased. As a result, the algorithm's overall bias is minimized.
- This algorithm is quite dependable. Even if a new data point is added to the dataset, the overall process is unaffected because while new data may change one tree, it is extremely unlikely to affect all trees [117].
- When both category and numerical information is used, the RF approach performs effectively.
- When data has missing values or has not been scaled correctly, the RF technique performs well.

The disadvantages of employing RF are:

- The intricacy of random forests is one of its key drawbacks. Due to the enormous number of decision trees combined, they required much greater processing resources.
- They take substantially longer to train than other equivalent algorithms due to their complexity [118].

## CHAPTER 3 – STATE OF THE ART



### 3. State of The Art

#### 3.1. Animal Models

Many studies of the role of the visual system [119]–[121] and the processes of developmental visual plasticity [122] have used genetically engineered mice, and many mouse models of visual system diseases have been developed and tested [123]–[125]. Despite the use of mice in vision studies, no basic knowledge about their spatial vision or how experimental manipulations of the visual system affect their vision is available. The lack of quick and simple behavioral methods to quantify vision in mice is one of the major causes of this deficiency [126].

Mice's spatial perception has been quantified using reinforcement-based visual discrimination tasks [127]. While these exercises have been used to assess the impact of experimental manipulations on the mouse's vision, they take a significant amount of time to produce valid psychophysical levels, and their application is effectively restricted to juvenile-adult mice since younger animals seem to lack the cognitive ability to easily master the tasks [127], [128].

Increased neural inhibition underpins cognitive and learning abnormalities in NF1, according to studies on NF1 mice [129]–[131], [13]. Neurofibromin interacts with the hyperpolarization-activated cyclic nucleotide-gated (HCN), a voltage-gated ion channel that mediates an inward cationic current that modulates neuronal excitability [132]. In adult NF1 mice, pharmacological stimulation of HCN channels can improve electrophysiological and spatial learning deficiencies [133].

In contrast to the hippocampus origin of the spatial learning loss in NF1 animals, cognitive abnormalities in NF1 humans may develop largely in the cortex. While hippocampal plasticity stays high throughout life [134], cortical plasticity decreases once important developmental periods have passed. As a result, NF1 may produce cortical development deficiencies that cannot be rectified by therapy at a later age [135].



### **3.2. Electroretinogram Applied to the Study of Autism**

The shape of the ERG is believed to be altered in certain neurological disorders. The growing use of the ERG in psychological illnesses, as well as its capacity for distinguishing symptoms dependent on the ERG waveform, has been highlighted in a recent systematic study [136]. For e.g., smaller LA a- and b-wave amplitudes as well as longer b-wave peak periods were observed in schizophrenia, and a delayed cone b-wave period to peak was found in depression [137]. The ERG a-wave amplitudes under LA and DA conditions were recently used to distinguish schizophrenia from bipolar disorder [138]. These results suggest that the ERG can detect variations in the form of synaptic transmission despite the fact that the same CNS neurotransmitters are involved. The ERG's overlapping interactions with genes implicated in ASD and schizophrenia [139], as well as similar changes in a- and b-wave amplitudes and b-wave time to peak in schizophrenia [138] and those reported in this study, suggest that it could aid our understanding of a wide range of psychiatric disorders, including ASD [10], [136]. As a non-invasive and reliable indicator of retinal function in response to fleeting bursts of light, the ERG has the ability to aid our interpretation of neurodevelopmental and neurodegenerative disorders [10].

Differences in the ERG waveform in people with ASD could assist our comprehension of the biology of the factors that cause ASD. There have only been three human trials on the retinal activity of people with ASD conducted to date. The first two studies, published 30 years earlier, found a smaller DA-ERG b-wave in a diverse number of children with ASD [140], as well as disparities between siblings and probands within a population [141]. This result was recently verified in a small sample of adults with ASD [21]. Constable et al. (2016) have looked at the LA-ERG b-wave amplitude and discovered that it was lower at different flash intensities. Constable et al. (2016)'s novel LA-ERG findings are backed up by reports of altered ERGs in mouse models of neurodevelopmental diseases such as ASD [35], [3], Fragile X syndrome and ADHD [142]. The greater sophistication of the cone pathways makes the LA-ERG an effective instrument for probing the detail of a retina's reaction to light [10], [68], and the LA-ERG is a faster and more suitable assay than the DA-ERG since it does not need dark adaptation period.

Some studies used full-field electroretinogram (ffERG) recordings to investigate retinal activity [143],[144]. Experiments were carried out under scotopic (rod-dominated)

and photopic (cone-dominated) conditions in order to explore rod-versus cone-driven pathways more extensively. The observations were similar to those of an inbred strain of mice with typical levels of social interaction and repeated activities, which is commonly used as a control for BTBR mice in autism research [145]. Under both scotopic and photopic conditions, the results point to retina-based changes, mainly in the cone pathway, and robustly improved visual recognition of finer spatial information and more complex contrasts at higher spatial frequencies [20].

### 3.3. ERG Processing and Points of Interest Detection

The Herrera et al. [146] ERGs were sent to an acquisition system, where the data is processed and shown in a graph for proper illness treatment [147]. A front-end design of the high-pass filter described by Spinelli et al. for AC coupling was utilized for each lead; the cutoff frequency to eliminate dc was 0.16Hz. A low pass filter (fourth grade Butterworth) is employed to reduce high frequency noise in the following step [148]. Its cutoff frequency is 300 Hz. A band stop filter, with a rejection range of 57 to 63 Hz, is also included in the system, which eliminates the 60 Hz AC power line signal [149]. Finally, two amplifier stages with a minimum of 40dB and a maximum of 100dB are installed. To complete this project, a MATLAB application (Figure 3.1) was created to capture the signal from the PC sound card. The signal received from the cornea has a maximum frequency component on the order of 250 Hz. The biological signal is vulnerable to ambient noise due to its magnitude of a few microvolts; the majority of this noise is removed by the biopotentials amplifier's pass band filter, but there is a portion that is not destroyed since it is in the filtered band [1, 5, 6]. They used MATLAB to create a Butterworth filter to remove the noise in this situation.

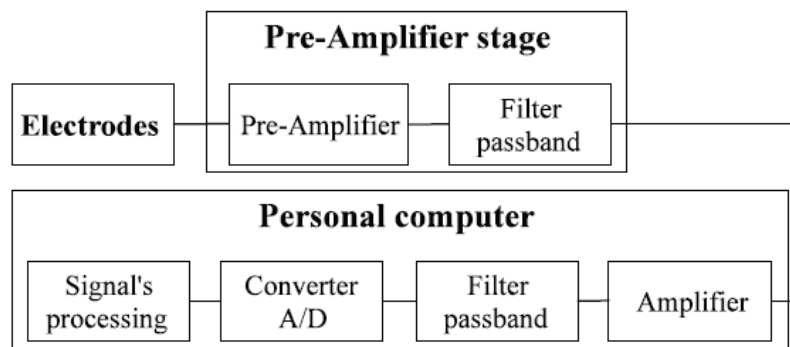


Figure 3.1 - Block diagram of the electroretinography used in [146].

In Gauvin M., Lina J-M and Lachapelle P.(2014) [150], ERG waves from both eyes were averaged to create a single waveform with a pre-stimulus baseline of 20ms and a duration of 150ms (sampling rate: 3413.33Hz). The a-wave amplitude was measured from the prestimulus baseline to the ERG's most negative trough, whereas the b-wave amplitude was measured from the a-wave trough to the highest positive peak of the ERG that followed the a-wave. Peak timings were calculated from the beginning of the flash to the peak of the a- and b-waves [151]. These ERG measurements will be referred to as time domain measurements since they are taken in the time domain. The fast Fourier transform technique implemented in MATLAB was used to perform frequency domain analysis of the ERG. They were able to compute the FFT coefficients for frequencies ranging from 0 to 1706.66Hz in increments of 6.66Hz using the size (512 data points) and sample frequency (3413.33Hz) of our ERG waveforms. Due to the limitations imposed by our recording bandwidth (1–1000Hz), we confined our study to frequencies spanning from 0 to 300Hz in order to minimize artifactual contamination (such as that predicted by the Nyquist-Shannon sampling theorem [152]). The time domain analysis revealed two major ERG components, one peaking at  $13.53 \pm 1.55$ ms (mean SD in our 40 subjects) with an amplitude of  $32.21 \pm 5.11$   $\mu$ V (identified as the a-wave in Figure 3.2) and the other peaking at  $30.98 \pm 1.33$  ms with an amplitude of  $104.81 \pm 18.66$   $\mu$ V (identified as the b-wave in Figure 3.2). The FA, such as that produced using the FFT, can be used to identify the frequency components that contribute to the origin of the ERG [150].

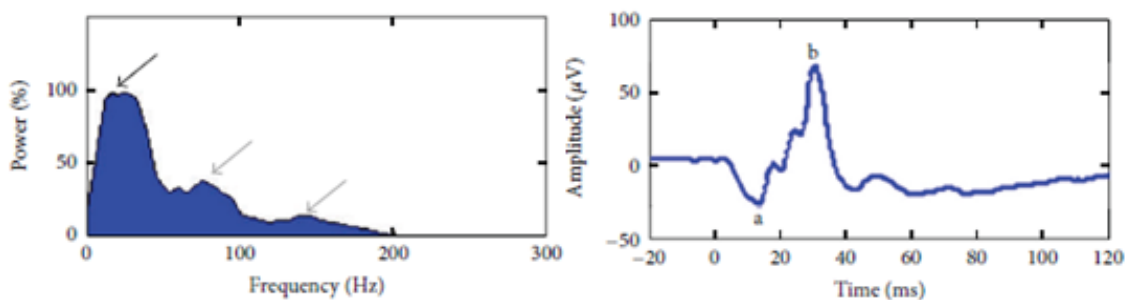


Figure 3.2 - FA of a composite ERG, averaged from 40 subjects, showing the 3 typical frequency components that contribute to the ERG (~30Hz: a- and b-waves contribution, black arrow; ~75 Hz and ~150Hz: oscillatory potentials (OPs) contribution, gray arrows) [150].

According to Creel D. and Yu M. [57], a rate of 30 Hz is commonly used to determine if a retina's cone physiology is excellent. The lowest and higher frequency limitations for recording OPs components are 75 to 100 Hz and 300 to 1000 Hz, respectively. Analyzing the OPs with digital filtering and frequency spectrum analysis using a Fast Fourier Transform is more convenient. The frequency spectrum is computed from the raw ERG waveform during this procedure, and the amplitudes of the components in different frequencies are calculated. The frequency spectrum of the experimental group may be directly compared to that of the control group. Another technique is to extract the OPs waveform using band-pass filtering, which selects components of the frequency spectrum in the region of 100–150 Hz. The amplitudes of the several OPs wavelets may then be examined separately [153].

A phased procedure is used in Alaql A [154]. Graduate Thesis to achieve the best answer, and each stage will be detailed in this section. The ERG data gathering procedure is depicted in Figure 3.3 as a phased approach. To eliminate unwanted frequencies, a band pass filter is utilized [155]. The bandwidth of the filter used in this application is generally 0.3 Hz-500 Hz. The filtered signal is captured by an analog to digital converter and sent to the processing unit [154]. The ERG response is then shown in time domain on the computer using a display unit. It can also save data for further analysis, as well as collect several ERG signals and average them to eliminate noise [155]. A response can be either a Scotopic or a Photopic ERG signal, depending on the light hue and intensity settings as well as the start period.

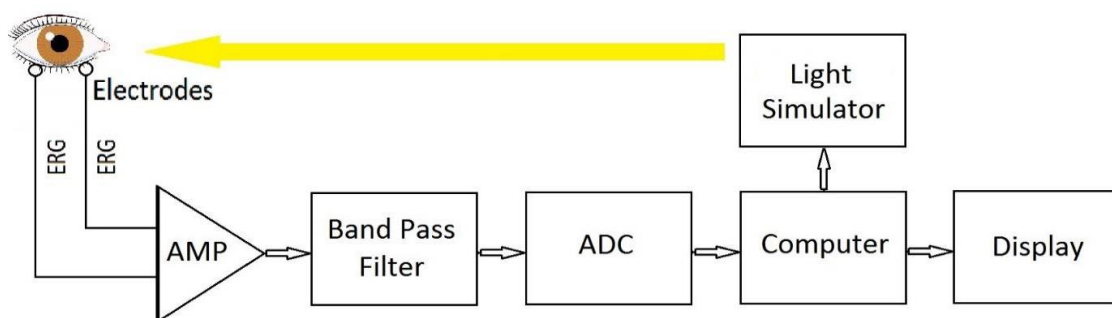


Figure 3.3 - ERG Data Collection Block Diagram used in [154].

A sampling frequency of 2000 Hz was used to sample the averaged signal collected. The ERG response is a 16-bit signal with a sample frequency of 2000 Hz, which

has been averaged from 10 raw recorded responses to remove noise. The initial negative peak (a-wave) and the subsequent positive peak (b-wave) are measured from the base line, and the implicit time from  $t=0$  ms. The implicit time of the highest point of the wave's peak, as well as the amplitude of the wave's peak, are used to apply the time domain properties of a-wave and b-wave ERG signals. A-wave has an implied time of 16.5 milliseconds and a voltage value of -28.7 microvolts at its maximum point. The ERG's greatest peak is the B-wave, which has an amplitude of 66.9 microvolts and an implied duration of 28 milliseconds. The duration difference between the a-wave and b-wave critical points is 11.5 milliseconds, while the amplitude difference between the two peaks is 95.6 microvolts. The ERG response has been split into five signals, each with a specific frequency spectrum. In this part, a breakdown of ERG components is performed using DWT and Castro's ERG Model. The ERG model of Castor was used to eliminate the a-wave and b-wave components of the signal in this section of the thesis. The breakdown of ERG components is depicted in Figure 3.4 as a block diagram [154].

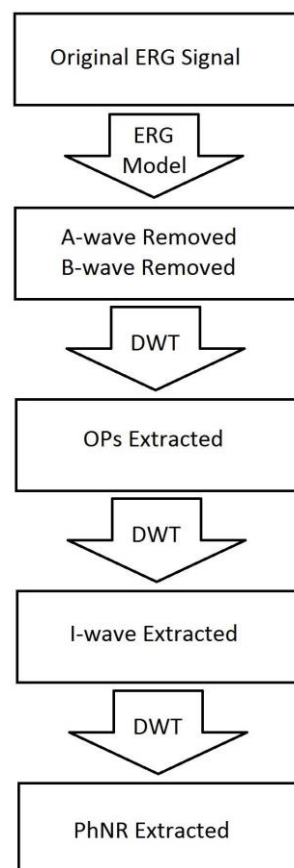


Figure 3.4 - ERG Components Decomposition Process of [154].

### 3.4. Statistical Analysis

Ten issues of The American Journal of Pathology were chosen by Mata D. and Milnerat D. [80], for evaluation between January 2014 and December 2018. The type and number of statistical tests provided per article were studied in the papers published in the issues. There were 195 articles found in the ten issues, with 93% of them claiming to have used one or more statistical tests. There was a total of 426 statistical tests reported, with an average of two tests per article. Figure 3.5 shows an overview of the statistical tests presented in the publications. These included normality tests, P-value correction methods for multiple testing, two-sample parametric and nonparametric tests, multi-sample parametric and nonparametric tests, post hoc tests, tests for evaluating categorical variable differences, correlation analysis, generalized linear models, survival analysis, and other specialized methods. Parametric tests were thus overused, accounting for 54% of tests. Two-sample parametric tests were the most common, accounting for 32% of all tests, followed by multisample parametric testing, which accounted for 22% of all tests. Only 8% of two-sample tests reported were nonparametric. 68% of studies reporting multisample tests did not conduct post hoc tests to investigate differences between study groups. Only a few studies adjusted P values to account for multiple testing. Finally, despite the fact that numerous researches supplied data that might have been analyzed utilizing correlation, regression, and survival analysis approaches, they were underutilized (Figure 3.5).

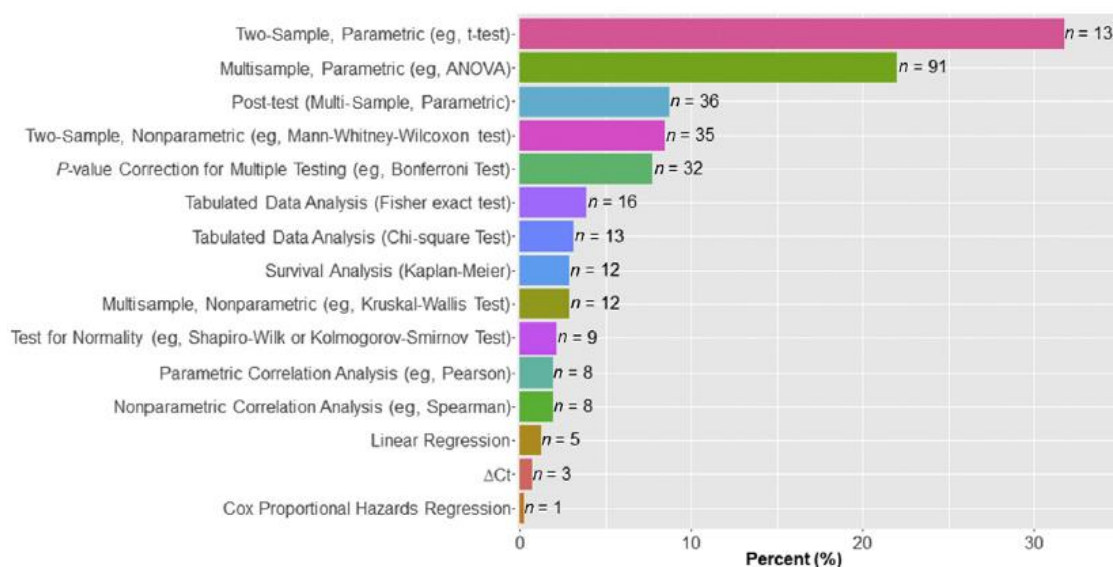


Figure 3.5 - Statistical tests utilized by the articles surveyed by [80]. A bar chart is shown with the breakdown of test type, total number encountered, and percentage of total. The graph shows all tests (not all articles).

### **3.4.1. T-test**

Due to its resilience, the heavy-tailed Student-t distribution has gotten a lot of attention from elements like statistical modeling [156], [157] or autoregression issues [158] instead of the Gaussian and its mixture. The Student-t model has recently been proposed as an alternative to the Gaussian on state estimation, allowing for non-Gaussianity in the model.

### **3.4.2. Two-Way ANOVA**

Tukey [159], who examined the variances of variance component estimation for balanced data under the assumptions of independence and normality in 1956, was one of several academics interested in finite population effects for variance component estimation. The finite population correction, on the other hand, would be connected to the estimate of variances if one sampled from limited populations. The predicted values of mean squares in trials with balanced data were next considered by Cornfield and Tukey (1956) [160]. To establish the formulae for crossing and nested classifications, they employed a model with enough generality and flexibility. Furthermore, Tukey (1957) [161], presented the variance components for one-way classification for unbalanced data, while Searle and Henderson (1961) [162], discussed the two-way classification model with one fixed factor for unbalanced data. Following that, Hartley (1967) [163], developed a general procedure for directly yielding the numerical values of the coefficients in the formulas of expected mean squares (EMS) for one-way and two-way classifications with unequal numbers when sampling from an infinite population using random and mixed models. Mathematical formulae for the numerical coefficients needed to generate the variance and covariance formulas for anticipated mean squares were beneficial. Following that, Searle and Fawcett (1970) [164], investigated the EMS in variance component models with random effects collected from finite populations. They came up with a rule for transforming expectations from infinite to limited population models. It may also be used to both balanced and unbalanced data, as well as nested and cross classifications, assuming the set levels for each factor are believed to be finite. Simmachan, Borkowski, and Budsaba (2012) [165], calculated the EMS of treatments and error for random effects in only the one-way ANOVA model with normal errors, assuming a finite population.

The predicted mean squares for the random effects in the random and mixed effects models in the two-factor factorial model assuming finite populations for A, B, and AB interaction effects were determined in Suphirat C, Chomtee B., and Borkowski J. study [166]. When the random effects are sampled from limited populations, the anticipated mean square formulae for components A, B, and the AB interaction are the same as in the infinite population scenario. The values of the variance components, on the other hand, are the most significant differences. They are supposed to follow normal distributions in the infinite case, whereas they are the variances of finite populations in the finite case. The anticipated mean square of error for a finite population is equivalent to the expected mean square of error for an infinite population in an imbalanced situation. Because they are dependent on the multiplier values of the population variances, the predicted value of mean square in component A, B, and the AB interaction will not be the same. They are the variances of finite populations in the finite situation.

As an example, Hui F et al. [167] utilized 20 healthy people and 15 people with glaucoma in their study. A portable device was used to capture photopic ERGs in one eye per participant utilizing a sequence of red flashes on a blue background. A repeated measures (RM) 2-way ANOVA was utilized to compare controls to glaucoma, with frequency nested inside, to evaluate changes related with interstimulus frequency and the ERG. When there was a significant difference between groups, Tukey's multiple comparisons approach was utilized. While there were minor variations in amplitude and timing with frequency, the a-wave (amplitude:  $F = 1.74$ ,  $P = 0.15$ ) and b-wave (amplitude:  $F = 1.65$ ,  $P = 0.17$ ) showed no significant differences. However, the photopic negative response (PhNR) was likewise attenuated more in the glaucoma group than in the controls ( $F = 4.84$ ,  $P = 0.03$ ).

### **3.5. Classification Algorithm**

Neural networks, SVM, decision trees, and rule-based classifiers are examples of machine learning approaches. They are automated tools that need little human intervention during data processing. R [168], Scikitlearn [169], Statistics and machine learning MATLAB toolbox [170], and WEKA [171] are only a few examples of software packages with inbuilt machine learning methodologies.



A small number of reviews have been published on the use of machine learning in the study of autism [172]–[178]. The majority of evaluations have only touched on one or a few facets of ASD (the role of classification during the diagnosis process, application of a certain machine learning class of algorithms, differentiating between features of autism and ADHD, identifying small sets of features to shorten diagnosis time among others). For instance, Pratap, et al. [175], Wall et al. [179], Bone et al. [173], and Lopez Marcano et al. [178], looked at how alternative algorithms, such as neural networks and tree models (decision tree and RF), may be used to speed up the ASD diagnosis process. Bone et al. [173] and Bone et al. [177], used the same algorithms to synthesize and re-examine the results and methods of Wall et al. [179]. The authors pointed out many drawbacks, including eliminating difficult-to-classify cases, which leads to skewed accuracy, the lack of a real-world clinical context throughout the evaluation process, and the use of inadequate ASD codes to develop the classification system. Experimental reviews of six machine learning algorithms were undertaken by Duda et al. [172] and Chu et al. [180] in order to establish the best fitting model for ADHD and ASD. Without a particular focus on autism, Wolfers et al. [176], explored typical issues associated with mental diseases, such as limited sample sizes, external validity, and machine learning algorithmic obstacles.

Most recent studies claim to have developed a machine learning approach for automated ASD detection, however in most cases, the researchers are just repurposing existing machine learning algorithms and applying them to autism datasets independently. SVM, such as in the studies of Bone et al. [177], Duda et al. [172] and Kosmicki et al. [181], logistic regression and decision trees, such as in Wall et al. [182] and Wall et al. [179], and self-organizing map and naive Bayes, such as in Pratap and Kanimozhiselvi [183], and Pratap et al. [175], are common algorithms used in the training phase. The researchers wanted to improve sensitivity, specificity, and classification accuracy, as well as distinguish between ASD and ADHD. Consequently, several copies of the input dataset (different features) are trained to maximize the metrics, with the ASD prediction system claiming to be the version with the greatest performance outcomes.

### 3.5.1. Random Forest

There are numerous articles in the literature that present RF machine learning algorithms to achieve different goals, be it classification or linear regression. In this section different research papers are presented that apply this type of algorithms to the study of autism.

Sluban et al. (2012) [184], built on the work of Petric et al. (2007) [185], who used text mining to discover an unusual link between ASD and calcineurin. The authors searched the PubMed database for 15,243 abstracts using phrases that connect ASD and calcineurin. The authors used naive Bayes, RF, and SVM classification techniques to find groups of outlier texts that link ASD with calcineurin. Outliers detected by at least two of the categorization methods were also assembled into union and Bmajority sets by the authors. Between 70% and 90% of the bridge phrases were discovered in less than 5% of all texts in the sample across the five outlier selections.

Chen et al. (2015) [186], analyzed neuroimaging data for diagnostic categorization purposes using machine learning models, including RF. For a sample of 126 people with ASD and 126 people with typically developing, low-motion resting-state functional MRI (rs-fMRI) scans were employed. Age, nonverbal IQ, and head motion were used to match the participants. A matrix of functional connection between 220 identified areas of interest served as the foundation for diagnostic categorization. An RF achieved the highest degree of diagnostic classification accuracy of the models examined, at 91%, with a sensitivity of 89% and a specificity of 93%, using the top 100 areas of interest. When applied to the top 10 regions of interest, the RF had a 75 % sensitivity, and a 75 % specificity. The large number of locations required to diagnose ASD with good accuracy might indicate that ASD biomarkers are dispersed rather than centralized in the brain. RF classifiers have also been utilized to create ASD screening systems that are both inexpensive and effective.

RF has also been employed for ASD surveillance and monitoring. The Autism and Development Disabilities Monitoring (ADDM) Network is responsible for population-based monitoring of ASD in children aged 8 in the United States. To assess a child's diagnostic status, physicians used to manually analyze developmental exams. Maenner et al. (2016) [187], used the 2008 Georgia ADDM data to train an RF classifier in order to identify children who match the ASD surveillance requirements. A bag-of-words technique with term-frequency-inverse-document-frequency (Tf-idf) weighting

was used to preprocess 5396 assessments from 601 children with ASD and 561 children with TD. To (1) find words and phrases suitable for categorizing ASD and (2) categorize ASD, RF classifiers were utilized. The classification model was evaluated on 9811 assessments from 754 children with ASD and 696 children with TD. The final RF of 3000 trees had an accuracy of 86.5 %, a sensitivity of 84 %, a specificity of 89.2 %, and an AUC of 0.932. Machine learning, according to the authors, can assist distinguish youngsters who match the monitoring requirements; nevertheless, this model should be used as a filter rather than a final classification tool.

On a dataset of 2925 patients, Duda et al. (2016) [172], used six machine learning methods to identify ASD from ADHD instances (2775 ASD cases and 150 ADHD cases). The goal of the study was to use electronic and digital apps to reduce the time it took to pre-diagnose ADHD and ASD. The study used 65 characteristics from the Simplex Simon Collection (SSC) version 1532, which are based on the Social Responsiveness Scale (SRS), a parent-administered questionnaire used to assess autistic tendencies. The authors pre-processed the data in the machine learning algorithms trials by deleting cases and controls with more than four incomplete responses on their sheets. As a result, the input dataset is limited to data samples having five missing responses. Furthermore, the authors used forward feature selection and cross validation during the training phase of the classification algorithms to minimize data dimensionality to less than 10 features. Furthermore, the authors modified the data by under sampling to a ratio of 1.5:1 before developing the classification model in order to balance the class labels. Six characteristics from the SRS data remained after pre-processing, according to the results. The majority of the evaluated machine learning algorithms, particularly functions-based algorithms like logistic regression, obtained excellent classification accuracy (usually better than 95%), but decision tree-based algorithms like RF had poor accuracy. There was no obvious path forward for identifying the difficult cases that overlapped ASD and ADHD.

Based on a parental questionnaire and behaviors observed in home recordings, Abbas et al. (2018) [188], merged two separate classifiers to produce an ASD screening tool. Multiple repositories were utilized to harvest Autism Diagnostic Interview – Revised (ADI-R) and Autism Diagnostic Observation Schedule (ADOS) scoresheets from children ages 18 to 84 months, which were used to train an RF for a parental questionnaire and an RF video classifier, respectively, using clinical diagnosis as the target variable. ADI-R interviews were given to a random sample of low-risk youngsters to assist balance

the results. Because language development has been shown to influence the presentation of ASD, the classifiers were trained and evaluated individually on children aged 4 and under. A total of 2299 children with ASD, 100 children with TD, and 287 children with another diagnosis were used to train the parental classifier. Also, 3310 children with ASD, 585 children with TD, and 364 children with another diagnosis were used to train the video classifier. The existence and intensity of behaviors, as evaluated by analysts watching two to three 1-minute semi-structured home films, were employed as inputs by the video classifier once it had been trained. Based on the ROC curves, the final diagnosis used logistic regression on the questionnaire and video classifier results and outperformed other established screening tools such as the Modified Checklist for Autism in Toddlers (MCHAT; Robins et al. 2014 [189]).



## CHAPTER 4 – MATERIALS AND METHODS



## 4. Materials and Methods

### 4.1. Data Acquisition and Pre-Processing

Neurofibromatosis type 1 is a neurodevelopmental disease with adult cognitive implications. However, little is known about the effects on the visual system and how these may be associated with and predict cognitive deficits.

The RETI-port/scan 21 unit from the Roland Consult Stasche & Finger GmbH includes the stimulator units and the data recording and analyzing system. Electrophysiological test unit is usable for scotopic and photopic ERG and it can be adapted for rodent ERG by using ring cornea electrodes and needle reference electrodes.

A preamplifier is located near the subject in the biosignal amplifier. A database stores all the subject's information as well as the outcomes. The signal and averaged curves from all channels can be monitored. The system automatically sets point markers and calculates major parameters in the analyze mode [190].

In Figure 4.1 it is possible to see the analysis interface of the RETI-port program along with the window responsible for applying digital filters by equalizer to extract the characteristics, in this case to obtain the b-wave.

This program has other features such as it is possible to see on top-left of figure 4.1, allowing the user to access the program Selector and Controls, other than the analysis interface. In this interface it is possible to see the ERG recorded for the different light intensity stimulus, apply filters to feature extraction, manually select the points of interest, and see the amplitudes and latencies collected for each channel.



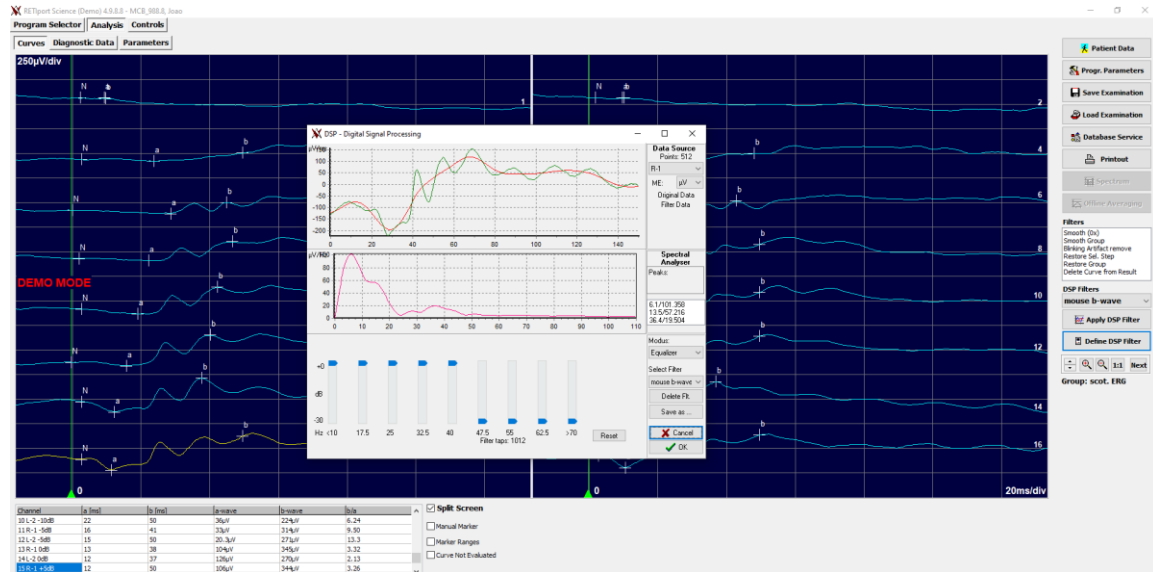


Figure 4.1 - Analysis Interface of RETI-port software.

This process of analysis presents different problems and difficulties for the user such as: There is a high lack of automation in the process of signal collection since after the collection the user needs to manually apply filters for extraction of b-wave and OPs for each light intensity. Difficulty in identifying regions and points of interest, as the user needs prior knowledge of the typical ranges of each component to manually select the point of interest. Method of data analysis merely numerical through the table of values obtained after the extraction of characteristics, not facilitating the visualization and meaning of the results.

Besides the signal processing difficulties, it is not known what correlation these data have and whether they differentiate between pathological and non-pathological. Therefore, it can be stated that these data need a statistical study with several ERGs to define groups of differentiating characteristics.

## 4.2. Animals

In this study we used a transgenic animal model of NF1, both males and females. All animals were genotyped, which allowed us to determine genotype group each animal belongs, either heterozygous NF1 (*Nf1*<sup>+/+</sup>) or wild-type (WT).

Male and female mice (8 weeks-old) were anesthetized with intraperitoneal injection of 80 mg/kg ketamine and 5 mg/kg xylazine. The animals were maintained at  $22 \pm 1^\circ\text{C}$  on a 12h light/12h dark cycle, with access to water and food ad libitum. For pupil dilation eye drops of 0.5% tropicamine were used.

The choice of the mouse as a model is due to its similarities in terms of mechanisms and characteristics when expressing the mutation in the NF1 gene compared to humans. The 98% similarity rate of the NF1 gene product when compared to humans makes them the best choice to study cognitive and behavioral manifestations, which are also observed in humans with this condition [191].

## 4.3. Light stimulation

A Ganzfeld stimulator [190] was used to deliver light stimuli. Based on recommendations for ERG procedure [192] and four different ERG responses were recorded:

- Scotopic Luminance Responses: The dark-adapted animals were exposed to a sequence of white light flashes of seven different intensities (0.0095 to 9.49 cd-s/m<sup>2</sup>) three times at 0.1 Hz.
- Photopic Adaptometry: Bright white flashes (9.49 cd-s/m<sup>2</sup>) were delivered three times at 1.3 Hz at the commencement of light adaptation and at 2, 4, 8, and 16 minutes to measure the light adaptation process using a white background light (25 cd/m<sup>2</sup>).
- Photopic Luminance Responses: White flashes of seven different light intensities (0.0095 to 9.49 cd-s/m<sup>2</sup>) were delivered three times at 1.3 Hz against a white background light (25 cd/m<sup>2</sup>).
- Photopic Flicker: White brilliant flashes (3.00 and 9.49 cd-s/m<sup>2</sup>) were delivered 10 times at 6.3 Hz against a white background light (25 cd/m<sup>2</sup>).

#### **4.4. ERG Recordings**

In the present work, only the scotopic luminance responses were analyzed since they represent a richer signal in rodent ERG. Future works will continue to explore other ERG tests. ERGs were obtained after overnight dark adaptation, none of the animals was injected with drugs or received any treatment.

Before the ERG recording, the pupil was fully dilated with topical tropicamide (0.5%). Celluvisc® eye drops were sufficient to maintain stable corneal potential (impedance < 6 kohm) through the entire recording protocol. The body temperature of the animals was maintained with a heating pad set to 37°C during the procedure. The electrical responses were recorded with a gold wire electrode placed at the cornea, a reference electrode placed at the head, and a ground electrode in the tail. Electrode impedance did not exceed 6 kohm during the entire procedure. The ERG waveforms were recorded with a band width of 1 to 300 Hz and sampled at 3.4 kHz (except for flicker test in which a 0.65 kHz sampling rate was used) by a digital acquisition system (Roland Consult GmbH, Brandenburg, Germany), and they were analyzed with the MATLAB and Python.

#### **4.5. Database**

Each file represents a tested individual, includes his or her identification, sex, test date, and the collected ERGs, corresponding to 16 readings taken with eight different light intensities for each eye. Each electroretinogram is composed of 512 points representing 150 milliseconds of recording. The intensities tested were infrared light as the lowest light intensity and 7 readings for each eye with intensities varying between -25dB and +5dB, always adding +5dB in each new reading. A total of 60 files were made available, 17 female and 43 male individuals for a final number of 30 Wild-type and 30 NF1 pathological individuals. For some of these individuals their visual acuity was collected, as well as some notes regarding reading and signal quality. Table in attachment A represents the database used in this paper.

## CHAPTER 5 – DEVELOPMENT



## 5. Development

The development of the topic goes through three main phases. The first phase consists of reading, processing and point detection all ERGs received as Excel files. For this stage two programs with different functions were developed. The second phase of the development consists of the statistical analysis of the ERG components detected by the first phase of the theme development process. For statistical analysis of the features t-tests and two-way ANOVA analysis were performed. For the development of the last phase consisting of testing the ability to predict cognitive deficits in ERGs, an algorithm of the RF classification was used.

### 5.1. The Solution – Electroretinogram

As a solution to the problem presented by the analysis interface of the RETI-port program, two programs were developed:

- a) One for reading, processing and detect points of interest in the 16 channels recorded for each individual, developed in MATLAB for the use of the laboratory.
- b) Another for analysis of multiple ERGs for the same light intensity, in order to solve the lack of automation and difficulty in identifying points of interest, making the whole analysis simpler, developed in Python.

For both programs the same process and digital filters defined in the previous solution were applied. In Figure 5.1 we can observe the filters applied by equalizer for a) the extraction of the b-wave peak, which is a low-pass filter with cutoff frequency at 47.5 Hz and b) for the extraction of oscillatory potentials with a high-pass filter for frequencies above 60 Hz.

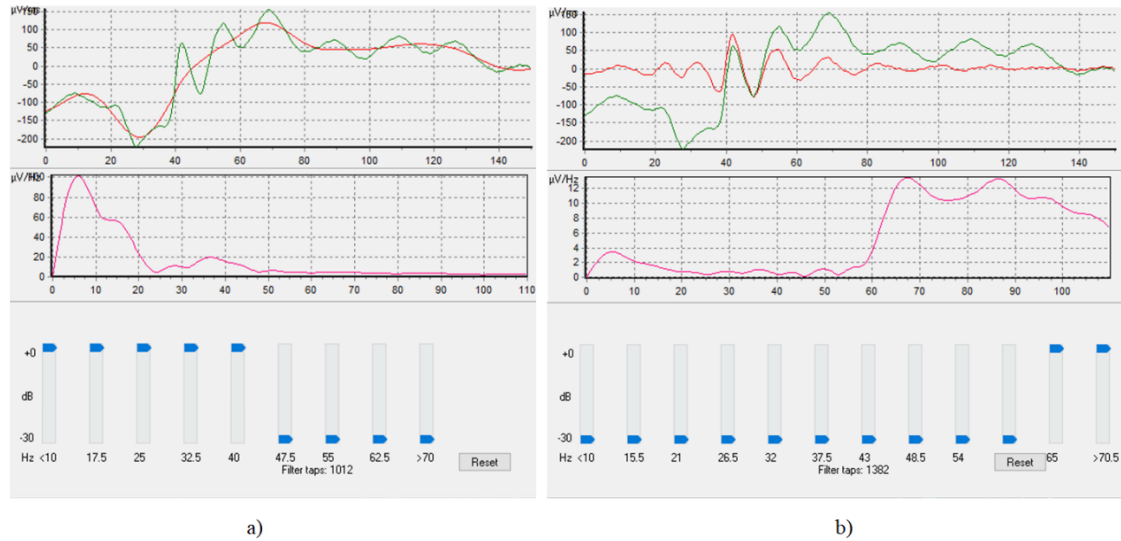


Figure 5.1 - Filters applied by equalizer in RETI-port. a) (left) the extraction of the b-wave peak with low-pass filter with cutoff frequency at 47.5 Hz. b) (right) for the extraction of oscillatory potentials with a high-pass filter for frequencies above 60 Hz. In each image there are two graphs, the first one shows the original signal in green, the filtered signal in red, and the second graph shows the distribution of frequencies after the application of the filter.

In order to clarify the process to be implemented in the solution, we built the pipeline represented in Figure 5.2, in which the pre-stimulus baseline, the first 16 ms, is disregarded. All the components under study were collected after applying the respective filter to the original signal.

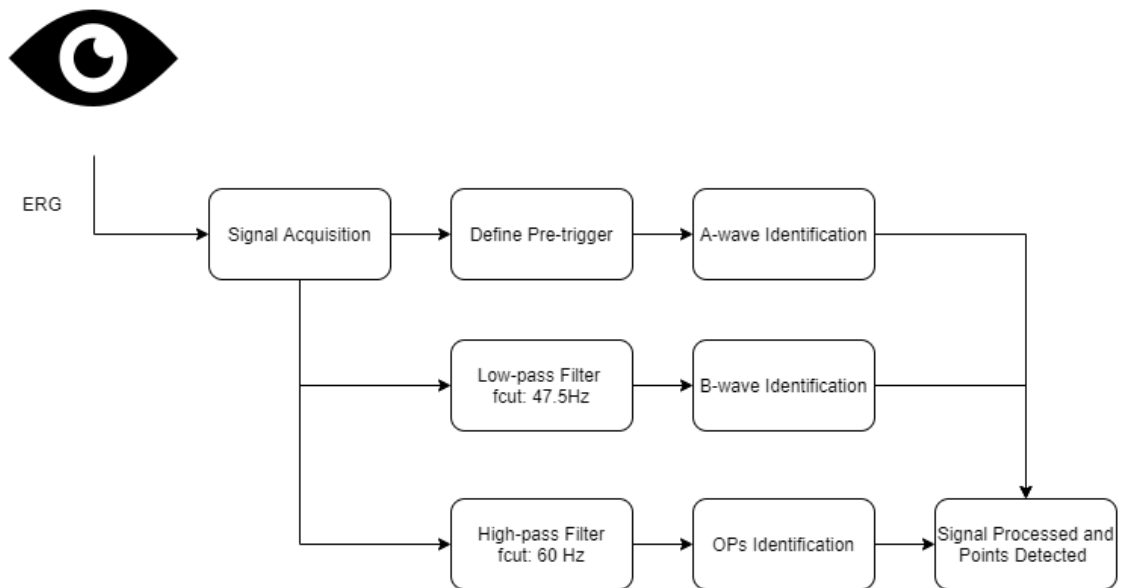


Figure 5.2 - Pipeline used in the signal processing and points detection.

While the program developed in MATLAB is mainly intended to analyze all the ERGs collected for the same individual, for the 7 light intensities tested, the program developed in Python, although it also has the function of analyzing a single file, is intended to analyze several files (different individuals) for the same light intensity, in order to find sex or genetic similarities.

## **5.2. The Solution – Statistic Analysis**

For the first exploratory test we want to compare the samples by genotype and by sex, individually. Once the dataset has:

- Dependent variable that is continuous
- Independent variable that is categorical
- Independent samples/groups - There is no relationship between the subjects in each sample. This means that:
  - Subjects in the first group cannot also be in the second group
  - No subject in either group can influence subjects in the other group
  - No group can influence the other group
- Random sample of data from the population

That said, two independent t-tests were performed, one to sex and other to genotype, the Independent t-test examines the means of the two independent groups to see if statistical evidence exists that the related population means differ substantially [83].

A two-way ANOVA is used to determine how the mean of a quantitative variable varies when two category factors are changed. A two-way ANOVA was employed in this study to see how the two independent factors affected the dependent variables when they were combined.

## **5.3. The Solution – Classification Algorithm**

To develop a basic classification algorithm, we used scikit-learn, a library in Python that provides many unsupervised and supervised learning algorithms. It is built upon some of the technology like NumPy, pandas, and Matplotlib.



The functionality that scikit-learn provides include Regression, Classification, Clustering, Model selection and Preprocessing.

A comparison of a several classifiers in scikit-learn on synthetic datasets is shown in Figure 5.3. The point of this example is to illustrate the nature of decision boundaries of different classifiers [169].

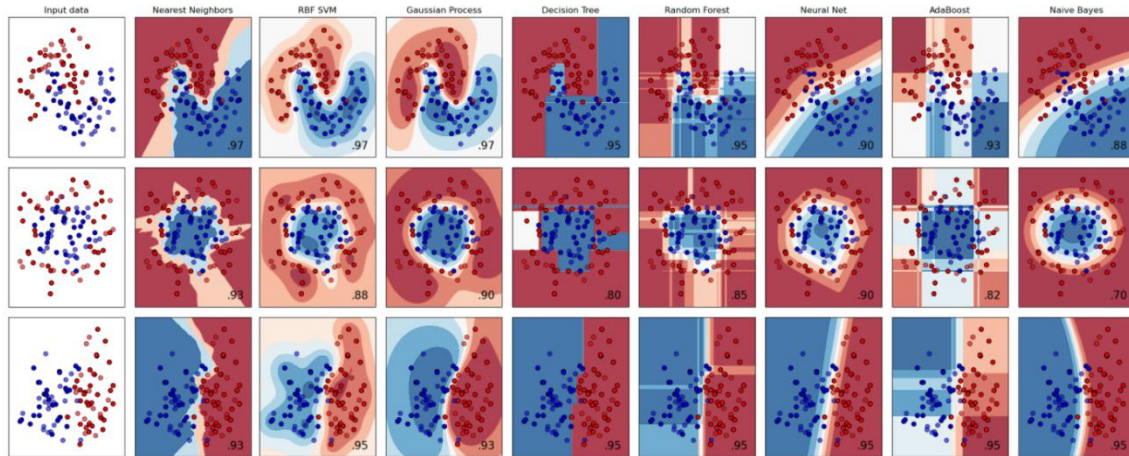


Figure 5.3 - Comparison between some scikit-learn algorithms by [169].

The dataset is expected to behave like the dataset in the third row of figure 4.4, and so at an early stage of this development, RF was used to predict the genotype of the individuals tested, since it was one of the algorithms that showed in [169], an accuracy of 0.95. In addition, there are many other advantages to using this type of algorithm such as:

- It outperforms the decision tree algorithm in terms of accuracy.
- It is a useful tool for dealing with missing data.
- Without hyper-parameter adjustment, it can provide a fair forecast.
- It overcomes the problem of decision tree overfitting.
- At the node's splitting point in every random forest tree, a subset of characteristics is chosen at random [117].

## CHAPTER 6 – EVALUATION AND RESULTS



## 6. Evaluation and Results

### 6.1. Electretinogram processing and Points Detection

After collecting the ERGs it is possible to export an Excel file with the collected data, this file has a common data arrangement among all files, being constituted initially with a header with information about the laboratory, the animal and the signal collection, then it presents the data table but only 128 points per line for each channel (each reading consists of 512 points), which means that to read the complete ERG one must access the first line of each channel, and connect with the continuation of the same signal that happens 16 lines below this one, and so on.

As mentioned before, this point was developed in two environments. In MATLAB the main objective is the analysis of the various channels for the same ERG and therefore, in this point no distinction is made between pathological and non-pathological. After reading the file a visual representation of all the channels is built, represented in figure 6.1, being the channels on the left side (odd numbers) the representation of the right eye tests and vice-versa.

The signal was converted to the time scale knowing that the total reading time is 0.15 seconds, knowing that these are divided into 512 points we can state that each point represents 0.29 milliseconds and therefore that the sampling frequency is 3406.7 Hz.

In all signal processing the first 16 milliseconds of the signal are disregarded since they represent the pre-trigger baseline recording, in other words, it is the time the acquisition system records voltage measurements before the light flash is delivered. The light flash instant is represented in Figure 6.1 by the vertical blue line.

The animal whose ERG is represented in figure 6.1 has the ID 929.6. Checking the Table in Attachment A we know that it is a wild-type male individual that apparently had no reading problems such as outside noise or movement during the test.

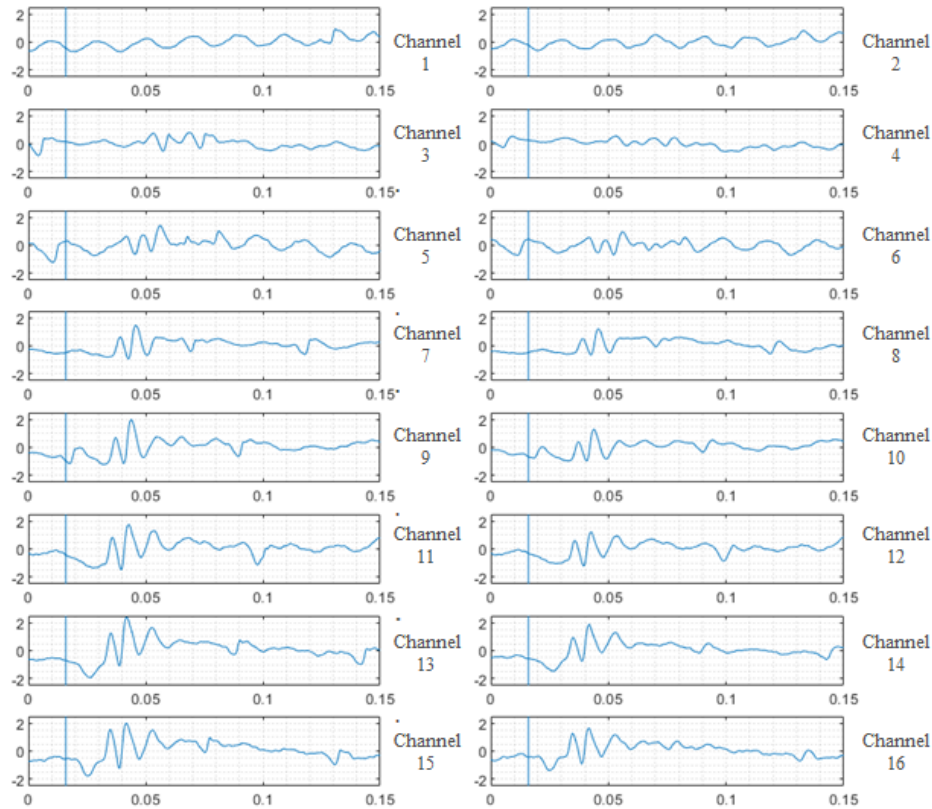


Figure 6.1 - Original ERGs, all the 16 channels recorded with infrared light and 7 other light intensities, for both eyes, in MATLAB. The ERGs shown on the left side correspond to readings taken with the right eye and vice versa. The blue vertical line corresponds to the default, normal reaction latency.

After viewing all channels of the ERG, the signal processing step begins, following the process described previously in Figure 4.3.

A previous study on the estimation of the window in milliseconds (latencies) where the waves appear according to the intensity of the luminous flash was done for the two lowest and the two highest luminous intensities, to restrict the search for the points and therefore, make the reading more correct. The represents the estimations 6.1.

Table 6.1 - Estimation of the window in milliseconds (latencies) where the waves appear according to the intensity of the luminous flash.

Light Intensity	a-wave	b-wave	OP1	OP2	OP3	OP4
1	not detected	(43-86) ms	not detected	not detected	not detected	not detected
2	not detected	(33-87) ms	(19-31) ms	(28-39) ms	(35-48) ms	(44-60) ms
6	(8-19) ms	(28-59) ms	(11-17) ms	(19-26) ms	(26-39) ms	(35-54) ms
7	(9-13) ms	(26-55) ms	(13-16) ms	(19-26) ms	(26-39) ms	(37-53) ms

Figure 6.2 is an example of the processing performed for just one of the channels, channel 5. The same process is repeated for all 16 available.

A-wave a is identified directly in the original signal as the minimum peak of the signal between point 81 and 120 since all peaks corresponding to a-wave happen up to this point. This identification corresponds to the upper left graph in figure 6.2.

After identifying the a-wave, we proceed to apply a fifth-order Butterworth low-pass filter with cutoff frequency at 47.5 Hz. This filter allows discarding all oscillations of frequency higher than the typical maximum frequency of b-wave to facilitate its detection and corresponding amplitude latency. The identification of this wave is depicted in Figure 6.2 in the upper right graph.

Finally, to identify the oscillatory potentials, a fifth-order Butterworth high-pass filter with a 60 Hz cutoff frequency was applied, so as to display only the higher frequency oscillations that correspond to the oscillatory potentials. MATLAB's findpeaks function was used to determine the position of the oscillatory potentials, this function returns a vector with the local maxima (peaks) of the input signal vector, data. A local peak is a data sample that is larger than its two neighboring samples. This identification is shown in the bottom graph of Figure 6.2.

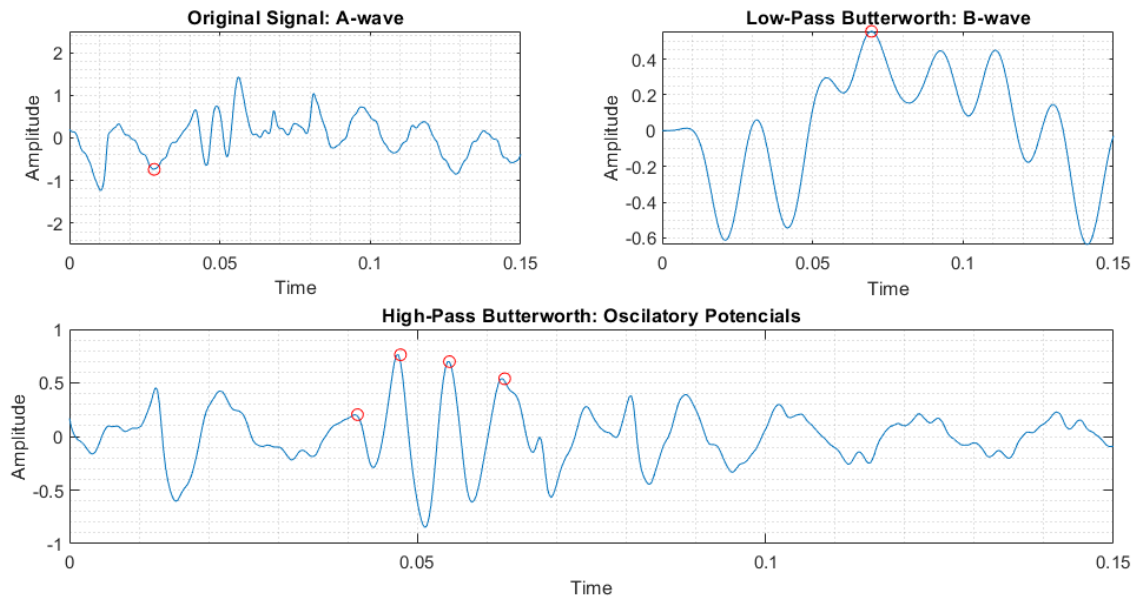


Figure 6.2 - Points detected after filters were applied in MATLAB. The top left graph shows the original signal, and the red dot the detection made of the a-wave. The top right graph is the signal after application of the defined low-pass filter and the red dot represents the detection made of the b-wave in the wave. Finally, in the bottom graph we see the application of the low-pass filter and the detection of oscillatory potentials (red dots).

In the case that the user does not want to see the point detection per channel, a loop was created that performs the same procedure for all channels and returns the collected information.

As mentioned before, the same process was done in Python but this time with the intention of analyzing several files at the same time. However, it is also possible to apply the developed code to a single file and build visualization graphs similar to those obtained in MATLAB, figure 6.3 is the graph representation of the individual 929.6. obtained in Python, equivalent to figure 6.1, where the red vertical line is equivalent to the light flash instant.

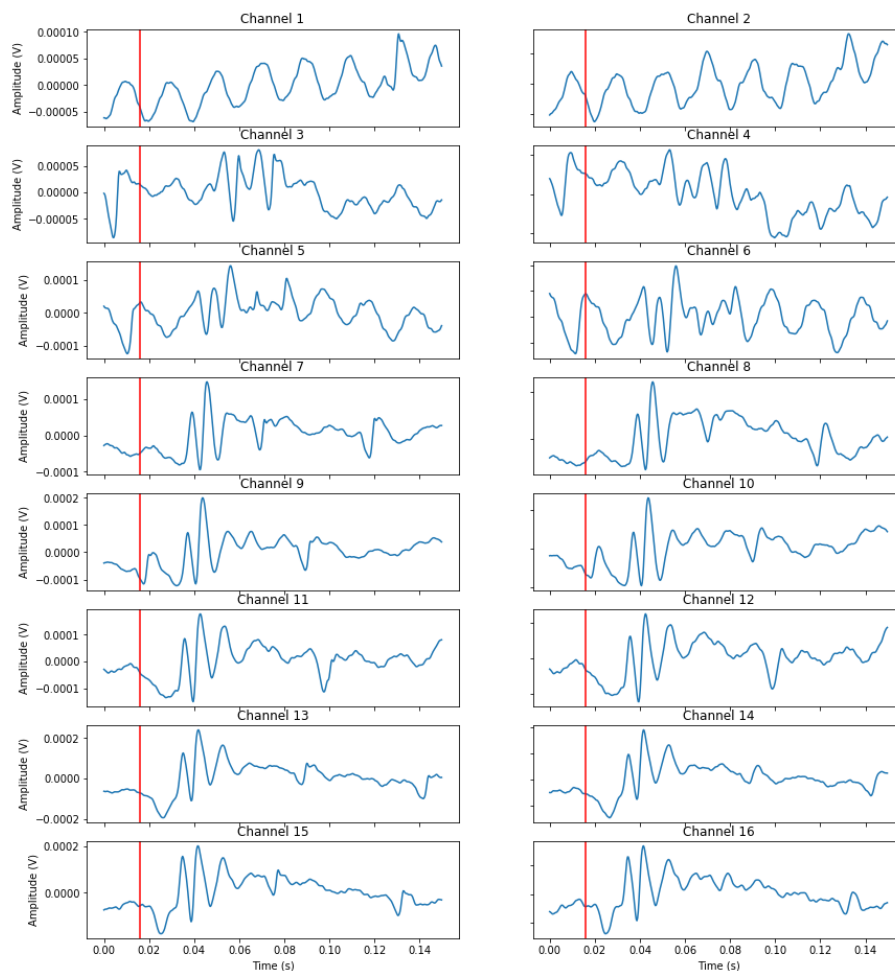


Figure 6.3 - Original ERGs, all the 16 channels recorded with infrared light and 7 other light intensities, for both eyes, in Python. The ERGs shown on the left side correspond to readings taken with the right eye and vice versa. The blue vertical line corresponds to the default, normal reaction latency.

For point detection the process performed was the same as described above and represented in figure 5.3. Figure 6.4 shows the detection performed in Python for channel 15.

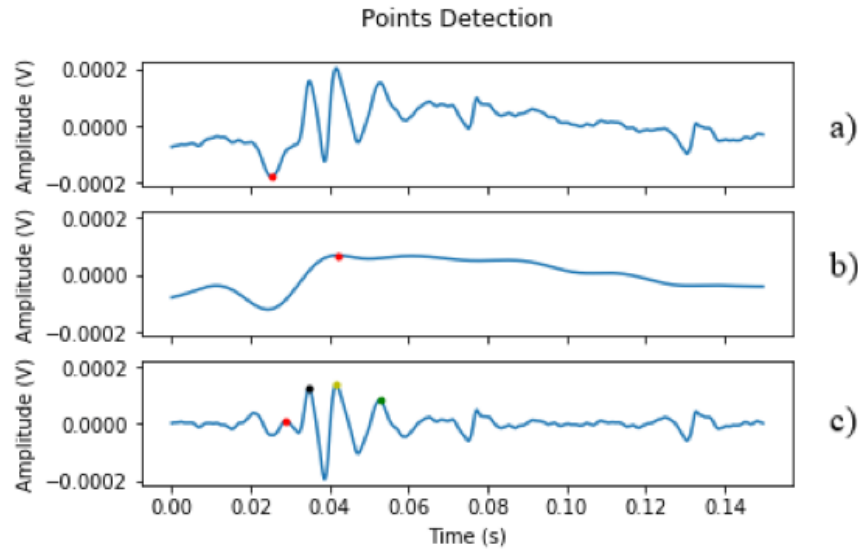


Figure 6.4 - Points detected after filters were applied in Python. a) a-wave detected in the original signal. b) b-wave detected after low-pass filter. c) Oscillatory Potentials detected after high-pass filter.

Since the main objective of this development is to analyze the points detected for several waveforms/animals at the same time, in order to find similarities between them for groups between sexes and genotypes, previous separation of files the entry was made, ie, with the prior information of sex and genotype of the file, and this was stored in a variable of its own.

After collecting the files by lists, dividing them by sex and genotype, the files for each list are read and the points for each file are detected, by means of cycles, which go through all the files on the list in question, performing the same signal processing on each of them, in the end, when the characteristics for the analysis of a respective file are found, they are stored in lists for the respective characteristic, sex and genotype.

The reading of the signals and their graphical representation was done similarly to what was developed in MATLAB. The point detection was done in a slightly different way since it is intended to analyze the features by defining the light intensity applied, unlike what was developed in MATLAB, which was intended to analyze the points of interest for all light intensities applied to an individual. Since the statistical analysis will



be applied only to the two strongest light intensities, we took as normal latency intervals of the ERG components, those shown in Table 6.1. The a-wave is searched for between points 81 and 200 and found by min function. The a-wave amplitude is measured from the baseline to the a-wave trough, where baseline is the average value of the first 3 ms after the reaction latency. The b-wave detection is made after the application of a fifth-order Butterworth low-pass filter with cutoff frequency at 47.5 Hz and found between point 100 and 300 by the max function. The b-wave amplitude is the amplitude from a-wave peak to b-wave peak. Finally, to identify the oscillatory potentials, a fifth-order Butterworth high-pass filter with a 60 Hz cutoff frequency was applied. The OPs were searched between the a-wave peak and point 239 (according to Table 6.1 is the limit range for OP4) and found by find\_peaks function from scipy.signal library. The amplitude of the first oscillatory potential is measure from a-wave peak to the first OP peak, the other 3 OPs are measure from the previous valley to the peak of the OP. Sometimes an ERG can have only 3 OPs, in this case the OP4 columns have ND as Not Detected.

The process was repeated for all the files expect for ID 943.7 that was noticed with extreme noise in Attachment A. The Table with all the points detected to the 59 files analyzed for Channel 15, is presented in Attachment B.

The average values found for each of the characteristics under study are shown in Table 6.2. The reading, processing and detection of points of interest from all files is useful for the statistical analysis of the data performed in the following development point.

Table 6.2 - Mean values obtained for each feature in study for WT and NF1.

	Wild-Type	Neurofibramatosis Type 1
<b>A-wave Amplitude (V)</b>	-0.0001279	-0.0001291
<b>A-wave Latency (s)</b>	0.0272259	0.0276172
<b>B-wave Amplitude (V)</b>	0.0002910	0.0003205
<b>B-wave Latency (s)</b>	0.0625640	0.0642480
<b>OP1 Amplitude (V)</b>	0.0001997	0.0002215
<b>OP1 Latency (s)</b>	0.0310042	0.0309766
<b>OP2 Amplitude (V)</b>	0.0001172	0.0001251
<b>OP2 Latency (s)</b>	0.0386416	0.0384863
<b>OP3 Amplitude (V)</b>	0.0002011	0.0002119
<b>OP3 Latency (s)</b>	0.0478852	0.0474316
<b>OP4 Amplitude (V)</b>	0.0000934	0.0001057

OP4 Latency (s)

0.0602574

0.0589648

## 6.2. Statistical Analysis

A dataset of 59 animals was considered, 29 Wild-type and 30 NF1. The analysis was performed only for the two highest light intensities, considering channel 13 (6th light intensity for the right eye) and channel 15 (7th light intensity for the right eye). At this point only the analysis for channel 15 was presented, based on the data collected in the previous section and represented in the figure in attachment B.

First, to check if there is any visible difference between clusters two Scatter plots were created, one for the a and b waves, Figure 6.5 a) and one for the OPs, Figure 6.5 b).

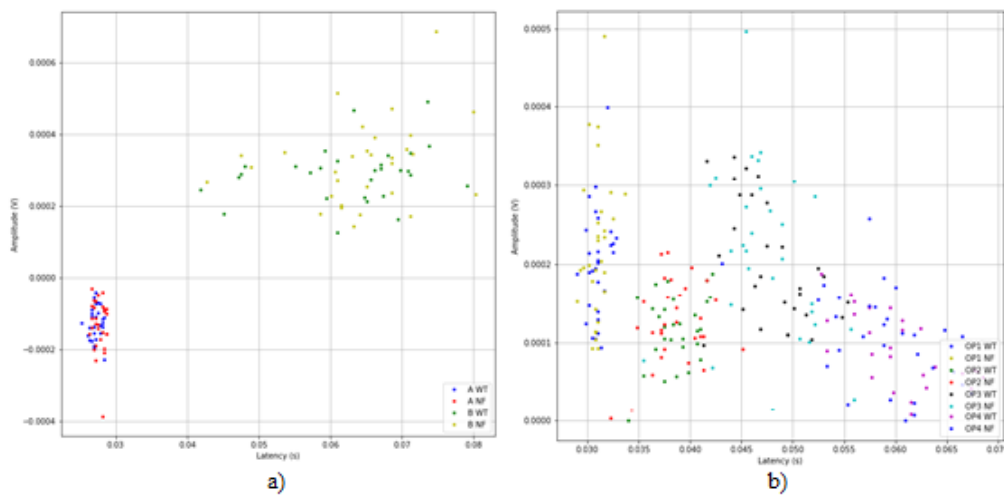


Figure 6.5 - Scatter plot of oscillatory potentials.

Through the analysis of Figures 6.5 and 6.6 we can see that no clear differences between genotypes, with the exception of a-wave, where there seems to be a tendency of greater latency and a greater range of amplitudes for NF1. To check more specifically whether there are significant differences between groups, two t-tests, one to compare genotypes and one to compare sexes, and a two-way ANOVA were performed.

All tests are used to decide whether to accept or reject the null hypothesis. The hypotheses to be considered in this statistical analysis for each trait under study are:

- Null hypothesis: There are no statistically significant differences between groups.

- Alternative hypothesis: There are statistically significant differences between groups and therefore this may be a differentiating characteristic between groups.

If statistically significant differences between groups are found, the characteristics in question can be used in the future as determining factors for the diagnosis of pathology.

### 6.2.1. T-test – Genotype

T-test was performed for the independent variable Genotype with  $\alpha = 0.05$  (95% confidence level). 59 files were considered however one of the ERG did not show 4 OPs but only 3.

Recalling what was presented before in Section 2.6.6.1, the test works by checking the means from two samples to see if they are significantly different from each other. It does this by calculating the standard error in the difference between means.

We can interpret the statistic value in a two-tailed test by comparing it to the positive critical value, as follows:

- If  $|t\text{-statistic}| \leq \text{critical value}$ : Accept null hypothesis.
- If  $|t\text{-statistic}| > \text{critical value}$ : Reject the null hypothesis.

The p-value can then be compared to the significance level ( $\alpha$ ), 0.05, to determine if the null hypothesis can be rejected:

- If  $p > \alpha$ : Accept null hypothesis.
- If  $p \leq \alpha$ : Reject null hypothesis [83].

The library `scipy.stats` was used to perform the t-test to each one of the characteristics. The summary of all the results is presented in Table 6.3.

Table 6.3 - T-test Table for Genotype.

	<b>T-stat</b>	<b>DF</b>	<b>CV</b>	<b>P-value</b>
<b>a(V)</b>	0.0750401	57	1.6720289	0.9404456
<b>a(s)</b>	-1.9807585	57	1.6720289	<b>0.0524512</b>
<b>b(V)</b>	-1.1428225	57	1.6720289	0.2578898
<b>b(s)</b>	-0.7203082	57	1.6720289	0.4742789
<b>OP1(V)</b>	-1.0252876	57	1.6720289	0.3095591
<b>OP1(s)</b>	0.1147859	57	1.6720289	0.9090182
<b>OP2(V)</b>	-0.6175279	57	1.6720289	0.5393459
<b>OP2(s)</b>	0.2440262	57	1.6720289	0.8080868

<b>OP3(V)</b>	-0.4395313	57	1.6720289	0.6619386
<b>OP3(s)</b>	0.4323773	57	1.6720289	0.6670986
<b>OP4(V)</b>	-0.8603927	56	1.6725223	0.3932413
<b>OP4(s)</b>	1.0130848	56	1.6725223	0.3153770

By analyzing Table 6.3 we can see that no p-value is statistically significant ( $<0.05$ ), however the p-value for the latency of the a-wave is very close to being so, it is also observed that no T-stat is statistically significant ( $|t\text{-stat}| > CV$ ). Therefore, it can be concluded that the only characteristic under study that can represent a differentiating parameter between genotypes is the a-wave latency.

### 6.2.2. T-test – Sex

T-test was performed for the independent variable Sex with  $\alpha = 0.05$  (95% confidence level). 59 files were considered, 16 female and 43 male individuals, however one of the ERG did not show 4 OPs but only 3.

To decide whether or not to accept the null hypothesis, in each case, we should compare the results as described above. Figure 6.4 shows the results obtained for each of the characteristics under analysis.

Table 6.4 - T-test Table for Sex.

	<b>T-stat</b>	<b>DF</b>	<b>CV</b>	<b>P-value</b>
<b>a(V)</b>	1.5984970	57	1.6720289	0.1154616
<b>a(s)</b>	-0.2409656	57	1.6720289	0.8104465
<b>b(V)</b>	-1.1652362	57	1.6720289	0.2487767
<b>b(s)</b>	0.5292036	57	1.6720289	0.5987192
<b>OP1(V)</b>	-1.1085502	57	1.6720289	0.2722798
<b>OP1(s)</b>	1.8174021	57	1.6720289	0.0744131
<b>OP2(V)</b>	-1.3137871	57	1.6720289	0.1941812
<b>OP2(s)</b>	2.8436851	57	1.6720289	<b>0.0061813</b>
<b>OP3(V)</b>	-2.5693850	57	1.6720289	<b>0.0128289</b>
<b>OP3(s)</b>	2.8086445	57	1.6720289	<b>0.0068023</b>
<b>OP4(V)</b>	2.5401528	56	1.6725223	<b>0.0138814</b>
<b>OP4(s)</b>	-1.8755496	56	1.6725223	0.0659339

By analyzing Table 6.4 we can see that the p-values that are statistically significant ( $<0.05$ ) are the latency of the second and third OP and the amplitudes of the third and fourth OP. It is also observed that for the same parameters, the T-stat is also statistically significant ( $|t\text{-stat}| > CV$ ), with the addition of the latency of the first and fourth OB. Therefore, it can be concluded that the latencies and amplitudes of some OPs are sex differentiating factors and the null hypothesis should therefore be rejected in these cases.

### 6.2.3. Two-Way ANOVA

Since t-test is not able to evaluate potential interactions between sex and genotype, a two-way ANOVA was performed in order to verify, which may be relevant for the differentiation between samples.

A boxplot was generated to see the distribution of the data by characteristic, showing in Figure 6.6 the graphs for the a- and b-waves, in Figure 6.7 for the two firsts OPs and in Figure 6.8 for the third and fourth OPs. Using the boxplot, we can easily detect the differences between the different types, comparing sex and genotype.

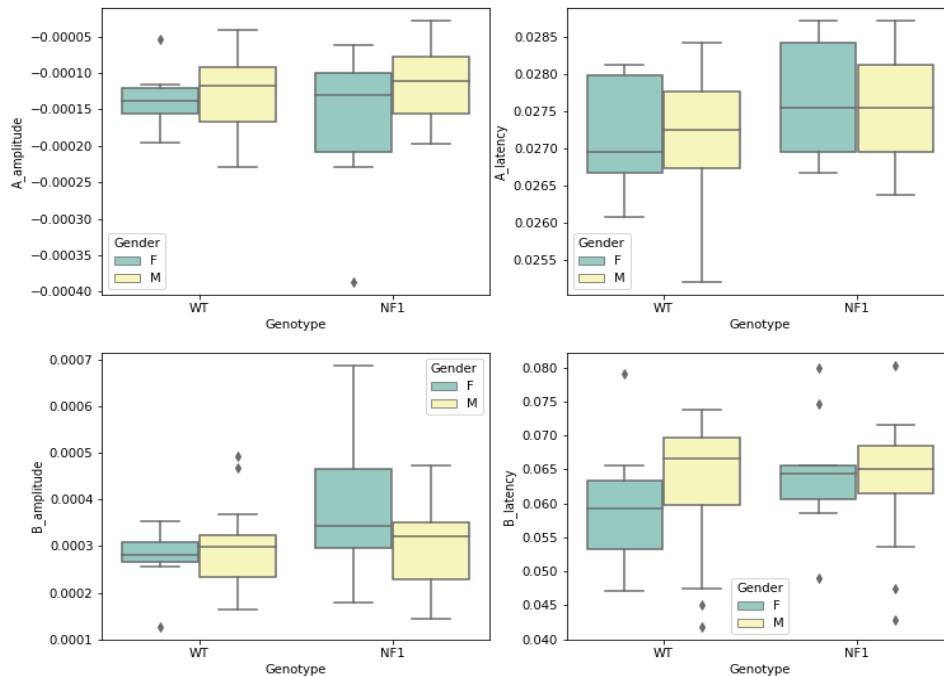


Figure 6.6 - Boxplot of a and b wave, comparing sex and genotype.

By observing the graphs in figure 6.6 we can see that the distributions are different between groups, but the interaction with the most evident differences appears to be in relation to the amplitude of the b-wave in males, since the range of values in this case is much wider in NF1.

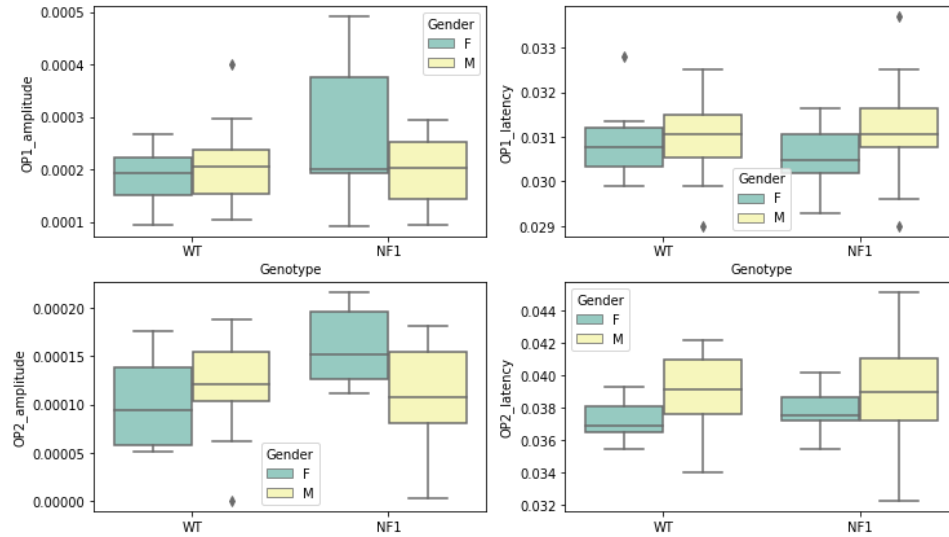


Figure 6.7 - Boxplot of the first and second oscillatory potentials, comparing sex and genotype.

From the graphs in figure 6.7 we can see that the distributions are different between groups, but there are no apparent significant differences, and there is no clear distribution characteristic to point to.

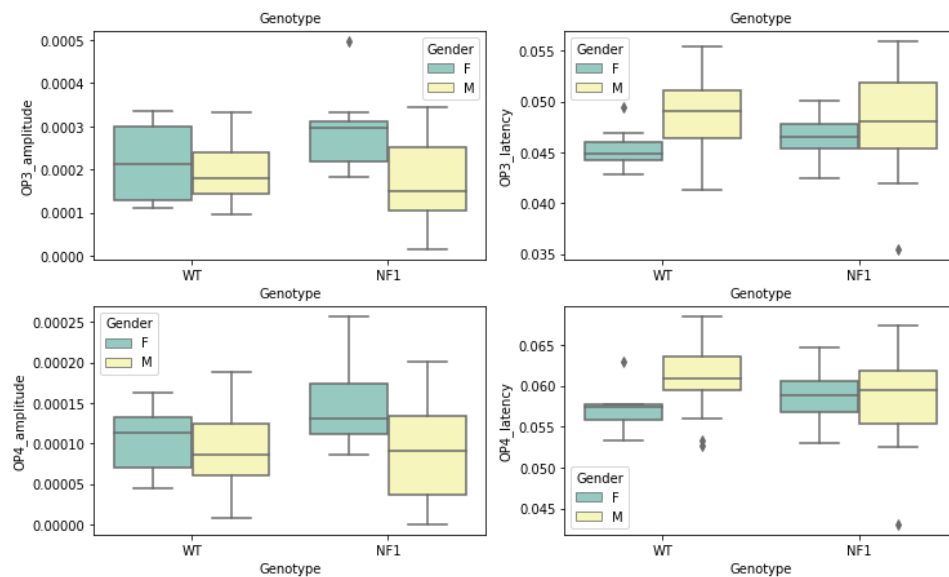


Figure 6.8 - Boxplot of the third and fourth oscillatory potentials, comparing sex and genotype.

Finally, the graphs in Figure 6.8 appear to be a distinguishing factor for some characteristics, with minor differences in the mean value or range.

It is important to point out that visual analysis only provides indicative information that cannot be taken into account to distinguish groups, only to confirm statistical values obtained.

All the functions used to elaborate the ANOVA analysis were imported from `statsmodels.api` and `statsmodels.formula.api` libraries.

Visual analysis and the Shapiro test were used to test the assumptions, for all the characteristics tested. The standardized residuals lie around the 45-degree line, which suggests that the residuals were approximately normally distributed and the distribution does appear approximately normal for the majority of the data. The Shapiro-Wilk test confirmed that there's no normal distribution of residuals.

### 6.2.3.1. A-wave Amplitude

Table 6.5 presents the ANOVA table, where *df* corresponds to the degrees of freedom, *sum\_sq* means sum of squares, *mean\_sq* is the mean of the squares which is the previous value divided by the *df*, *F* is the F-ratio that represents the mean square of the term divided by the residual mean square and *PR(>F)* is the p-value that is inversely proportional to the F-ratio.

Table 6.5 - ANOVA table for the a-wave amplitude.

	<b>df</b>	<b>sum_sq</b>	<b>mean_sq</b>	<b>F</b>	<b>PR(&gt;F)</b>
<b>C(Genotype)</b>	1.0	1.018882e-11	1.018882e-11	0.002912	0.957158
<b>C(Sex)</b>	1.0	1.376032e-08	1.376032e-08	3.933197	<b>0.052344</b>
<b>C(Genotype):C(Sex)</b>	1.0	6.448443e-09	6.448443e-09	1.843199	0.180121
<b>Residual</b>	55.0	1.924179e-07	3.498507e-09	NaN	NaN

As the p-value obtained from ANOVA analysis for genotype, sex and interaction are not statistically significant ( $p < 0.05$ ), it is concluded that genotype type does not significantly affect the production outcome, and sex does not significantly affect the production outcome and also the interaction of genotype and sex does not significantly

affect the production outcome. However, the effect of sex has a p-value close to being significant.

Although the p-values are not significant, the interaction graph (also called profile graph) in figure 6.9 can give some additional information.

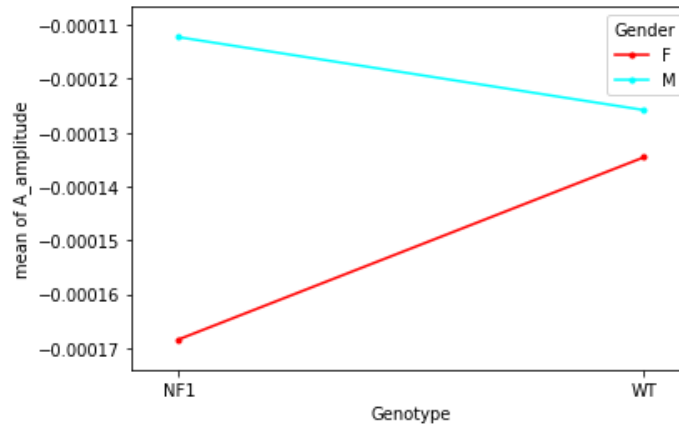


Figure 6.9 - Interaction plot for the a-wave amplitude.

Although in the graph in Figure 6.19, the interaction effect seems significant between genotype and sex because the lines are not parallel (approximately parallel factor lines indicate no interaction - additive model), it is not statistically significant as seen in ANOVA results.

Although the ANOVA table showed no significant interactions, these may exist between specific groups individually, so multiple pairwise comparison (Post-hoc comparison) analysis using Tukey's HSD test was performed, the results of which are shown in Table 6.6.

The comparisons that are relevant and answer the experimental question were performed instead of comparing all to all, since this increases the p value because of the correction. For example, it would not be relevant to compare WT-M with NF1-F (and similar) because it has two variables implied and only ANOVA is able to answer this. Therefore, we performed 4 comparisons in which one variable was kept in order to better understand which groups vary more. It is preformed the comparisons that are relevant and answer the experimental question rather than comparing all to all, since that increases the p value because of the correction. For example, it would not be relevant to compare WT-M with NF1-F (and similar) because it has two variables implied and only ANOVA is



able to answer this. Therefore, we performed 4 comparisons in which one variable was kept in order to better understand which groups vary more.

Table 6.6 - Tukey's table for the a-wave amplitude.

group1	group2	Diff	Lower	Upper	q-value	p-value
(WT, F)	(WT, M)	0.000009	-0.000059	0.000077	0.482499	0.9
(NF1, F)	(NF1, M)	0.000056	-0.000006	0.000118	3.364519	0.093144
(WT, F)	(NF1, F)	0.000034	-0.000045	0.000113	1.602955	0.651943
(WT, M)	(NF1, M)	0.000014	-0.000034	0.000061	1.059602	0.864805

By analyzing the p-values in Table 6.6 from Tukey's test we can confirm that there is no significant interaction.

#### 6.2.3.2. A-wave Latency

For the a-wave latency we performed the same process as described for the a-wave amplitude, starting by analyzing the ANOVA table, Table 6.7, in search of statistically significant p-values.

Table 6.7 - ANOVA table for the a-wave latency.

	df	sum_sq	mean_sq	F	PR(>F)
<b>C(Genotype)</b>	1.0	2.229614e-06	2.229614e-06	3.747270	0.058041
<b>C(Sex)</b>	1.0	8.666840e-09	8.666840e-09	0.014566	0.904376
<b>C(Genotype):C(Sex)</b>	1.0	3.053460e-08	3.053460e-08	0.051319	0.821624
<b>Residual</b>	55.0	3.272484e-05	5.949971e-07	NaN	NaN

Once the p-values obtained from the ANOVA analysis for genotype, sex, and interaction are not statistically significant ( $p < 0.05$ ), it is concluded that genotype as well as sex or the interaction genotype:sex has no significant impact on the output outcome, though the genotype effect has a p-value that is close to being significant, which could mean that this can be a differentiating factor between groups.

Although the p-values do not seem to be significant we should analyze the interaction plot, Figure 6.10.

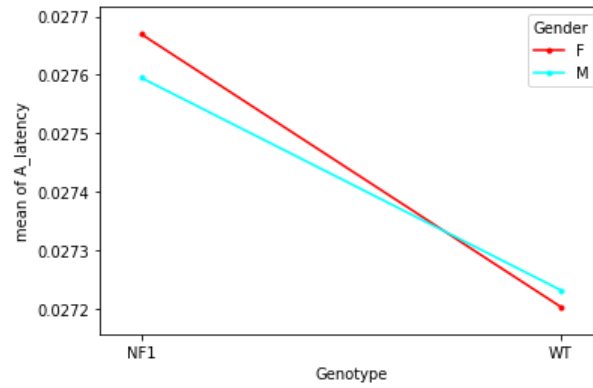


Figure 6.10 - Interaction plot for the a-wave latency.

In the graph in Figure 6.10, it's possible to understand that this is quite different from what happens for the wave amplitude, since in this case the interaction effect is not significant between genotype and sex because the lines are almost parallel. Even so, Tukey's table was generated, Table 6.8, to confirm the results.

Table 6.8 - Tukey's table for the a-wave latency.

group1	group2	Diff	Lower	Upper	q-value	p-value
(WT, F)	(WT, M)	0.000029	-0.000858	0.000915	0.120562	0.900000
(NF1, F)	(NF1, M)	0.000074	-0.000740	0.000889	0.342396	0.900000
(WT, F)	(NF1, F)	0.000465	-0.000565	0.001495	1.691798	0.617139
(WT, M)	(NF1, M)	0.000362	-0.000261	0.000986	2.176004	0.423337

By analyzing the p-values in Table 6.6 from Tukey's test we can confirm that there is no significant interaction.

### 6.2.3.3. B-wave Amplitude

Table 6.9 shows the ANOVA table for the b-wave amplitude.

Table 6.9 - ANOVA table for b-wave amplitude.

	df	sum_sq	mean_sq	F	PR(>F)
<b>C(Genotype)</b>	1.0	1.086186e-08	1.086186e-08	1.168358	0.284456
<b>C(Sex)</b>	1.0	1.845110e-08	1.845110e-08	1.984696	0.164525
<b>C(Genotype):C(Sex)</b>	1.0	3.927857e-08	3.927857e-08	4.225008	0.044593
<b>Residual</b>	55.0	5.113177e-07	9.296685e-09	NaN	NaN

Since the p-value obtained from the ANOVA analysis for genotype and sex are not statistically significant ( $p < 0.05$ ), it is concluded that genotype and sex does not significantly affect the output outcome. However, the interaction of genotype and sex have significantly affected the output outcome since the p-value is smaller than 0.05.

To verify whether there appear to be significant differences between sex and/or genotype, we created the interaction graph of Figure 6.11.

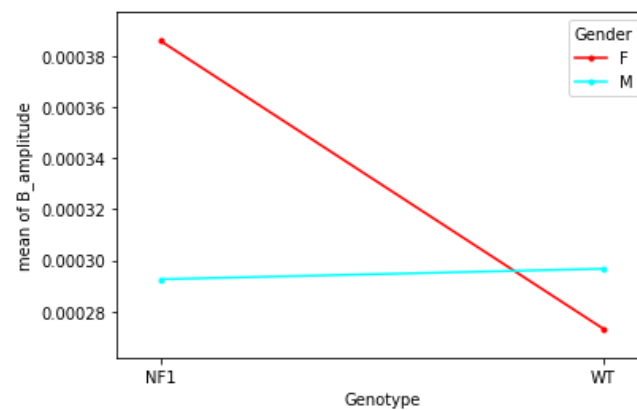


Figure 6.11 - Interaction plot for b-wave amplitude.

In the graph in Figure 6.11, the interaction effect is significant between genotype and sex because the lines are not parallel. It can be seen that for males there are almost no visible differences, but among females the difference is clear, the mean value for the group (NF1, F) is higher than the mean value for the groups (WT, F) and (WT, M).

To confirm the ANOVA table that showed significant interactions, the post-hoc comparison was performed using Tukey's HSD test, the results are shown in Table 6.10.

Table 6.10 - Tukey's table for b-wave amplitude.

group1	group2	Diff	Lower	Upper	q-value	p-value
(WT, F)	(WT, M)	0.000023	-0.000087	0.000134	0.793882	0.900000
(NF1, F)	(NF1, M)	0.000093	-0.000009	0.000195	3.433535	0.083776
(WT, F)	(NF1, F)	0.000113	-0.000016	0.000241	3.278360	0.106398
(WT, M)	(NF1, M)	0.000004	-0.000074	0.000082	0.197716	0.900000

By analysing the p-values in Table 6.10 from Tukey's test it's possible to see that there is no significant interaction. This is contradictory to the ANOVA table, which showed that there were significant differences in the interaction between sex and genotype. Thus, considering that the interaction that was highlighted as relevant in the analysis of the graph in figure 6.11 was between the group (NF1, F) with (WT, F) and (WT, M), if we check the p-values of these interactions relative to the others, we can see that they are indeed the most significant interactions, although the p-value is not statistically significant. The discrepancy between the p-value of the ANOVA table and the Tukey table can be due to outliers that are directly affecting the power of the analysis between gene and genotype.

#### 6.2.3.4. B-wave Latency

For the b-wave latency we performed the same process as described for the b-wave amplitude, starting by analysing the ANOVA table, Table 6.11, in search of statistically significant p-values.

Table 6.11 - ANOVA table for b-wave latency.

	df	sum_sq	mean_sq	F	PR(>F)
<b>C(Genotype)</b>	1.0	0.000046	0.000046	0.566472	0.454874
<b>C(Sex)</b>	1.0	0.000030	0.000030	0.364494	0.548503
<b>C(Genotype):C(Sex)</b>	1.0	0.000040	0.000040	0.492018	0.485986
<b>Residual</b>	55.0	0.004507	0.000082	NaN	NaN

Because the p-values for genotype, sex, and interaction from the ANOVA analysis are not statistically significant ( $p > 0.05$ ), it is concluded that genotype has no effect on the output outcome, sex has no effect on the output outcome, and the interaction of genotype and sex has no effect on the output outcome.

The interaction graph (also known as a profile graph) in Figure 6.12 can provide some extra information, even though the p-values are not significant.

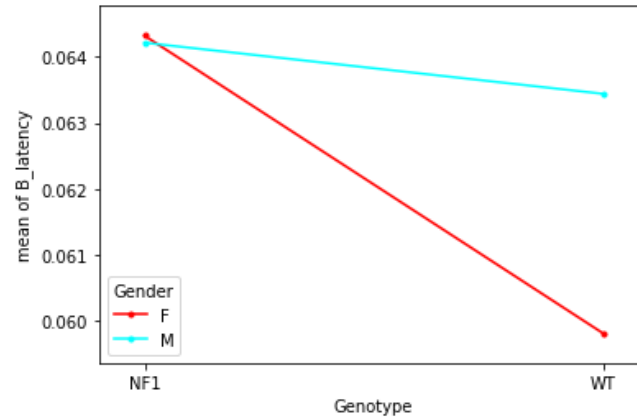


Figure 6.12 - Interaction plot for b-wave latency.

The interaction effect between genotype and sex seems to be apparent since the lines in Figure 6.12 are not parallel. When comparing sex in NF1, males have nearly no noticeable differences, while females have a distinct difference: the mean value for the group (NF1, F) is greater than the mean value for the groups (WT, F).

Tukey's HSD test was used as a post-hoc comparison to confirm the ANOVA table, which revealed significant interactions; the results are presented in Table 6.12.

Table 6.12 - Tukey's table for b-wave latency.

Group 1	Group 2	Diff	Lower	Upper	q-value	p-value
(WT, F)	(WT, M)	0.003634	-0.006774	0.014041	1.308153	0.767432
(NF1, F)	(NF1, M)	0.000107	-0.009448	0.009662	0.041941	0.900000
(WT, F)	(NF1, F)	0.004515	-0.007571	0.016602	1.399824	0.731520
(WT, M)	(NF1, M)	0.000775	-0.006542	0.008092	0.396826	0.900000

We can check that there is no significant interaction by looking at the p-values in Table 6.12 from Tukey's test.

### 6.2.3.5. OP1 Amplitude

Now begins the analysis of OP, this being the section of analysis to the amplitude of the first OP, we present Table 6.13 which contains the ANOVA analysis.

Table 6.13 - ANOVA table for the first oscillatory potential amplitude.

	df	sum_sq	mean_sq	F	PR(>F)
<b>C(Genotype)</b>	1.0	5.853487e-09	5.853487e-09	0.923205	0.340840
<b>C(Sex)</b>	1.0	1.148363e-08	1.148363e-08	1.811184	0.183888
<b>C(Genotype):C(Sex)</b>	1.0	2.437590e-08	2.437590e-08	3.844539	0.054980
<b>Residual</b>	55.0	3.487219e-07	6.340398e-09	NaN	NaN

Since the p-value obtained from the ANOVA analysis for genotype, sex and interaction are not statistically significant ( $p < 0.05$ ), it is concluded that genotype, sex and the interaction of genotype and sex does not significantly affect the output outcome, however the interaction of genotype/sex has a p-value close to being significant.

Although the p-values are not significant, the interaction graph in Figure 6.13 can give some additional information.

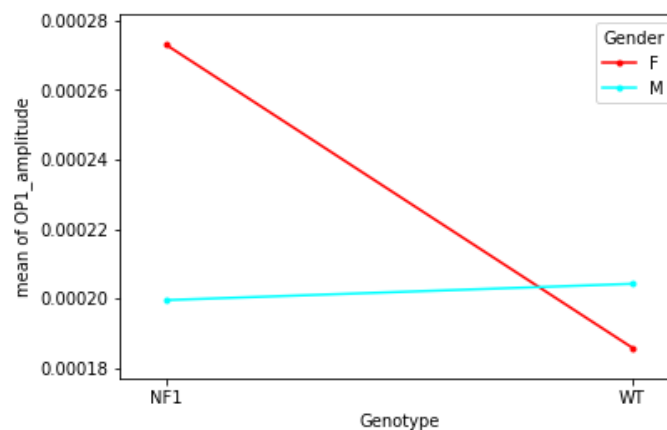


Figure 6.13 - Interaction plot for the first oscillatory potential amplitude.

Because the lines in Figure 6.13 are not parallel, the interaction effect between genotype and sex may be substantial. Males have almost no visible differences, and the same applies when comparing sexes in WT, but females have a clear difference: the mean value for the group (NF1, F) is higher than the mean value for the groups (WT, F) and (WT, M).

The post-hoc comparison was done using Tukey's HSD test to corroborate the ANOVA table that demonstrated significant interactions; the findings are provided in Table 6.14.

Table 6.14 - Tukey's table for the first oscillatory potential amplitude.

group1	group2	Diff	Lower	Upper	q-value	p-value
(WT, F)	(WT, M)	0.000018	-0.000073	0.000110	0.755439	0.900000
(NF1, F)	(NF1, M)	0.000074	-0.000011	0.000158	3.277309	0.106569
(WT, F)	(NF1, F)	0.000087	-0.000019	0.000194	3.075814	0.143049
(WT, M)	(NF1, M)	0.000005	-0.000060	0.000069	0.273597	0.900000

We can validate that there is no significant interaction by looking at the p-values in Table 6.6 from Tukey's test.

#### 6.2.3.6. OP1 Latency

Table 6.15 represents the ANOVA table for the latency of the first OP.

Table 6.15 - ANOVA table for the first oscillatory potential latency.

	df	sum_sq	mean_sq	F	PR(>F)
<b>C(Genotype)</b>	1.0	2.420727e-12	2.420727e-12	0.000003	0.998633
<b>C(Sex)</b>	1.0	2.500964e-06	2.500964e-06	3.060403	0.085800
<b>C(Genotype):C(Sex)</b>	1.0	1.305210e-06	1.305210e-06	1.597172	0.211635
<b>Residual</b>	55.0	4.494605e-05	8.172009e-07	NaN	NaN

Since the p-value obtained from the ANOVA analysis for genotype, sex and interaction are not statistically significant ( $p < 0.05$ ), it is concluded that genotype does not significantly affect the output outcome, sex does not significantly affect the output outcome and the interaction of genotype and sex does not significantly affect the output outcome. Although the p-values are not significant, the interaction graph in Figure 6.14 can give some additional information.

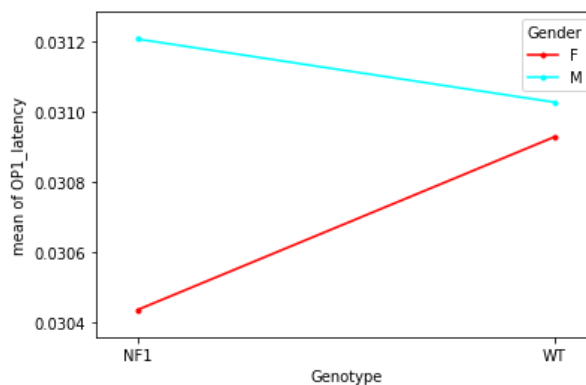


Figure 6.14 - Interaction plot for the first oscillatory potential latency.

In the graph in Figure 6.14, the interaction effect seem significant between genotype and sex because the lines are not parallel since approximately parallel factor lines indicate no interaction. This interaction is also called an ordinal interaction because the lines do not intersect. We can see that the means for females are always lower than the means for males.

Although the ANOVA table showed no significant interactions, these may exist between specific groups individually, so a multi-pair comparison analysis (post-hoc comparison) was performed using Tukey's HSD test, the results of which are shown in Table 6.16.

Table 6.16 - Tukey's table for the first oscillatory potential latency.

group1	group2	Diff	Lower	Upper	q-value	p-value
(WT, F)	(WT, M)	0.000099	-0.000940	0.001138	0.356628	0.9
(NF1, F)	(NF1, M)	0.000772	-0.000182	0.001726	3.031166	0.152443
(WT, F)	(NF1, F)	0.000493	-0.000714	0.001700	1.530197	0.680444
(WT, M)	(NF1, M)	0.000180	-0.000551	0.000911	0.923496	0.9

Tukey's table confirm that there is no relevant interaction for this characteristic.

#### 6.2.3.7. OP2 Amplitude

For the amplitude of the second oscillatory potential, the Table 6.17 presents the ANOVA analysis.

Table 6.17 ANOVA table for the second oscillatory potential amplitude.

	df	sum_sq	mean_sq	F	PR(>F)
<b>C(Genotype)</b>	1.0	6.583688e-10	6.583688e-10	0.311406	0.579083
<b>C(Sex)</b>	1.0	4.310945e-09	4.310945e-09	2.039063	0.158958
<b>C(Genotype):C(Sex)</b>	1.0	1.518078e-08	1.518078e-08	7.180461	0.009704
<b>Residual</b>	55.0	1.162799e-07	2.114180e-09	NaN	NaN

The ANOVA table shows that the relevant interaction is between sex and genotype, presenting a p-value smaller than 0,05.

To check if interactions are evident, the interaction plot shown in Figure 6.15 was created.



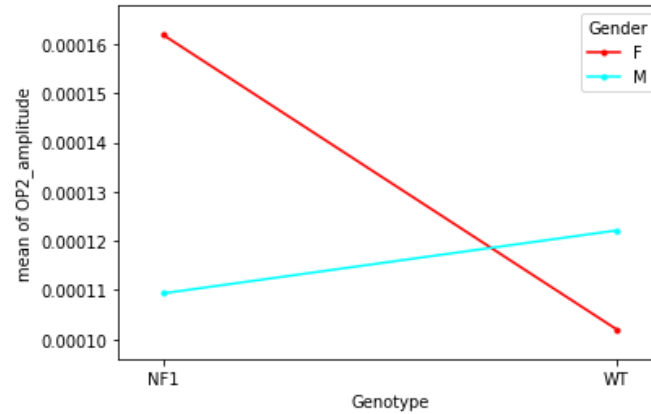


Figure 6.15 - Interaction plot for the second oscillatory potential amplitude.

We can see that for males there are almost no visible differences, but among females the difference is clear, the mean value for the group (NF1, F) is higher than the average of the groups (WT, F).

We know that treatment differences are statistically significant because of ANOVA analysis, but ANOVA does not tell us which treatments are substantially different from one another. To determine the pairs of significant different treatments, we will use Tukey's honestly significantly different (HSD) test to do multiple pairwise comparison (post hoc comparison) analysis for all unplanned comparisons presented in Table 6.18.

Table 6.18 - Tukey's table for the second oscillatory potential amplitude.

group1	group2	Diff	Lower	Upper	q-value	p-value
(WT, F)	(WT, M)	0.000020	-0.000033	0.000073	1.425765	0.721357
(NF1, F)	(NF1, M)	0.000052	0.000004	0.000101	4.050462	0.029307
(WT, F)	(NF1, F)	0.000060	-0.000002	0.000121	3.650524	0.058858
(WT, M)	(NF1, M)	0.000013	-0.000024	0.000050	1.287403	0.775561

By analysing the p-values in Table 6.18 from Tukey's test it is possible to observe that exist significant interaction exists between genders in individuals NF1 and the p-value for the interaction between (WT, F) and (NF1, F) is close to be significant (0,059).

### 6.2.3.8. OP2 Latency

Table 6.19 presents de ANOVA table for the second OP latency.

Table 6.19 - ANOVA table for the second oscillatory potential latency.

	df	sum_sq	mean_sq	F	PR(>F)
<b>C(Genotype)</b>	1.0	6.907996e-08	6.907996e-08	0.012030	0.913060
<b>C(Sex)</b>	1.0	2.536500e-05	2.536500e-05	4.417346	0.040169
<b>C(Genotype):C(Sex)</b>	1.0	1.252463e-06	1.252463e-06	0.218118	0.642323
<b>Residual</b>	55.0	3.158175e-04	5.742136e-06	NaN	NaN

As the p-value obtained from the ANOVA analysis for sex is statistically significant ( $p < 0.05$ ), we conclude that sex significantly affects the production outcome. Since the sex effect is significant, let's view the interaction graph in Figure 6.16 for interaction effects.

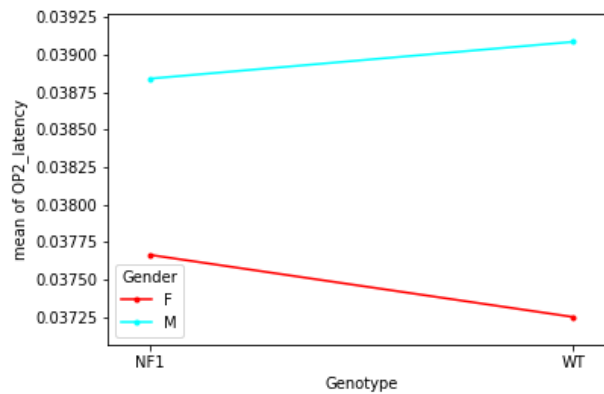


Figure 6.16 - Interaction plot for the second oscillatory potential latency.

In the interaction plot, the interaction effect is not significant between genotype and sex because the lines are close to parallel which indicates that there is no genotype/genotype interaction as the ANOVA indicates. However, the means differ in genotype, as determined by the ANOVA table.

ANOVA analysis shows us that treatment differences are statistically significant, but it doesn't tell us which treatments are significantly different from one another. We will use Tukey's honestly significantly difference (HSD) test, Table 6.20, to undertake multiple pairwise comparison (post hoc comparison) analysis for all unplanned comparisons to discover the pairs of significant different treatments.

Table 6.20 - Tukey's table for the second oscillatory potential latency.

group1	group2	Diff	Lower	Upper	q-value	p-value
(WT, F)	(WT, M)	0.001836	-0.000919	0.004591	2.496707	0.301010
(NF1, F)	(NF1, M)	0.001177	-0.001353	0.003706	1.742809	0.597154
(WT, F)	(NF1, F)	0.000414	-0.002786	0.003613	0.484685	0.900000
(WT, M)	(NF1, M)	0.000245	-0.001691	0.002182	0.474739	0.900000

Tukey's table confirm that the only relevant interaction is between sex.

### 6.2.3.9. OP3 Amplitude

Now, for the amplitude of the third OP, the Table 6.21 presents the ANOVA analysis.

Table 6.21 - ANOVA table for the third oscillatory potential amplitude.

	df	sum_sq	mean_sq	F	PR(>F)
<b>C(Genotype)</b>	1.0	6.412174e-10	6.412174e-10	0.082638	0.774834
<b>C(Sex)</b>	1.0	5.873044e-08	5.873044e-08	7.569023	0.008024
<b>C(Genotype):C(Sex)</b>	1.0	2.564107e-08	2.564107e-08	3.304553	0.074536
<b>Residual</b>	55.0	4.267624e-07	7.759316e-09	NaN	NaN

The ANOVA table suggests that sex is a determining factor for distinguishing an OP3, it also indicates that there may be relevant gene/genotype interactions and therefore one should pay attention to the Tukey table. First, I should look at the interactions plot presented in figure 6.17.

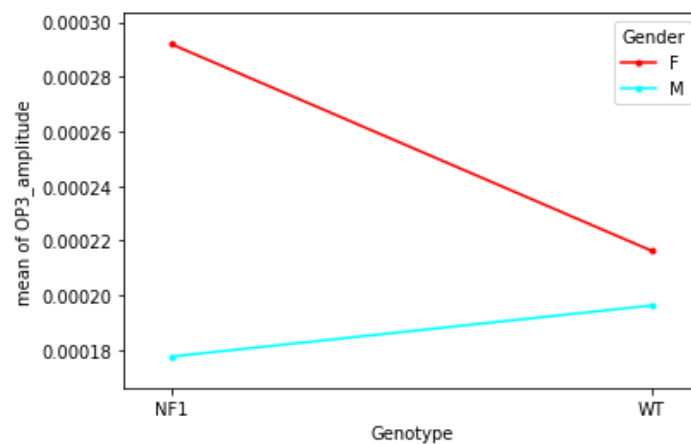


Figure 6.17 - Interaction plot for the third oscillatory potential amplitude.

By the analysis of figure 6.17 we can see that the averages of the WT individuals have a lower range of values than the NF1 individuals. There is a clear difference between sexes, with all female individuals having higher mean values than male individuals, and there are also significant differences between NF1 female individuals and WT individuals. For all comparisons, it's used Tukey's honestly significant difference test, Table 6.22, to conduct post hoc comparison analysis to find the pairs of significant distinct treatments.

Table 6.22 - Tukey's table for the third oscillatory potential amplitude.

<b>group1</b>	<b>group2</b>	<b>Diff</b>	<b>Lower</b>	<b>Upper</b>	<b>q-value</b>	<b>p-value</b>
(WT, F)	(WT, M)	0.000020	-0.000081	0.000121	0.737586	0.900000
(NF1, F)	(NF1, M)	0.000114	0.000021	0.000207	4.604684	0.010158
(WT, F)	(NF1, F)	0.000076	-0.000042	0.000193	2.409764	0.331619
(WT, M)	(NF1, M)	0.000019	-0.000053	0.000090	0.983574	0.894590

By the analysis of Table 6.22, it's confirmed that there's relevant interactions in sex and between (NF1, M) and (NF1, F).

#### 6.2.3.10. OP3 Latency

As previous performed, the ANOVA table is presented (Table 6.23).

Table 6.23 - ANOVA table for the third oscillatory potential latency.

	<b>df</b>	<b>sum_sq</b>	<b>mean_sq</b>	<b>F</b>	<b>PR(&gt;F)</b>
<b>C(Genotype)</b>	1.0	0.000001	0.000001	0.092418	0.762273
<b>C(Sex)</b>	1.0	0.000067	0.000067	4.316029	0.042437
<b>C(Genotype):C(Sex)</b>	1.0	0.000008	0.000008	0.526931	0.470978
<b>Residual</b>	55.0	0.000854	0.000016	NaN	NaN

ANOVA analysis only suggests that sex is a determinant parameter for differentiating groups.

The interaction plot is presented in Figure 6.18.

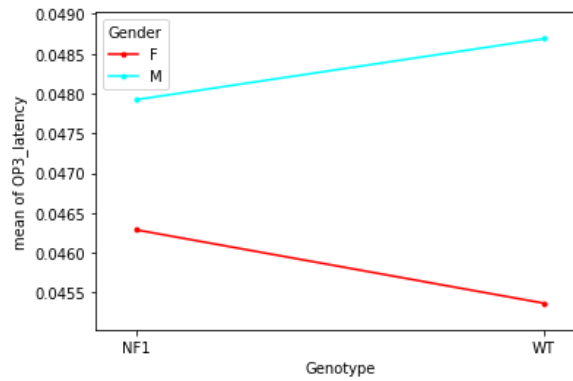


Figure 6.18 - Interaction plot for the third oscillatory potential latency.

In the graph in Figure 6.18, the interaction effect may not be significant between genotype and sex because the lines are almost parallel (approximately parallel factor lines indicate no interaction - additive model). This interaction is also called an ordinal interaction because the lines do not intersect. However, there are clear differences between sexes since the values for female individuals are higher than the values presented for males. These assumptions should be verified by analyzing Table 6.24.

Table 6.24 - Tukey's table for the third oscillatory potential latency.

group1	group2	Diff	Lower	Upper	q-value	p-value
(WT, F)	(WT, M)	0.003318	-0.001214	0.007850	2.743196	0.223819
(NF1, F)	(NF1, M)	0.001632	-0.002528	0.005793	1.469964	0.704040
(WT, F)	(NF1, F)	0.000921	-0.004342	0.006184	0.655548	0.900000
(WT, M)	(NF1, M)	0.000765	-0.002421	0.003951	0.899419	0.900000

By analysing the p-values in Table 6.24 from Tukey's test it's possible to verify that sex is the only relevant parameter.

### 6.2.3.11. OP4 Amplitude

ANOVA analysis is presented in Table 6.25.

Table 6.25 - ANOVA table for the fourth oscillatory potential amplitude.

	df	sum_sq	mean_sq	F	PR(>F)
<b>C(Genotype)</b>	1.0	1.519228e-09	1.519228e-09	0.572236	0.452600
<b>C(Sex)</b>	1.0	1.699741e-08	1.699741e-08	6.402288	0.014290

<b>C(Genotype):C(Sex)</b>	1.0	6.007560e-09	6.007560e-09	2.262822	0.138234
<b>Residual</b>	55.0	1.460193e-07	2.654897e-09	NaN	NaN

As the p-value obtained from the ANOVA analysis for sex is statistically significant ( $p < 0.05$ ), we conclude that sex significantly affects the production outcome. Since the sex effect is significant, let's view the interaction graph in Figure 6.19 for interaction effects.

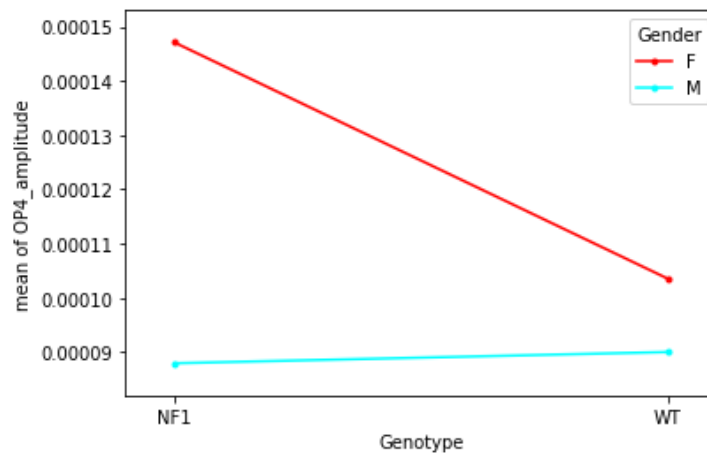


Figure 6.19 - Interaction plot for the fourth oscillatory potential amplitude.

In the interaction plot, the interaction effect is not significant between genotype and sex because the lines are close to parallel which indicates that there is no genotype/genotype interaction which is in accordance with ANOVA result.

ANOVA analysis shows us that treatment differences are statistically significant, but it doesn't tell us which treatments are significantly different from one another. We will use Tukey's honestly significantly difference (HSD) test, Table 6.26, to undertake multiple pairwise comparison (post hoc comparison) analysis for all unplanned comparisons to discover the pairs of significant different treatments.

Table 6.26 - Tukey's table for the fourth oscillatory potential amplitude.

group1	group2	Diff	Lower	Upper	q-value	p-value
(WT, F)	(WT, M)	0.000013	-0.000046	0.000073	0.852965	0.900000
(NF1, F)	(NF1, M)	0.000059	0.000005	0.000114	4.074637	0.028043
(WT, F)	(NF1, F)	0.000044	-0.000025	0.000112	2.373884	0.344988
(WT, M)	(NF1, M)	0.000002	-0.000040	0.000044	0.186529	0.900000

Tukey's table confirm that sex is a relevant interaction but is also shows that the interaction (WT, M)/(NF1, F) is relevant since it has a p-value smaller than 0,05.

### 6.2.3.12. OP4 Latency

To find statistical relevant values for the latency of OP4, the Table 6.27 was generated to perform the ANOVA analysis.

Table 6.27 - ANOVA table for the fourth oscillatory potential latency.

	df	sum_sq	mean_sq	F	PR(>F)
<b>C(Genotype)</b>	1.0	0.000021	0.000021	0.937541	0.337150
<b>C(Sex)</b>	1.0	0.000052	0.000052	2.300833	0.135032
<b>C(Genotype):C(Sex)</b>	1.0	0.000035	0.000035	1.534657	0.220676
<b>Residual</b>	55.0	.001246	0.000023	NaN	NaN

Because the p-values for genotype, sex, and interaction from the ANOVA analysis are not statistically significant ( $p > 0.05$ ), it is concluded that genotype has no effect on the output outcome, sex has no effect on the output outcome, and the interaction of genotype and sex has no effect on the output outcome.

The interaction graph in Figure 6.20 can provide some extra information, even though the p-values are not significant.

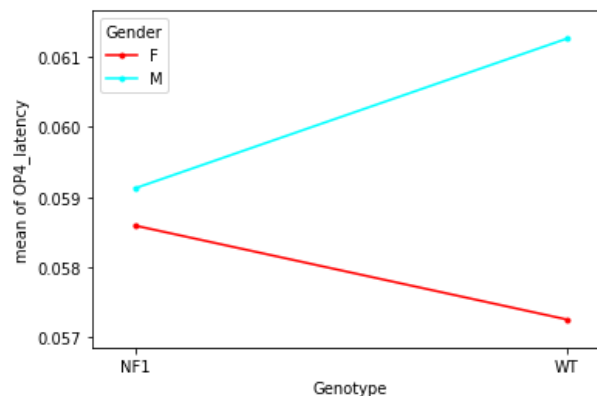


Figure 6.20 - Interaction plot for the fourth oscillatory potential latency.

The interaction effect between genotype and sex seems to be significant since the lines in Figure 6.20 are not parallel. When comparing sex in NF1, males and females have

nearly no noticeable differences, while in WT have a distinct difference: the mean value for the group (WT, M) is greater than the mean value for the groups (WT, F).

Tukey's HSD test was used as a post-hoc comparison to confirm the ANOVA table, which revealed significant interactions; the results are presented in Table 6.28.

Table 6.28 - Tukey's table for the fourth oscillatory potential latency.

group1	group2	Diff	Lower	Upper	q-value	p-value
(WT, F)	(WT, M)	0.004004	-0.001469	0.009477	2.741293	0.224360
(NF1, F)	(NF1, M)	0.000530	-0.004494	0.005555	0.395336	0.900000
(WT, F)	(NF1, F)	0.001339	-0.005016	0.007695	0.789576	0.900000
(WT, M)	(NF1, M)	0.002134	-0.001713	0.005982	2.078693	0.463574

We can check that there is no significant interaction by looking at the p-values in Table 6.28 from Tukey's test.

### 6.3. Classification Algorithm

As mentioned before, the algorithm chosen to study the possibility of determining an individual's genotype by analyzing his ERG was Random Forest (RF), based on the bibliography. To develop it, all the functions used belong to the sklearn library.

An algorithm was created that is intended to be able to make binary decisions and for this the RandomForestClassifier() function was used.

Initially the dataset was prepared, being the points detected at the end of the step presented in section 6.1, the WT genotype was replaced by 0 and the NF1 by 1 to start training the algorithm.

An algorithm study was conducted to study which number of decision trees would have the highest accuracy. The results are shown in figure 6.21.



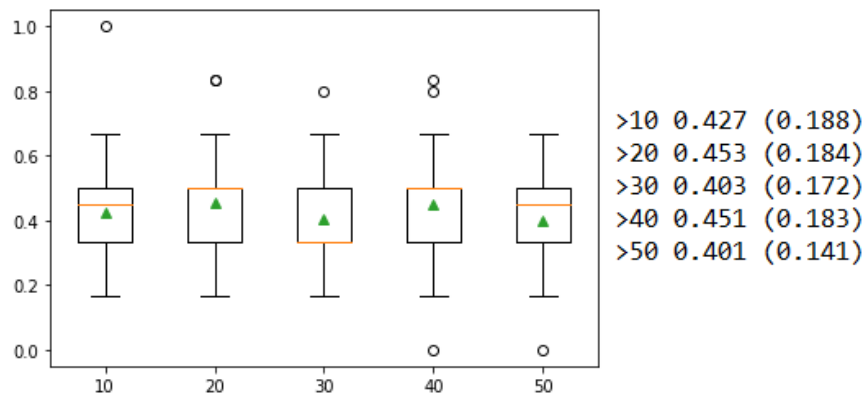


Figure 6.21 - Decision Trees number exploration.

Regarding the results of this analysis, the algorithm was trained with 40 decision trees.

The function `train_test_split` receives the data to train and the size of the test, in this case a test was performed with 60% of the initial dataset and splits data into training and testing sets. To train the algorithm the function `RandomForestClassifier` is then applied that also takes `n_estimators` as a parameter, the number of trees used is 40 trees.

The results obtained are shown in Figure 6.22, where the graph on the left shows the actual genotypes tested and the graph on the right or predicted by the algorithm.

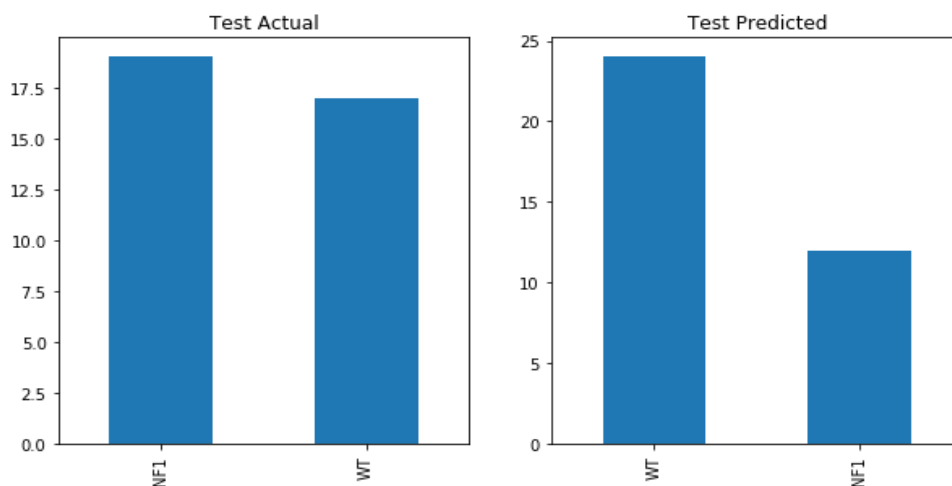


Figure 6.22 - Results of the application of the algorithm.

It can be seen that some results do not correspond with the actual genotype of the test. It remains to be evaluated the algorithm, so the confusion matrix and a classification report were generated, the confusion matrix is represented in Table 6.29.

Table 6.29 - Confusion Matrix of predictions.

	<b>Real Value</b>	
	Positive	Negative
<b>Predicted Value</b>		
Positive	12	5
Negative	12	7

Some results do not correspond with the actual genotype of the test. It remains to evaluate the algorithm, so the confusion matrix and a classification report were generated, the confusion matrix is represented in Table 6.28.

Table 6.30 - Classification Report of the Algorithm.

	<b>Precision</b>	<b>Recall</b>	<b>F1-score</b>	<b>Support</b>
<b>WT</b>	0.50	0.71	0.59	17
<b>NF1</b>	0.58	0.37	0.45	19
<b>Accuracy</b>	-	-	0.53	36
<b>Macro avg</b>	0.54	0.54	0.52	36
<b>Weighted avg</b>	0.54	0.53	0.51	36

The accuracy achieved for by our random forest classifier with 40 trees is 52,78%, being higher, as previously analyzed, in the detection of WT (59%).

The reported averages include macro average (averaging the unweighted mean per label), weighted average (averaging the support-weighted mean per label), and sample average (only for multilabel classification).



## CHAPTER 7 – CONCLUSIONS



## 7. Conclusions

This section presents a general summary of all the work done, exploring the main results obtained and objectives achieved, and referring the main limitations of the work.

### 7.1. Conclusion

One of the initial objectives of this development was to automate and facilitate the reading, processing and detection of points of interest of ERGs, since the currently implemented solution, the RETI-port software, presents problems and difficulties for the user such as: lack of automation in the process of signal collection since after the collection the user needs to manually apply filters for extraction of b-wave and OPs for each light intensity, difficulty in identifying regions and points of interest, as the user needs prior knowledge of the typical ranges of each component to manually select the point of interest. In addition, the method of data analysis is merely numerical through the table of values obtained after the extraction of characteristics, which do not facilitate the visualization, and meaning of the results. As a solution to the problem presented by the analysis interface of the RETI-port program, two programs were developed. While the program developed in MATLAB is mainly intended to analyze all the ERGs collected for the same individual, for the 7 light intensities tested, the program developed in Python, although it also has the function of analyzing a single file, it is intended to analyze several files for the same light intensity. About this development it is possible to conclude that both programs reached the automation objectives and are a good alternative to the current process, being the Python program more complete and robust, since, having the capacity to perform the same processing as the one developed in MATLAB, it presents capabilities such as multiple file analysis, distinction by genotype and sex, more infographic alternatives such as plots, scatter plots, box plots, interaction plots, QQ-plots and histograms. Although MATLAB also has the equivalent functions, these were only developed in Python since the entire development of the statistical analysis and classification algorithm required it.

Besides the signal processing difficulties, it was not known what correlation these data have and whether they differentiate between pathological and non-pathological. Therefore, these data needed a statistical study with several ERGs to define groups of

differentiating characteristics. Two independent t-tests were performed, one to sex and other to genotype, to see if statistical evidence exists that the related population means differ substantially. A two-way ANOVA was employed in this study to see how the two independent factors affected the dependent variables when they were combined.

The results of each test applied to each of the collected signal characteristics for the two tested intensities (2 highest intensities) are summarized in Table 6.1.

Table 7.1 - Differential parameters found in the statistical analyses.

Characteristics	Intensity 6		Intensity 7	
	T-test	Two-way ANOVA	T-test	Two-way ANOVA
<b>a-Wave Amplitude (V)</b>	Sex	Sex	-	≈ Sex
<b>a-Wave Latency (s)</b>	-	-	Genotype	≈ Genotype
<b>b-Wave Amplitude (V)</b>	-	-	-	-
<b>b-Wave Latency (s)</b>	-	-	-	-
<b>OP1 Amplitude (V)</b>	Sex	Sex and Sex:Genotype	-	-
<b>OP1 Latency (s)</b>	-	-	-	-
<b>OP2 Amplitude (V)</b>	Sex	Sex and Sex:Genotype	-	(Sex:Genotype
<b>OP2 Latency (s)</b>	-	-	Sex	Sex
<b>OP3 Amplitude (V)</b>	-	-	Sex	Sex and Sex:Genotype
<b>OP3 Latency (s)</b>	-	-	Sex	Sex
<b>OP4 Amplitude (V)</b>	-	-	Sex	Sex and Sex:Genotype
<b>OP4 Latency (s)</b>	-	-	-	-

It can be concluded from the analysis of table 6.1 that ERG parameters mainly related to inhibitory oscillatory activity reveal subtle sex-dependent alterations. For various oscillatory potentials males and females exhibit opposite changes associated with the transgenic background. The parameter that, in the ERG analysis of the highest light intensity, revealed itself as differentiating between groups by genotype was the a-wave latency, which was noticeably higher in individuals with NF1. Therefore, this characteristic of the signal represents the main effect of NF1 on the visual system circuitry.

Finally, it was intended to test the ability to predict previously reported cognitive deficits by using the ERG features to form a machine learning classifier based on the

significant clusters found for some interactions between individuals, a classifier that is intended to be able to receive a signal and return the likely diagnosis. Based on the literature, a simple RF algorithm was created to predict the genotype of the individuals tested. The algorithm created showed a low accuracy (53%), some results do not correspond with the actual genotype of the test, this is due to the fact that the differences between genotypes are not clear or easily detected. The algorithm can be improved by increasing the number of files available, restricting the reading by sex or even analyzing only male individuals since the sex differences found in ERG data can confuse the algorithm and are a small, unbalanced portion of the dataset.

In conclusion, the thesis objectives were achieved, having automated the process of reading, processing and detecting dots, having found the characteristic of the signal representing the main effect of NF1 on the visual system and having tested the ability to predict previously reported cognitive deficits by using the ERG features.

## **7.2.Future Work**

Regarding the work done, there are some processes that can be improved in the future, such as the statistical analysis that could be performed for all the different light intensities, once there are the latency estimates to restrict the search windows in order to improve the detection of points of interest. The machine learning classificatory algorithm can be improved by increasing the dataset size and better defining the differentiating parameters between genotypes. Other types of algorithms should also be tested in order to find the best possible accuracy.

In order to better support the hypothesis of differences in the visual system in individuals with neurodevelopmental disorders, several other non-invasive imaging techniques and neurophysiology of the visual system should be used in the future to ascertain the diagnostic potential of each technique, these include optical coherence tomography (OCT), optomotor test performance (OMR) and functional magnetic resonance imaging (fMRI). The computer tools developed in this work should be improved in order to perform the analysis of images and performances in the various techniques and correlation between the modalities.





## References

- [1] “Autism spectrum disorders,” *World Health Organization* , 2019. [Online]. Available: <https://www.who.int/news-room/fact-sheets/detail/autism-spectrum-disorders>. [Accessed: 30-Mar-2021].
- [2] American Psychiatric Association, *Diagnostic and Statistical Manual of Mental Disorders*. American Psychiatric Association, 2013.
- [3] E. M. Guimarães-Souza, C. Joselevitch, L. R. G. Britto, and S. Chiavegatto, “Retinal alterations in a pre-clinical model of an autism spectrum disorder,” *Mol. Autism*, vol. 10, no. 1, Apr. 2019.
- [4] D. Dierker *et al.*, “Resting-state Functional Magnetic Resonance Imaging in Presurgical Functional Mapping: Sensorimotor Localization,” *Neuroimaging Clinics of North America*, vol. 27, no. 4. W.B. Saunders, pp. 621–633, 01-Nov-2017.
- [5] “Human Eye Details | Human Eye structure and their Details Function.” [Online]. Available: <https://www.atoznews24.com/human-eye-structure-and-their-details/>. [Accessed: 30-Mar-2021].
- [6] “The human eye: structure and function,” *Choice Rev. Online*, vol. 37, no. 06, pp. 37-3340-37–3340, Feb. 2000.
- [7] H. Alipour, H. Namazi, H. Azarnoush, and S. Jafari, “Complexity-based analysis of the relation between moving visual stimuli and human eye movement,” *Fractals*, vol. 27, no. 3, May 2019.
- [8] G. A. Lutty and D. S. McLeod, “Development of the hyaloid, choroidal and retinal vasculatures in the fetal human eye,” *Progress in Retinal and Eye Research*, vol. 62. Elsevier Ltd, pp. 58–76, 01-Jan-2018.
- [9] S. Sato, R. Frederiksen, M. C. Cornwall, and V. J. Kefalov, “The retina visual cycle is driven by cis retinol oxidation in the outer segments of cones,” *Vis. Neurosci.*, vol. 34, 2017.
- [10] J. Lavoie, M. Maziade, and M. Hébert, “The brain through the retina: The flash electroretinogram as a tool to investigate psychiatric disorders,” *Progress in Neuro-Psychopharmacology and Biological Psychiatry*, vol. 48. Prog Neuropsychopharmacol Biol Psychiatry, pp. 129–134, 03-Jan-2014.

- [11] H. Wassle and B. B. Boycott, "Functional architecture of the mammalian retina," *Physiological Reviews*, vol. 71, no. 2. *Physiol Rev*, pp. 447–480, 1991.
- [12] J. Chen, L. Mi, C. P. Chen, H. Liu, J. Jiang, and W. Zhang, "Design of foveated contact lens display for augmented reality," *Opt. Express*, vol. 27, no. 26, 2019.
- [13] J. Gonçalves *et al.*, "Testing the excitation/inhibition imbalance hypothesis in a mouse model of the autism spectrum disorder: In vivo neurospectroscopy and molecular evidence for regional phenotypes," *Mol. Autism*, vol. 8, no. 1, Sep. 2017.
- [14] J. Y. An *et al.*, "Genome-wide de novo risk score implicates promoter variation in autism spectrum disorder," *Science (80-. )*, vol. 362, no. 6420, p. 19, Dec. 2018.
- [15] J. Doherty, M. Cooper, and A. Thapar, "Advances in our understanding of the genetics of childhood neurodevelopmental disorders," *Evidence-Based Mental Health*, vol. 21, no. 4. BMJ Publishing Group, pp. 171–172, 01-Nov-2018.
- [16] J. Grove *et al.*, "Identification of common genetic risk variants for autism spectrum disorder," *Nat. Genet.*, vol. 51, no. 3, pp. 431–444, Mar. 2019.
- [17] M. D. Thyne, H. M. Bednarz, A. J. Herringshaw, E. B. Sartin, and R. K. Kana, "The impact of atypical sensory processing on social impairments in autism spectrum disorder," *Developmental Cognitive Neuroscience*, vol. 29. Elsevier Ltd, pp. 151–167, 01-Jan-2018.
- [18] S. H. Baum, R. A. Stevenson, and M. T. Wallace, "Behavioral, perceptual, and neural alterations in sensory and multisensory function in autism spectrum disorder," *Progress in Neurobiology*, vol. 134. Elsevier Ltd, pp. 140–160, 01-Nov-2015.
- [19] C. E. Robertson and S. Baron-Cohen, "Sensory perception in autism," *Nature Reviews Neuroscience*, vol. 18, no. 11. Nature Publishing Group, pp. 671–684, 18-Oct-2017.
- [20] N. Cheng *et al.*, "Atypical visual processing in a mouse model of autism," *Sci. Rep.*, vol. 10, no. 1, pp. 1–15, 2020.
- [21] P. A. Constable *et al.*, "Light-Adapted Electroretinogram Differences in Autism Spectrum Disorder," *J. Autism Dev. Disord.*, vol. 50, no. 8, pp. 2874–2885, 2020.
- [22] F. D'Angelo *et al.*, "The molecular landscape of glioma in patients with

- Neurofibromatosis 1,” *Nat. Med.*, vol. 25, no. 1, pp. 176–187, Jan. 2019.
- [23] J. Campian and D. H. Gutmann, “CNS tumors in neurofibromatosis,” *Journal of Clinical Oncology*, vol. 35, no. 21. American Society of Clinical Oncology, pp. 2378–2385, 20-Jul-2017.
- [24] K. I. Ly and J. O. Blakeley, “The Diagnosis and Management of Neurofibromatosis Type 1,” *Medical Clinics of North America*, vol. 103, no. 6. W.B. Saunders, pp. 1035–1054, 01-Nov-2019.
- [25] D. H. Gutmann, R. E. Ferner, R. H. Listernick, B. R. Korf, P. L. Wolters, and K. J. Johnson, “Neurofibromatosis type 1,” *Nat. Rev. Dis. Prim.*, vol. 3, no. 1, pp. 1–17, Feb. 2017.
- [26] M. Bergoug, M. Doudeau, F. Godin, C. Mosrin, B. Vallée, and H. Bénédicti, “Neurofibromin Structure, Functions and Regulation,” *Cells*, vol. 9, no. 11. NLM (Medline), 27-Oct-2020.
- [27] K. P. Boyd, B. R. Korf, and A. Theos, “Neurofibromatosis type 1,” *Journal of the American Academy of Dermatology*, vol. 61, no. 1. NIH Public Access, pp. 1–14, Jul-2009.
- [28] K. North, “Neurofibromatosis type 1,” *Am. J. Med. Genet. - Semin. Med. Genet.*, vol. 97, no. 2, pp. 119–127, 2000.
- [29] “Neurofibromatosis 1,” *NORD (National Organization for Rare Disorders)*, 2017. [Online]. Available: <https://rarediseases.org/rare-diseases/neurofibromatosis-type-1-nf1/>. [Accessed: 29-Mar-2021].
- [30] L. Mottron, M. Dawson, I. Soulières, B. Hubert, and J. Burack, “Enhanced perceptual functioning in autism: An update, and eight principles of autistic perception,” *Journal of Autism and Developmental Disorders*, vol. 36, no. 1. J Autism Dev Disord, pp. 27–43, Jan-2006.
- [31] D. R. Simmons, A. E. Robertson, L. S. McKay, E. Toal, P. McAleer, and F. E. Pollick, “Vision in autism spectrum disorders,” *Vision Research*, vol. 49, no. 22. Pergamon, pp. 2705–2739, 10-Nov-2009.
- [32] J.-A. Little, “Vision in children with autism spectrum disorder: a critical review,” *Clin. Exp. Optom.*, vol. 101, no. 4, pp. 504–513, Jul. 2018.

- [33] M. Wrzesińska, J. Kapias, K. Nowakowska-Domagala, and J. Kocur, “Visual impairment and traits of autism in children,” *Psychiatr. Pol.*, vol. 51, no. 2, pp. 349–358, 2017.
- [34] D. Zhang *et al.*, “Altered visual cortical processing in a mouse model of MECP2 duplication syndrome,” *Sci. Rep.*, vol. 7, no. 1, pp. 1–14, Dec. 2017.
- [35] X. Zhang *et al.*, “Retinal defects in mice lacking the autism-associated gene Engrailed-2,” *Neuroscience*, vol. 408, pp. 177–190, Jun. 2019.
- [36] L. Kéïta, J. Guy, C. Berthiaume, L. Mottron, and A. Bertone, “An early origin for detailed perception in Autism Spectrum Disorder: Biased sensitivity for high-spatial frequency information,” *Sci. Rep.*, vol. 4, no. 1, pp. 1–6, Jul. 2014.
- [37] C. Deruelle, C. Rondan, B. Gepner, and C. Tardif, “Spatial frequency and face processing in children with autism and Asperger syndrome,” *J. Autism Dev. Disord.*, vol. 34, no. 2, pp. 199–210, Apr. 2004.
- [38] T. Yamasaki *et al.*, “Enhanced Fine-Form Perception Does Not Contribute to Gestalt Face Perception in Autism Spectrum Disorder,” *PLoS One*, vol. 12, no. 2, p. e0170239, Feb. 2017.
- [39] L. Kéïta, L. Mottron, and A. Bertone, “Far visual acuity is unremarkable in autism: Do we need to focus on crowding?,” *Autism Res.*, vol. 3, no. 6, pp. 333–341, Dec. 2010.
- [40] M. A. Albrecht *et al.*, “Brief report: Visual acuity in children with autism spectrum disorders,” *J. Autism Dev. Disord.*, vol. 44, no. 9, pp. 2369–2374, Mar. 2014.
- [41] C. E. Robertson, D. J. Kravitz, J. Freyberg, S. Baron-Cohen, and C. I. Baker, “Tunnel vision: Sharper gradient of spatial attention in autism,” *J. Neurosci.*, vol. 33, no. 16, pp. 6776–6781, Apr. 2013.
- [42] H. C. Koh, E. Milne, and K. Dobkins, “Spatial contrast sensitivity in adolescents with autism spectrum disorders,” *J. Autism Dev. Disord.*, vol. 40, no. 8, pp. 978–987, Aug. 2010.
- [43] L. T. van Elst, M. Bach, J. Blessing, A. Riedel, and E. Bubl, “Normal visual acuity and electrophysiological contrast gain in adults with high-functioning autism spectrum disorder,” *Front. Hum. Neurosci.*, vol. 9, no. AUGUST, p. 460, Aug. 2015.

- [44] E. Courchesne, "Brainstem, cerebellar and limbic neuroanatomical abnormalities in autism," *Curr. Opin. Neurobiol.*, vol. 7, no. 2, pp. 269–278, 1997.
- [45] M. Kaplan, S. M. Edelson, and J. A. L. Seip, "Behavioral changes in autistic individuals as a result of wearing ambient transitional prism lenses," *Child Psychiatry Hum. Dev.*, vol. 29, no. 1, pp. 65–76, 1998.
- [46] J. T. Chok, D. D. Reed, A. Kennedy, and F. L. Bird, "A Single-Case Experimental Analysis of the Effects of Ambient Prism Lenses for an Adolescent With Developmental Disabilities," *Behav. Anal. Pract.*, vol. 3, no. 2, pp. 42–51, Dec. 2010.
- [47] B. Abdolrahimzadeh, D. C. Piraino, G. Albanese, F. Cruciani, and S. Rahimi, "Clinical Ophthalmology Dovepress Neurofibromatosis: an update of ophthalmic characteristics and applications of optical coherence tomography," 2016.
- [48] H. AC and G. DH, "Neurofibromatosis type 1: a multidisciplinary approach to care," *Lancet. Neurol.*, vol. 13, no. 8, pp. 834–843, 2014.
- [49] S. M. Recupero *et al.*, "Lisch nodules in neurofibromatosis type 1 : Relationship to age and cutaneous neurofibromas," *Ann. Ophthalmol. Glaucoma*, vol. 28, no. 3, 1996.
- [50] M. J, C. IA, and B. TM, "Glaucoma and globe enlargement associated with neurofibromatosis type 1," *Ophthalmology*, vol. 116, no. 9, pp. 1725–1730, Sep. 2009.
- [51] A. S *et al.*, "Morphologic and vasculature features of the choroid and associated choroid-retinal thickness alterations in neurofibromatosis type 1," *Br. J. Ophthalmol.*, vol. 99, no. 6, pp. 789–793, Jun. 2015.
- [52] P. Topcu-Yilmaz, B. Kasim, and H. Kiratli, "Investigation of retinal nerve fiber layer thickness in patients with neurofibromatosis-1," *Jpn. J. Ophthalmol.*, vol. 58, no. 2, pp. 172–176, 2014.
- [53] D. L. McCulloch *et al.*, "ISCEV Standard for full-field clinical electroretinography (2015 update)," *Doc. Ophthalmol.*, vol. 130, no. 1, Jan. 2015.
- [54] A. G. Robson *et al.*, "ISCEV guide to visual electrodiagnostic procedures," *Doc. Ophthalmol.*, vol. 136, no. 1, Feb. 2018.

- [55] H. E. A. Bicas, “Electro-oculography in the investigation of oculomotor imbalance-I basic aspects,” *Vision Res.*, vol. 12, no. 5, pp. 993–1010, 1972.
- [56] G. B. Arden, A. Barrada, and J. H. Kelsey, “New clinical test of retinal function based upon the standing potential of the eye,” *Br. J. Ophthalmol.*, vol. 46, no. 8, pp. 449–467, 1962.
- [57] M. Yu, D. Creel, and A. Iannaccone, *Handbook of clinical electrophysiology of vision*. 2019.
- [58] R. F. Miller and J. E. Dowling, “Intracellular responses of the Müller (glial) cells of mudpuppy retina: their relation to b-wave of the electroretinogram,” *J. Neurophysiol.*, vol. 33, no. 3, pp. 323–341, 1970.
- [59] T. E. Ogden and C. J. Bassi, “New Methods in Clinical Electrophysiology,” in *New Methods of Sensory Visual Testing*, Springer New York, 1989, pp. 68–93.
- [60] M. Yu and N. S. Peachey, “Use of direct current electroretinography for analysis of retinal pigment epithelium function in mouse models,” in *Methods in Molecular Biology*, vol. 1753, Humana Press Inc., 2018, pp. 103–113.
- [61] S. Ueno, M. Kondo, M. Ueno, K. Miyata, H. Terasaki, and Y. Miyake, “Contribution of retinal neurons to d-wave of primate photopic electroretinograms,” *Vision Res.*, vol. 46, no. 5, pp. 658–664, Mar. 2006.
- [62] F. Naarendorp and G. E. Williams, “The d-wave of the rod electroretinogram of rat originates in the cone pathway,” *Vis. Neurosci.*, vol. 16, no. 1, pp. 91–105, Jan. 1999.
- [63] L. Wachtmeister, “Oscillatory potentials in the retina: What do they reveal,” *Prog. Retin. Eye Res.*, vol. 17, no. 4, pp. 485–521, Oct. 1998.
- [64] M. Nagaya *et al.*, “Pikachurin protein required for increase of cone electroretinogram B-wave during light adaptation,” *PLoS One*, vol. 10, no. 6, Jun. 2015.
- [65] M.-C. Blum, B. Solf, A. Hunold, and S. Klee, “Effects of Ocular Direct Current Stimulation on Full Field Electroretinogram,” *Front. Neurosci.*, vol. 15, p. 49, Feb. 2021.
- [66] D. L. McCulloch *et al.*, “ISCEV Standard for full-field clinical electroretinography

- (2015 update),” *Doc. Ophthalmol.*, vol. 130, no. 1, Jan. 2015.
- [67] K. Stingl *et al.*, “Full-field electroretinography, visual acuity and visual fields in Usher syndrome: a multicentre European study,” *Doc. Ophthalmol.*, vol. 139, no. 2, pp. 151–160, Oct. 2019.
  - [68] D. L. McCulloch *et al.*, “ISCEV extended protocol for the stimulus–response series for light-adapted full-field ERG,” *Doc. Ophthalmol.*, vol. 138, no. 3, pp. 205–215, Mar. 2019.
  - [69] J. C. Park, H. E. Moss, and J. J. McAnany, “Electroretinography in idiopathic intracranial hypertension: comparison of the pattern ERG and the photopic negative response,” *Doc. Ophthalmol.*, vol. 136, no. 1, pp. 45–55, Feb. 2018.
  - [70] D. Vatcher *et al.*, “Revealing a retinal facilitatory effect with the multifocal ERG,” *Doc. Ophthalmol.*, vol. 138, no. 2, pp. 117–124, Apr. 2019.
  - [71] M. G. Nittmann, A. J. Aher, J. Kremers, and R. Tzekov, “Relationship between stimulus size and different components of the electroretinogram (ERG) elicited by flashed stimuli,” *Doc. Ophthalmol.*, vol. 142, no. 2, pp. 213–231, Apr. 2020.
  - [72] G. Benchorin, M. Calton, M. Beaulieu, and D. Vollrath, “Assessment of Murine Retinal Function by Electroretinography,” *BIO-PROTOCOL*, vol. 7, no. 7, 2017.
  - [73] L. J. Frishman, “Electroretinography,” *Curated Ref. Collect. Neurosci. Biobehav. Psychol.*, no. March 2016, pp. 1–5, 2016.
  - [74] A. K. Abbas and R. Bassam, “Phonocardiography Signal Processing,” *Synth. Lect. Biomed. Eng.*, vol. 31, pp. 1–189, Apr. 2009.
  - [75] A. Rizal, A. A. Adz-dzikri, M. Arik, and G. Fauzi, “Classification of Normal and Abnormal Heart Sound using Continuous Wavelet Transform and ResNet-50,” *Technol. Reports Kansai Univ.*, vol. 62, no. 05, pp. 2595–2601, 2020.
  - [76] F. Zangeneh-Nejad and R. Fleury, “Topological analog signal processing,” *Nat. Commun. 2019 101*, vol. 10, no. 1, pp. 1–10, May 2019.
  - [77] F. Serbet, T. Kaya, and M. T. Ozdemir, “Design of digital IIR filter using Particle Swarm Optimization,” *2017 40th Int. Conv. Inf. Commun. Technol. Electron. Microelectron. MIPRO 2017 - Proc.*, pp. 202–204, Jul. 2017.
  - [78] L. H. Cherif, M. Mostafi, and S. M. Debbal, “Digitals Filters in Heart Sound



- Analysis,” *Int. J. Clin. Med. Res. Int. J. Clin. Med. Res.*, vol. 1, no. 3, pp. 97–108, 2014.
- [79] “Statistical Analysis: Definition, Examples - Statistics How To.” [Online]. Available: <https://www.statisticshowto.com/statistical-analysis/>. [Accessed: 25-Oct-2021].
- [80] D. A. Mata and D. A. Milner, “Statistical Methods in Experimental Pathology: A Review and Primer,” *Am. J. Pathol.*, vol. 191, no. 5, pp. 784–794, 2021.
- [81] F. C, W. H, L. N, and T. XM, “Log transformation: application and interpretation in biomedical research,” *Stat. Med.*, vol. 32, no. 2, pp. 230–239, Jan. 2013.
- [82] M. P, P. CM, S. U, G. A, S. C, and K. A, “Descriptive statistics and normality tests for statistical data,” *Ann. Card. Anaesth.*, vol. 22, no. 1, pp. 67–72, Jan. 2019.
- [83] P. Mishra, C. M. Pandey, U. Singh, A. Gupta, C. Sahu, and A. Keshri, “Descriptive Statistics and Normality Tests for Statistical Data,” *Ann. Card. Anaesth.*, vol. 22, no. 1, p. 67, Jan. 2019.
- [84] I. Masic, S. M. Jankovic, and E. Begic, “PhD Students and the Most Frequent Mistakes during Data Interpretation by Statistical Analysis Software,” *Stud. Health Technol. Inform.*, vol. 262, pp. 105–109, 2019.
- [85] T. J and M. WJ, “Logistic Regression: Relating Patient Characteristics to Outcomes,” *JAMA*, vol. 316, no. 5, pp. 533–534, Aug. 2016.
- [86] von E. E, A. DG, E. M, P. SJ, G. PC, and V. JP, “The Strengthening the Reporting of Observational Studies in Epidemiology (STROBE) statement: guidelines for reporting observational studies,” *Lancet (London, England)*, vol. 370, no. 9596, pp. 1453–1457, 2007.
- [87] J. L. Rodgers and ; W Alan Nicewander, “Thirteen Ways to Look at the Correlation Coefficient,” *Am. Stat.*, vol. 42, no. 1, pp. 59–66, 1988.
- [88] A. G. Asuero, A. Sayago, and A. G. González, “The Correlation Coefficient: An Overview,” <https://doi.org/10.1080/10408340500526766>, vol. 36, no. 1, pp. 41–59, Jan. 2007.
- [89] B. PM *et al.*, “STARD 2015: an updated list of essential items for reporting diagnostic accuracy studies,” *BMJ*, vol. 351, Oct. 2015.

- [90] T. J and L. RJ, “Time-to-Event Analysis,” *JAMA*, vol. 315, no. 10, pp. 1046–1047, Mar. 2016.
- [91] S. MJ and H. MA, “Why Test for Proportional Hazards?,” *JAMA*, vol. 323, no. 14, pp. 1401–1402, Apr. 2020.
- [92] M. Porta, “A Dictionary of Epidemiology,” *A Dict. Epidemiol.*, Jul. 2016.
- [93] V. Amrhein, D. Trafimow, and S. Greenland, “Inferential Statistics as Descriptive Statistics: There Is No Replication Crisis if We Don’t Expect Replication,” <https://doi.org/10.1080/00031305.2018.1543137>, vol. 73, no. sup1, pp. 262–270, Mar. 2019.
- [94] S. Geisser and W. O. Johnson, “Modes of parametric statistical inference,” p. 192, 2006.
- [95] J. M. Bland and S. M. Kerry, “Statistics Notes: Weighted comparison of means,” *Br. Med. J.*, vol. 316, no. 7125, p. 129, Jan. 1998.
- [96] S. S. Skene, C. Bunce, N. Freemantle, and C. J. Doré, “Ophthalmic statistics note 9: Parametric versus non-parametric methods for data analysis,” *Br. J. Ophthalmol.*, vol. 100, no. 7, pp. 877–878, Jul. 2016.
- [97] L. JM, “Nonparametric Statistical Analysis,” *JAMA*, vol. 323, no. 20, pp. 2080–2081, May 2020.
- [98] K. R. (Karimassery R. . Sundaram, S. N. (Sada N. Dwivedi, and V. (Vishnu) Sreenivas, “Medical statistics : principles & methods,” p. 386, 2010.
- [99] McDonaldJH, *Introduction - Handbook of Biological Statistics*, 3rd ed. Baltimore, Maryland, U.S.A.: Sparky House Publishing; , 2014.
- [100] K. LS and G. CE, “Analysis of variance: is there a difference in means and what does it mean?,” *J. Surg. Res.*, vol. 144, no. 1, pp. 158–170, Jan. 2008.
- [101] Jaykaran, “How to select appropriate statistical test?,” *J. Pharm. Negat. Results*, vol. 1, no. 2, pp. 61–63, Oct. 2010.
- [102] T. C. Urdan, “Statistics in plain English,” p. 211, 2010.
- [103] “One-Sample T-Test in SPSS Statistics - Procedure, output and interpretation of the output using a relevant example | Laerd Statistics.” [Online]. Available: <https://statistics.laerd.com/spss-tutorials/one-sample-t-test-using-spss->

- statistics.php. [Accessed: 25-Oct-2021].
- [104] B. Barton, “Medical statistics : a guide to SPSS, data analysis and critical appraisal / Belinda Barton, Jennifer Peat,” 2014.
- [105] “Independent t-test in SPSS Statistics - Procedure, output and interpretation of the output using a relevant example | Laerd Statistics.” [Online]. Available: <https://statistics.laerd.com/spss-tutorials/independent-t-test-using-spss-statistics.php>. [Accessed: 25-Oct-2021].
- [106] “Dependent T-Test in SPSS Statistics - The procedure for running the test, generating the output and understanding the output using a relevant example | Laerd Statistics.” [Online]. Available: <https://statistics.laerd.com/spss-tutorials/dependent-t-test-using-spss-statistics.php>. [Accessed: 25-Oct-2021].
- [107] K. HY, “Analysis of variance (ANOVA) comparing means of more than two groups,” *Restor. Dent. Endod.*, vol. 39, no. 1, p. 74, 2014.
- [108] J. Lewsey, “Medical Statistics: A Guide to Data Analysis and Critical Appraisal,” *Ann. R. Coll. Surg. Engl.*, vol. 88, no. 6, p. 603, 2006.
- [109] “One-way ANOVA in SPSS Statistics - Step-by-step procedure including testing of assumptions.” [Online]. Available: <https://statistics.laerd.com/spss-tutorials/one-way-anova-using-spss-statistics.php>. [Accessed: 25-Oct-2021].
- [110] S. Lee and D. K. Lee, “What is the proper way to apply the multiple comparison test?,” *Korean J. Anesthesiol.*, vol. 71, no. 5, p. 353, Oct. 2018.
- [111] “One-way ANOVA - How to report the significance results, homogeneity of variance and running post-hoc tests | Laerd Statistics.” [Online]. Available: <https://statistics.laerd.com/statistical-guides/one-way-anova-statistical-guide-4.php>. [Accessed: 25-Oct-2021].
- [112] “Two-way ANOVA in SPSS Statistics - Step-by-step procedure including testing of assumptions | Laerd Statistics.” [Online]. Available: <https://statistics.laerd.com/spss-tutorials/two-way-anova-using-spss-statistics.php>. [Accessed: 25-Oct-2021].
- [113] S. Shalev-Shwartz and S. Ben-David, “From Theory to Algorithms,” *Underst. Mach. Learn. From Theory to Algorithms*, pp. 5–6, 2014.

- [114] T. O. Ayodele, “Types of Machine Learning Algorithms,” *New Adv. Mach. Learn.*, Feb. 2010.
- [115] “An introduction to machine learning with scikit-learn — scikit-learn 1.0.1 documentation.” [Online]. Available: <https://scikit-learn.org/stable/tutorial/basic/tutorial.html#machine-learning-the-problem-setting>. [Accessed: 25-Oct-2021].
- [116] “5 Types of Classification Algorithms in Machine Learning.” [Online]. Available: <https://monkeylearn.com/blog/classification-algorithms/>. [Accessed: 25-Oct-2021].
- [117] D. Denisko and M. M. Hoffman, “Classification and interaction in random forests,” *Proc. Natl. Acad. Sci.*, vol. 115, no. 8, pp. 1690–1692, Feb. 2018.
- [118] S. Basu, K. Kumbier, J. Brown, and B. Yu, “Iterative random forests to discover predictive and stable high-order interactions,” *Proc Natl Acad Sci USA*, vol. 115, no. 8, pp. 1943–1948, Feb. 2018.
- [119] A. Mendez and J. Chen, “Mouse models to study GCAP functions in intact photoreceptors,” *Adv. Exp. Med. Biol.*, vol. 514, pp. 361–388, 2002.
- [120] J. R. Sinclair, A. L. Jacobs, and S. Nirenberg, “Selective Ablation of a Class of Amacrine Cells Alters Spatial Processing in the Retina,” *J. Neurosci.*, vol. 24, no. 6, pp. 1459–1467, Feb. 2004.
- [121] S. E. Williams *et al.*, “Ephrin-B2 and EphB1 mediate retinal axon divergence at the optic chiasm,” *Neuron*, vol. 39, no. 6, pp. 919–935, Sep. 2003.
- [122] C. A. McMullen, F. H. Andrade, and J. S. Stahl, “Functional and Genomic Changes in the Mouse Ocular Motor System in Response to Light Deprivation from Birth,” *J. Neurosci.*, vol. 24, no. 1, pp. 161–169, Jan. 2004.
- [123] M. Hübener, “Mouse visual cortex,” *Current Opinion in Neurobiology*, vol. 13, no. 4. Elsevier Ltd, pp. 413–420, 2003.
- [124] J. H. Wilson and T. G. Wensel, “The Nature of Dominant Mutations of Rhodopsin and Implications for Gene Therapy,” in *Molecular Neurobiology*, 2003, vol. 28, no. 2, pp. 149–158.
- [125] J. Ambati *et al.*, “An animal model of age-related macular degeneration in

- senescent Ccl-2- or Ccr-2-deficient mice,” *Nat. Med.*, vol. 9, no. 11, pp. 1390–1397, Nov. 2003.
- [126] L. H. Pinto and C. Enroth-Cugell, “Tests of the mouse visual system,” *Mamm. Genome*, vol. 11, no. 7, pp. 531–536, 2000.
- [127] L. Gianfranceschi, A. Fiorentini, and L. Maffei, “Behavioural visual acuity of wild type and bcl2 transgenic mouse,” *Vision Res.*, vol. 39, no. 3, pp. 569–574, Feb. 2000.
- [128] G. T. Prusky and R. M. Douglas, “Developmental plasticity of mouse visual acuity,” *Eur. J. Neurosci.*, vol. 17, no. 1, pp. 167–173, Jan. 2003.
- [129] Y. Cui *et al.*, “Neurofibromin regulation of ERK signaling modulates GABA release and learning,” *Cell*, vol. 135, no. 3, p. 549, Oct. 2008.
- [130] C. RM *et al.*, “Mechanism for the learning deficits in a mouse model of neurofibromatosis type 1,” *Nature*, vol. 415, no. 6871, pp. 526–530, Jan. 2002.
- [131] C. Shilyansky *et al.*, “Neurofibromin regulates corticostriatal inhibitory networks during working memory performance,” *Proc. Natl. Acad. Sci. U. S. A.*, vol. 107, no. 29, pp. 13141–13146, Jul. 2010.
- [132] O. A *et al.*, “HCN channels are a novel therapeutic target for cognitive dysfunction in Neurofibromatosis type 1,” *Mol. Psychiatry*, vol. 20, no. 11, pp. 1311–1321, Nov. 2015.
- [133] S. MM, “Cortical HCN channels: function, trafficking and plasticity,” *J. Physiol.*, vol. 592, no. 13, pp. 2711–2719, Jul. 2014.
- [134] A. A, F. JE, and S. MJ, “Impermanence of dendritic spines in live adult CA1 hippocampus,” *Nature*, vol. 523, no. 7562, pp. 592–596, Jul. 2015.
- [135] E. Castrén, Y. Elgersma, L. Maffei, and R. Hagerman, “Treatment of Neurodevelopmental Disorders in Adulthood,” *J. Neurosci.*, vol. 32, no. 41, pp. 14074–14079, Oct. 2012.
- [136] P. Youssef, S. Nath, G. A. Chaimowitz, and S. S. Prat, “Electroretinography in psychiatry: A systematic literature review,” *European Psychiatry*, vol. 62. Elsevier Masson SAS, pp. 97–106, 01-Oct-2019.
- [137] M. Hébert, C. Mérette, T. Paccalet, A. M. Gagné, and M. Maziade,

- “Electroretinographic anomalies in medicated and drug free patients with major depression: Tagging the developmental roots of major psychiatric disorders,” *Prog. Neuro-Psychopharmacology Biol. Psychiatry*, vol. 75, pp. 10–15, Apr. 2017.
- [138] M. Hébert *et al.*, “The Electroretinogram May Differentiate Schizophrenia From Bipolar Disorder,” *Biol. Psychiatry*, vol. 87, no. 3, pp. 263–270, Feb. 2020.
- [139] M. Pathania, E. C. Davenport, J. Muir, D. F. Sheehan, G. López-Doménech, and J. T. Kittler, “The autism and schizophrenia associated gene CYFIP1 is critical for the maintenance of dendritic complexity and the stabilization of mature spines,” *Transl. Psychiatry*, vol. 4, no. 3, p. 374, Mar. 2014.
- [140] E. R. Ritvo, R. Ritvo, A. Yuwiler, A. Brothers, B. J. Freeman, and S. Plotkin, “Elevated daytime melatonin concentrations in autism: A pilot study,” *Eur. Child Adolesc. Psychiatry*, vol. 2, no. 2, pp. 75–78, Apr. 1993.
- [141] G. Realmuto, R. Purple, W. Knobloch, and E. Ritvo, “Electroretinograms (ERGs) in four autistic probands and six first-degree relatives,” *Can. J. Psychiatry*, vol. 34, no. 5, pp. 435–439, 1989.
- [142] R. Rossignol *et al.*, “Visual sensorial impairments in neurodevelopmental disorders: Evidence for a retinal phenotype in fragile X syndrome,” *PLoS One*, vol. 9, no. 8, p. 105996, Aug. 2014.
- [143] J. Kremers and N. Tanimoto, “Measuring retinal function in the mouse,” in *Methods in Molecular Biology*, vol. 1753, Humana Press Inc., 2018, pp. 27–40.
- [144] D. M. Waldner *et al.*, “Cone dystrophy and ectopic synaptogenesis in a *Cacna1f* loss of function model of congenital stationary night blindness (CSNB2A),” *Channels*, vol. 12, no. 1, pp. 17–33, Jan. 2018.
- [145] K. Z. Meyza and D. C. Blanchard, “The BTBR mouse model of idiopathic autism – Current view on mechanisms,” *Neuroscience and Biobehavioral Reviews*, vol. 76. Elsevier Ltd, pp. 99–110, 01-May-2017.
- [146] C. Herrera, A. Moreno, K. Chavez, L. Niño De Rivera, and V. Ponomaryov, “Acquisition and processing of ERG signals,” *2010 2nd Circuits Syst. Med. Environ. Appl. Work. CASME 2010*, pp. 10–13, 2010.
- [147] S. DE Estudios De Posgrado E Investigación and D. DE LUIS NIÑO RIVERA Y OYARZABAL México DF, “INSTITUTO POLITÉCNICO NACIONAL

ESCUELA SUPERIOR DE INGENIERÍA MECÁNICA Y ELÉCTRICA Unidad Culhuacán ‘DISEÑO Y CONSTRUCCIÓN DE UN EQUIPO PARA ELECTRORETINOGRFÍA,” 2009.

- [148] T. Instruments and I. Sloa, “Chapter 16 Active Filter Design Techniques Excerpted from Op Amps for Everyone Literature Number: SLOD006A.”
- [149] C. Sudalaimani, T. E. Thomas, N. Sivakumaran, S. R. Valsalam, S. P. Meethal, and E. Sathish, “Seizure prediction using general regression neural network,” *Proc. - TIMA 2017 9th Int. Conf. Trends Ind. Meas. Autom.*, Oct. 2017.
- [150] M. Gauvin, J. M. Lina, and P. Lachapelle, “Advance in ERG analysis: From peak time and amplitude to frequency, power, and energy,” *Biomed Res. Int.*, vol. 2014, 2014.
- [151] M. F. Marmor, A. B. Fulton, G. E. Holder, Y. Miyake, M. Brigell, and M. Bach, “ISCEV Standard for full-field clinical electroretinography (2008 update),” *Doc. Ophthalmol.*, vol. 118, no. 1, pp. 69–77, 2009.
- [152] H. Nyquist, “Certain topics in telegraph transmission theory,” *Proc. IEEE*, vol. 90, no. 2, pp. 280–305, 2002.
- [153] M. Yu and N. S. Peachey, “Attenuation of oscillatory potentials in nob2 mice,” *Doc. Ophthalmol.*, vol. 115, no. 3, p. 173, Nov. 2007.
- [154] D. CREEL, “Evaluating Hydroxychloroquine Toxicity With Multifocal Electroretinograpy,” *Retin. Today*, 2014.
- [155] G. Theses and A. Mohammad Alaql, “Scholar Commons Analysis and Processing of Human Electroretinogram,” 2016.
- [156] M. Svensén and C. M. Bishop, “Robust Bayesian mixture modelling,” *Neurocomputing*, vol. 64, no. 1-4 SPEC. ISS., pp. 235–252, Mar. 2005.
- [157] X. Wei and C. Li, “The Student’s t-hidden Markov model with truncated stick-breaking priors,” *IEEE Signal Process. Lett.*, vol. 18, no. 6, pp. 355–358, 2011.
- [158] J. Christmas and R. Everson, “Robust autoregression: Student-t innovations using variational bayes,” *IEEE Trans. Signal Process.*, vol. 59, no. 1, pp. 48–57, 2011.
- [159] J. Tukey, “Variances of Variance Components: I. Balanced Designs,” *Inst. Math. Stat.*, vol. 27, no. 3, 1956.

- [160] J. Cornfield and J. W. Tukey, "Average Values of Mean Squares in Factorials," *Ann. Math. Stat.*, vol. 27, no. 4, pp. 907–949, Dec. 1956.
- [161] J. W. Tukey, "Variances of Variance Components: II. The Unbalanced Single Classification," <https://doi.org/10.1214/aoms/1177707036>, vol. 28, no. 1, pp. 43–56, Mar. 1957.
- [162] S. R. Searle and C. R. Henderson, "Computing Procedures for Estimating Components of Variance in the Two-Way Classification, Mixed Model," *Biometrics*, vol. 17, no. 4, p. 607, Dec. 1961.
- [163] H. O. Hartley, "Expectations, Variances and Covariances of Anova Mean Squares by 'Synthesis,'" *Biometrics*, vol. 23, no. 1, p. 105, Mar. 1967.
- [164] S. R. Searle and R. F. Fawcett, "Expected Mean Squares in Variance Components Models Having Finite Populations," *Biometrics*, vol. 26, no. 2, p. 243, Jun. 1970.
- [165] T. Simmachan, J. J. Borkowski, and K. Budsaba, "Expected Mean Squares for the Random Effects One-Way ANOVA Model when Sampling from a Finite Population," *Thail. Stat.*, vol. 10, no. 1, pp. 121–128, 2012.
- [166] C. Suphirat, B. Chomtee, and J. J. Borkowski, "Expected mean squares for model effects in the two-way anova model when sampling from finite populations," *Songklanakarin J. Sci. Technol.*, vol. 43, no. 1, pp. 57–71, 2021.
- [167] F. Hui, J. Tang, X. Hadoux, M. Coote, and J. G. Crowston, "Optimizing a portable ERG device for glaucoma clinic: The effect of interstimulus frequency on the photopic negative response," *Transl. Vis. Sci. Technol.*, vol. 7, no. 6, 2018.
- [168] "R: The R Project for Statistical Computing." [Online]. Available: <https://www.r-project.org/>. [Accessed: 26-Oct-2021].
- [169] "scikit-learn: machine learning in Python — scikit-learn 1.0.1 documentation." [Online]. Available: <https://scikit-learn.org/stable/>. [Accessed: 26-Oct-2021].
- [170] "Statistics and Machine Learning Toolbox - MATLAB." [Online]. Available: <https://www.mathworks.com/products/statistics.html>. [Accessed: 26-Oct-2021].
- [171] "World's Fastest File System for HPC, AI, and Analytics at Scale | WekaIO." [Online]. Available: <https://www.weka.io/>. [Accessed: 26-Oct-2021].
- [172] D. M, M. R, H. N, and W. DP, "Use of machine learning for behavioral distinction



- of autism and ADHD,” *Transl. Psychiatry*, vol. 6, no. 2, 2016.
- [173] D. Bone, M. S. Goodwin, M. P. Black, C.-C. Lee, K. Audhkhasi, and S. Narayanan, “Applying Machine Learning to Facilitate Autism Diagnostics: Pitfalls and Promises,” *Springer*, 2014.
- [174] C. Frazier Norbury, “Editorial: The search for core symptoms - will this help clinical decision-making?,” *J. Child Psychol. Psychiatry*, vol. 57, no. 8, pp. 881–883, 2016.
- [175] A. Pratap and C. S. Kanimozhiselvi, “Predictive assessment of autism using unsupervised machine learning models,” *Int. J. Adv. Intell. Paradig.*, vol. 6, no. 2, pp. 113–121, 2014.
- [176] T. Wolfers, J. K. Buitelaar, C. F. Beckmann, B. Franke, and A. F. Marquand, “From estimating activation locality to predicting disorder: A review of pattern recognition for neuroimaging-based psychiatric diagnostics,” *Neurosci. Biobehav. Rev.*, vol. 57, pp. 328–349, Oct. 2015.
- [177] B. D, B. SL, B. MP, G. MS, Lord C, and N. SS, “Use of machine learning to improve autism screening and diagnostic instruments: effectiveness, efficiency, and multi-instrument fusion,” *J. Child Psychol. Psychiatry.*, vol. 57, no. 8, pp. 927–937, Aug. 2016.
- [178] J. Lopez Marcano, A. A. Beex, and C. Scott Bailey JoAnn Paul, “Classification of ADHD and Non-ADHD Using AR Models and Machine Learning Algorithms,” 2016.
- [179] D. P. Wall, R. Dally, R. Luyster, J.-Y. Jung, and T. F. DeLuca, “Use of Artificial Intelligence to Shorten the Behavioral Diagnosis of Autism,” *PLoS One*, vol. 7, no. 8, p. e43855, Aug. 2012.
- [180] K. C. Chu, H. J. Huang, and Y. S. Huang, “Machine learning approach for distinction of ADHD and OSA,” *Proc. 2016 IEEE/ACM Int. Conf. Adv. Soc. Networks Anal. Mining, ASONAM 2016*, pp. 1044–1049, Nov. 2016.
- [181] J. A. Kosmicki, V. Sochat, M. Duda, and D. P. Wall, “Searching for a minimal set of behaviors for autism detection through feature selection-based machine learning,” *Transl. Psychiatry 2015 52*, vol. 5, no. 2, pp. e514–e514, Feb. 2015.
- [182] D. P. Wall, J. Kosmicki, T. F. DeLuca, E. Harstad, and V. A. Fusaro, “Use of

- machine learning to shorten observation-based screening and diagnosis of autism,” *Transl. Psychiatry* 2012 24, vol. 2, no. 4, pp. e100–e100, Apr. 2012.
- [183] A. Pratap, C. S. Kanimozhiselvi, R. Vijayakumar, and K. V Pramod, “Soft Computing Models for the Predictive Grading of Childhood Autism-A Comparative Study,” *Int. J. Soft Comput. Eng.*, no. 4, pp. 2231–2307, 2014.
- [184] B. Sluban, M. Juršič, B. Cestnik, and N. Lavrač, “Exploring the Power of Outliers for Cross-Domain Literature Mining,” *Lect. Notes Comput. Sci. (including Subser. Lect. Notes Artif. Intell. Lect. Notes Bioinformatics)*, vol. 7250, pp. 325–337, 2012.
- [185] I. Petric, T. Urbancic, and B. Cestnik, “Discovering hidden knowledge from biomedical literature,” *Informatica*, vol. 31, no. 1, pp. 15–21, Mar. 2007.
- [186] C. P. Chen *et al.*, “Diagnostic classification of intrinsic functional connectivity highlights somatosensory, default mode, and visual regions in autism,” *NeuroImage Clin.*, vol. 8, pp. 238–245, Jan. 2015.
- [187] M. J. Maenner, M. Yeargin-Allsopp, K. V. N. Braun, D. L. Christensen, and L. A. Schieve, “Development of a Machine Learning Algorithm for the Surveillance of Autism Spectrum Disorder,” *PLoS One*, vol. 11, no. 12, p. e0168224, Dec. 2016.
- [188] H. Abbas, F. Garberson, E. Glover, and D. P. Wall, “Machine learning approach for early detection of autism by combining questionnaire and home video screening,” *J. Am. Med. Informatics Assoc.*, vol. 25, no. 8, pp. 1000–1007, Aug. 2018.
- [189] D. L. Robins, K. Casagrande, M. Barton, C.-M. A. Chen, T. Dumont-Mathieu, and D. Fein, “Validation of the Modified Checklist for Autism in Toddlers, Revised With Follow-up (M-CHAT-R/F),” *Pediatrics*, vol. 133, no. 1, pp. 37–45, Jan. 2014.
- [190] “RETI-port/scan 21.” [Online]. Available: <https://www.roland-consult.com/reti-port-scan-21.html>. [Accessed: 27-Oct-2021].
- [191] S. AJ *et al.*, “A mouse model for the learning and memory deficits associated with neurofibromatosis type I,” *Nat. Genet.*, vol. 15, no. 3, pp. 281–284, Mar. 1997.
- [192] R. SG, R. F, L. G. JF, and B. MG, “Recommendations for a toxicological screening ERG procedure in laboratory animals,” *Doc. Ophthalmol.*, vol. 110, no. 1, pp. 57–66, Jan. 2005.

## Attachments

### Attachment A

ID	Sex	Genotype	Visual Acuity	Notes
926.0.	F	WT	0,050	Noise
926.1.	F	WT	0,350	Noise
926.3.	F	NF1	0,400	Noise
926.4.	F	WT	0,350	Noise
926.5.	F	NF1	0,300	
926.6.	F	NF1	0,100	Noise
929.1.	M	NF1	0,400	
929.5.	M	NF1	0,350	Example of difficult b-wave filter at 0.3
929.6.	M	WT	0,300	
930.0.	F	NF1	0,400	Example of difficult OP times at 0.03
930.3.	F	WT	0,350	
930.4.	F	NF1	0,350	
942.0.	M	WT	0,400	
942.2.	M	WT	0,500	Example of difficult b-wave filter at 0.3
942.3.	M	NF1	0,500	
942.6.	M	WT	0,450	
943.1.	F	NF1	0,400	
943.4.	F	WT	0,450	Noise
943.5.	F	NF1	0,375	
943.7.	F	WT	0,350	Extreme noise
958.1.	M	NF1		Example of difficult b-wave filter at 9.49
958.3.	M	NF1		
958.4.	M	WT		Example of difficult b-wave filter at 0.3 and 9.49
958.6.	M	WT		
959.0.	F	WT		
959.2.	F	NF1		
959.5.	F	WT		
988.1.	M	NF1		Noise, OP not convincing
988.3.	M	WT		
988.5.	M	NF1		
988.7.	M	NF1		
988.8.	M	WT		
988.9.	M	WT		
990.0.	M	WT		
990.2.	M	WT		Noise
1005.0.	M	NF1	0,450	
1005.1.	M	NF1	0,400	No whiskers
1005.4.	M	NF1	0,450	PF repeated, the animal maybe moved

<b>1005.5.</b>	M	WT	0,400	No whiskers
<b>1005.8.</b>	M	NF1	0,450	
<b>1005.9.</b>	M	WT	0,400	
<b>1017.0.</b>	M	WT	0,400	
<b>1017.1.</b>	M	WT	0,450	
<b>1017.3.</b>	M	NF1	0,450	
<b>1018.2.</b>	F	NF1	0,500	
<b>1059.1.</b>	M	WT	0,500	
<b>1059.2.</b>	M	NF1	0,450	
<b>1059.3.</b>	M	NF1	0,400	
<b>1059.4.</b>	M	WT	0,400	Right eye with blood
<b>1059.8.</b>	M	WT	0,375	Right eye opaque
<b>1059.10.</b>	M	WT	0,400	Had more anesthesia than others
<b>1085.2.</b>	M	NF1	0,400	
<b>1085.3.</b>	M	WT	0,400	
<b>1085.4.</b>	M	NF1	0,400	
<b>1085.9.</b>	M	NF1	0,450	
<b>1085.10.</b>	M	WT	0,400	
<b>1087.0.</b>	M	NF1	0,400	
<b>1087.1.</b>	M	NF1	0,450	
<b>1087.7.</b>	M	NF1	0,450	
<b>1087.9.</b>	M	WT	0,500	

## Attachment B - Channel 15

Index	Genotype	Gender	A_amplitude	A_latency	B_amplitude	B_latency	OP1_amplitude	OP1_latency	OP2_amplitude	OP2_latency	OP3_amplitude	OP3_latency	OP4_amplitude	OP4_latency
0	WT	F	-0.000159778	0.0199219	0.00031209	0.0480469	0.000223024	0.0202148	4.694e-05	0.0301758	0.000133306	0.0369141	0.000309015	0.0442383
1	WT	F	-0.000152886	0.0216797	0.000256423	0.0791016	0.000191804	0.0304687	5.88104e-05	0.0354492	0.000211548	0.0427734	0.000127942	0.0533203
2	WT	F	-0.000125181	0.0219727	0.000306239	0.0585938	0.000236453	0.0231445	6.19787e-05	0.0328125	5.14525e-05	0.0375	0.000141895	0.0451172
3	WT	F	-0.000195801	0.0208008	0.000354521	0.0591797	0.000298368	0.0216797	3.19885e-05	0.0307617	0.000142888	0.0363281	0.000336557	0.0442383
4	WT	F	-5.41681e-05	0.0208008	0.000127585	0.0609375	0.00010068	0.0222656	2.30632e-05	0.0313477	5.76177e-05	0.0386719	0.000116625	0.046875
5	WT	F	-0.000115391	0.0219727	0.000274513	0.065625	0.000188274	0.0225586	2.55478e-05	0.0310547	9.44023e-05	0.0392578	0.000109456	0.0495117
6	WT	F	-0.00013882	0.0202148	0.000280918	0.047168	0.000154481	0.0219727	3.28438e-05	0.0298828	0.000175335	0.0366211	0.000288011	0.0448242
7	WT	M	-0.000170649	0.0210937	0.000467801	0.0632812	0.000324708	0.0216797	3.64237e-05	0.0307617	0.000154654	0.0383789	0.000278181	0.0474609
8	WT	M	-0.000228637	0.0222656	0.000492178	0.0735352	0.000399755	0.0319336	0.000188257	0.0421875	0.000151334	0.0553711	ND	ND
9	WT	M	-0.000188223	0.0210937	0.000223885	0.0647461	0.00012375	0.0219727	3.51489e-05	0.0310547	0.000104955	0.0392578	0.000222575	0.0489258
10	WT	M	-7.0136e-05	0.0210937	0.00022829	0.0673828	0.000139331	0.0213867	3.64083e-05	0.0310547	9.82292e-05	0.0407227	0.000169743	0.0506836
11	WT	M	-4.07424e-05	0.0210937	0.000164444	0.0694336	0.000105912	0.0219727	2.11501e-05	0.0307617	6.23449e-05	0.0398437	0.000109593	0.0495117
12	WT	M	-7.15090e-05	0.0216797	0.000299979	0.0697266	0.000219716	0.0222656	2.66809e-05	0.0325195	7.8404e-05	0.0410156	0.000103524	0.0518555
13	WT	M	-0.00013715	0.0219727	0.000304569	0.0670898	0.000226484	0.0325195	0.000157838	0.0418945	0.000185209	0.0530273	8.43019e-06	0.0615234
14	WT	M	-9.78463e-05	0.0213867	0.000316523	0.0670898	0.000237206	0.0222656	3.76924e-05	0.0322266	0.000116584	0.0410156	0.000134763	0.0512695
15	WT	M	-0.000175341	0.0205078	0.000298835	0.0708984	0.000260417	0.0222656	8.30853e-05	0.0310547	0.000179819	0.0416016	0.000195616	0.0524414
16	WT	M	-8.90286e-05	0.0222656	0.000287968	0.0711914	0.000190235	0.0301758	0.000114812	0.0407227	0.00016352	0.0506836	6.50997e-05	0.0676758
17	WT	M	-6.99488e-05	0.0213867	0.000301289	0.0662109	0.000134508	0.0263672	3.63213e-05	0.0316406	0.000134793	0.0404297	0.000143087	0.0500977
18	WT	M	-0.000126341	0.019043	0.000245692	0.0418945	0.000215036	0.0208008	5.04331e-05	0.0290039	0.000156954	0.0348633	0.000332087	0.0416016
19	WT	M	-9.89639e-05	0.0205078	0.000221589	0.0594727	0.000161695	0.0219727	3.23776e-05	0.0301758	0.000103706	0.0380859	0.000185249	0.046875
20	WT	M	-0.000153371	0.0208008	0.000311556	0.0550781	0.000236295	0.0219727	3.24090e-05	0.0310547	9.18951e-05	0.0366211	0.000245095	0.0442383
21	WT	M	-0.000107268	0.0205078	0.000349064	0.0711914	0.000250002	0.0216797	2.62892e-05	0.0298828	0.000122632	0.0383789	0.000222911	0.0474609
22	WT	M	-0.000196173	0.0208008	0.000367846	0.0738281	0.000318047	0.0219727	3.60159e-05	0.0301758	0.00017904	0.037793	0.000312898	0.046582
23	WT	M	-0.000173047	0.0202148	0.00029001	0.0474609	0.000214676	0.0216797	5.50452e-05	0.0307617	0.000141626	0.0375	0.000323423	0.0454102
24	WT	M	-0.000136038	0.0208008	0.000326028	0.0609375	0.000222435	0.0222656	4.60089e-05	0.0310547	0.000123589	0.0395648	0.000150622	0.0492187
25	WT	M	-0.000130963	0.0216797	0.000342601	0.0679687	0.000246879	0.0225586	4.47819e-05	0.0322266	0.000151798	0.0416016	0.000131891	0.0547852
26	WT	M	-8.86211e-05	0.0205078	0.000179274	0.0451172	0.000128105	0.0216797	3.15372e-05	0.0304687	0.000104875	0.0375	0.000173232	0.0462891
27	WT	M	-0.000188651	0.0208008	0.00029454	0.0571289	0.000223027	0.0216797	5.21116e-05	0.0310547	0.000119334	0.0375	0.000287979	0.0459961
28	WT	M	-0.000109344	0.0222656	0.000212818	0.0650391	0.000154122	0.0228516	2.11063e-05	0.0310547	7.38417e-08	0.039844	9.62354e-05	0.0413866
29	IF1	F	-6.21302e-05	0.0208008	0.00029696	0.0606445	0.000193505	0.0292369	0.0001521	0.0354492	0.000310804	0.0424805	0.000174413	0.0530273
30	IF1	F	-0.000386591	0.0219727	0.000687867	0.074787	0.000548669	0.0225586	4.87628e-05	0.0316406	0.000213587	0.037207	0.000497015	0.0454102
31	IF1	F	-0.000100407	0.0225586	0.000179398	0.0585938	0.000102174	0.0251953	1.13172e-05	0.0304687	0.000112904	0.0363281	0.000217416	0.0439453
32	IF1	F	-0.000199798	0.0208008	0.000421432	0.0644531	0.000376394	0.0222656	0.00014738	0.0301758	0.000215693	0.037793	0.00029602	0.046875
33	IF1	F	-0.000229402	0.0210937	0.000515082	0.0609375	0.000420747	0.0225586	4.54465e-05	0.0310547	0.000183449	0.0375	0.000333017	0.046582
34	IF1	F	-8.55251e-05	0.0222656	0.000343885	0.065625	0.000196722	0.0295898	0.0001114	0.037207	0.000217344	0.0454102	0.000108051	0.0568359
35	IF1	F	-0.000112221	0.0205078	0.000255015	0.0650391	0.000191049	0.0219727	3.627e-05	0.0304687	0.000126263	0.0366719	0.000183082	0.0480469
36	IF1	F	-0.00013067	0.0213867	0.000308288	0.0489258	0.000227862	0.0222656	2.4115e-05	0.0301758	0.000144432	0.0366719	0.000267761	0.0477539
37	IF1	F	-0.000208503	0.0222656	0.000464496	0.0799805	0.000352597	0.0310547	0.000196437	0.0401367	0.000304432	0.0500977	0.000116221	0.0647461
38	IF1	M	-2.90359e-05	0.0205078	0.000202083	0.0615234	0.000118628	0.0222656	2.36333e-05	0.0307617	7.49855e-05	0.0398437	0.000104933	0.0506836
39	IF1	M	-8.09629e-05	0.0208008	0.000228859	0.0600586	0.000140787	0.0225586	1.21546e-05	0.0310547	8.11921e-05	0.037207	0.000224798	0.0451172
40	IF1	M	-0.000189297	0.0210937	0.000341753	0.0474609	0.000268308	0.0222656	5.15784e-05	0.0310547	0.000181408	0.0388859	0.000343305	0.046875
41	IF1	M	-0.000127955	0.0210937	0.000350419	0.0536133	0.000250958	0.0219727	3.82574e-05	0.0310547	0.000160971	0.0395648	0.00025103	0.0489258
42	IF1	M	-9.37046e-05	0.0222656	0.000336003	0.0685547	0.000192824	0.0231445	2.71955e-05	0.0316406	0.000107767	0.0413086	0.000149369	0.0518555
43	IF1	M	-0.000197347	0.0222656	0.00039809	0.0711914	0.000307064	0.0231445	4.68075e-05	0.0322266	0.00018022	0.0416016	0.000285357	0.0521484
44	IF1	M	-8.71719e-05	0.0225586	0.000173075	0.0711914	0.00035e-05	0.0275391	1.80354e-05	0.0307617	1.41348e-05	0.0342773	6.86103e-05	0.0421875
45	IF1	M	-7.93605e-05	0.0219727	0.000237124	0.0685547	0.000174217	0.0231445	2.80634e-05	0.0316406	0.000107729	0.0410156	0.000123078	0.0521484
46	IF1	M	-0.000140253	0.0213867	0.000345896	0.0714844	0.000249377	0.0225586	3.74007e-05	0.0316406	0.000130838	0.0410156	0.000138066	0.0518555
47	IF1	M	-4.79512e-05	0.0213867	0.000320994	0.0685547	0.00021296	0.0228516	2.86551e-05	0.0313477	0.000105575	0.0404297	0.000100918	0.0515625
48	IF1	M	-0.000171983	0.0216797	0.000359241	0.0706055	0.000251058	0.0231445	5.27606e-05	0.0325195	0.000154354	0.0424805	0.00011664	0.0556642
49	IF1	M	-0.000155253	0.0225586	0.000392435	0.0662109	0.000288324	0.0231445	5.10933e-05	0.0336914	9.13784e-05	0.0451172	2.87809e-05	0.055957
50	IF1	M	-0.000137792	0.0205078	0.000338887	0.0629883	0.000290297	0.0219727	6.03271e-05	0.0313477	0.000169979	0.0395508	0.00020692	0.0489258
51	IF1	M	-4.14483e-05	0.0219727	0.000233259	0.0882734	0.000156749	0.0269531	3.84042e-06	0.0322266	7.76587e-05	0.0354492	0.000201362	0.0430664
52	IF1	M	-0.000155743	0.0225586	0.000267148	0.0427734	0.000234275	0.0316406	0.000119254	0.0348633	0.000299718	0.0418945	0.000154071	0.0524414
53	IF1	M	-7.788e-05	0.0205078	0.000177555	0.0461602	0.000127371	0.0219727	2.07473e-05	0.0307617	5.91891e-05	0.0363281	0.000148338	0.0439453
54	IF1	M	-0.000150907	0.0219727	0.000472432	0.0685547	0.000326635	0.0222656	1.29112e-05	0.0295898	0.000158205	0.037793	0.000338413	0.0459961
55	IF1	M	-0.000111385	0.0210937	0.000355499	0.0650391	0.000273014	0.0222656	4.6168e-05	0.0310547	0.000122534	0.0375	0.000239706	0.0459961
56	IF1	M	-6.45235e-05	0.0210937	0.000144288	0.0632812	9.72366e-05	0.0219727	3.4766e-05	0.0310547	6.55597e-05	0.0413086	1.50349e-05	0.0480469
57	IF1	M	-6.18827e-05	0.0208008	0.000195233	0.0615234	0.000158125	0.0216797	2.27291e-05	0.0307617	9.18746e-05	0.0375	0.000195397	0.0457031
58	IF1	M	-0.000156401	0.0202148	0.000273475	0.0609375	0.000208027	0.0216797	5.61071e-05	0.0307617	0.000115759	0.037207	0.000273093	0.0454102

## Attachment C - Channel 13

Index	Genotype	Gender	A_amplitude	A_latency	B_amplitude	B_latency	OP1_amplitude	OP1_latency	OP2_amplitude	OP2_latency	OP3_amplitude	OP3_latency	OP4_amplitude	OP4_latency
0	WT	F	-0.00022274	0.0251953	0.000326956	0.0723633	0.000227473	0.0298828	0.000133386	0.0375	0.000293854	0.0448242	0.000142042	0.0547852
1	WT	F	-0.000137532	0.0263672	0.000292592	0.0779297	0.000215635	0.0298828	0.000102112	0.0363281	0.000139254	0.0430664	0.000110338	0.0530273
2	WT	F	-0.47649e-05	0.0342773	0.000218766	0.065332	0.0001931	0.037793	0.000156237	0.0454102	7.78788e-05	0.0556641	3.05787e-05	0.0676758
3	WT	F	-0.000160911	0.028418	0.000409051	0.0714844	0.000387967	0.0366211	0.000345077	0.0445313	0.000172655	0.055957	5.46606e-05	0.0679687
4	WT	F	-6.47471e-05	0.0348633	0.000139539	0.0875977	0.00014656	0.0392578	0.000107127	0.047168	5.26544e-05	0.0574219	7.53099e-05	0.0635742
5	WT	F	-4.09388e-05	0.0263672	0.000110024	0.046582	9.44676e-05	0.0310547	4.90017e-05	0.037793	0.000110349	0.0457031	2.08416e-07	0.0509766
6	WT	F	-0.000114135	0.0290039	0.000300154	0.0662109	0.000193016	0.0319336	0.000103102	0.0395508	0.00013864	0.0489258	5.70678e-05	0.0629883
7	WT	F	-0.000168779	0.027832	0.000285779	0.0676758	0.000182167	0.0301758	0.0001558	0.0369141	0.000286019	0.0448242	0.000137849	0.0577148
8	WT	M	-0.000152059	0.028418	0.000477886	0.0678898	0.000283574	0.0316406	0.000156665	0.0386719	0.000277403	0.0477539	0.000131408	0.0609375
9	WT	M	-0.000169866	0.0295898	0.000448521	0.0744141	0.000312187	0.031055	0.000173196	0.0424805	0.000144871	0.0553711	ND	ND
10	WT	M	-0.000121906	0.028125	0.000252669	0.0679687	0.000130446	0.0310547	0.000114717	0.0395508	0.000215862	0.0489258	0.00010786	0.0624823
11	WT	M	-7.49668e-05	0.027832	0.000184127	0.065918	0.000149671	0.031055	8.29023e-05	0.0413086	0.000167701	0.0512695	8.21013e-05	0.065625
12	WT	M	-4.63739e-05	0.0292969	0.000234142	0.0676758	0.000112455	0.0298828	4.36417e-06	0.0328125	4.99921e-05	0.0404297	0.00010238	0.0495117
13	WT	M	-7.5258e-05	0.0301758	0.000162505	0.0685547	9.25699e-05	0.0328125	7.04855e-05	0.0413086	9.18125e-05	0.0515625	1.86261e-05	0.0618164
14	WT	M	-0.000125113	0.0290039	0.000247032	0.0553711	0.000152032	0.0319336	0.000149748	0.0427734	0.000195307	0.0539062	6.62802e-05	0.0605547
15	WT	M	-0.000129587	0.0290039	0.000337934	0.0676758	0.000197815	0.0313477	0.000137748	0.0410156	0.000187072	0.0512695	7.84681e-05	0.065918
16	WT	M	-0.000135226	0.0290039	0.000264875	0.075	0.000183466	0.0333984	0.000140844	0.0421875	0.000176598	0.0530273	5.41675e-05	0.0679687
17	WT	M	-8.82727e-05	0.0292969	0.000324515	0.0788086	0.000189754	0.031055	0.000107279	0.0407227	0.000171044	0.0509766	6.80375e-05	0.065918
18	WT	M	-4.80007e-05	0.0313477	0.000272869	0.0679687	0.000134845	0.0328125	0.000104083	0.0407227	0.000146785	0.0500977	1.7461e-06	0.0574219
19	WT	M	-0.000131817	0.0260742	0.000290489	0.0445313	0.000188404	0.0301758	0.00013926	0.0348633	0.000335822	0.0418945	0.000191162	0.0527344
20	WT	M	-0.000126544	0.0430664	0.00016128	0.0638672	0.000180076	0.046875	9.8524e-05	0.0594727	3.24473e-08	0.065332	ND	ND
21	WT	M	-0.000136238	0.028125	0.000284944	0.0723633	0.000173642	0.0290039	0.00011824	0.0369141	0.000261597	0.0445313	0.000127457	0.055957
22	WT	M	-6.51749e-05	0.028125	0.000281642	0.0647461	0.000174631	0.0295898	1.02491e-07	0.0345703	0.00011689	0.0383789	0.00019527	0.047168
23	WT	M	-0.000126913	0.028125	0.000342846	0.0667969	0.000222718	0.0304687	0.000165806	0.0380859	0.000305143	0.046582	0.000133568	0.0597656
24	WT	M	-0.000113937	0.028125	0.000310112	0.0726562	0.000214527	0.0298828	0.000177018	0.0375	0.000296607	0.0454102	0.000140532	0.0577148
25	WT	M	-9.74229e-05	0.0287109	0.000232434	0.065332	0.00016349	0.0322266	0.00012219	0.0392578	0.00015983	0.0503906	7.41637e-05	0.0624823
26	WT	M	-0.000114625	0.0287109	0.000270116	0.0550781	0.000146032	0.0325195	0.000150538	0.0418945	0.000151497	0.0533203	4.4415e-05	0.0694336
27	WT	M	-7.25663e-05	0.0266602	0.000221494	0.0609375	0.000134786	0.0307617	9.61811e-05	0.037793	0.00018536	0.0459961	8.38313e-05	0.058867
28	WT	M	-0.000162324	0.028418	0.00039219	0.065625	0.000266419	0.0319336	0.000116377	0.0380859	0.000268045	0.0462891	0.000179345	0.0574219
29	WT	M	-0.000180065	0.028418	0.000194799	0.0527344	0.000136929	0.0328125	9.79321e-05	0.0418945	8.53448e-05	0.0539062	1.89535e-05	0.0676758
30	WT	F	-0.000190672	0.0263672	0.000292656	0.0726562	0.00017241	0.0304687	0.000116165	0.0357422	0.000295315	0.0424805	0.000148948	0.0536133
31	WT	F	-0.000278232	0.0319336	0.00050071	0.0676758	0.000533835	0.037207	0.000520667	0.0457031	0.000227132	0.05625	4.95957e-05	0.0591797
32	WT	F	-0.000107132	0.0407227	0.000178933	0.047168	0.000170366	0.0439453	0.00010149	0.0547852	2.65982e-05	0.0624823	3.86122e-05	0.0691406
33	WT	F	-8.36073e-05	0.0301758	0.000323838	0.0650391	0.000326834	0.0380859	0.000258469	0.046875	0.000123527	0.0609375	ND	ND
34	WT	F	-0.00016315	0.0275391	0.000350359	0.0691406	0.000206741	0.0307617	0.000171053	0.0375	0.000325736	0.046582	0.000162761	0.058867
35	WT	F	-6.21639e-05	0.0269531	0.000255628	0.0492187	0.000140868	0.0298828	0.000125754	0.0375	0.000243957	0.0459961	0.000131749	0.0568359
36	WT	F	-0.000125199	0.028418	0.000226909	0.0665039	0.000166969	0.0316406	0.00011244	0.0386719	0.000170088	0.0495117	8.88152e-05	0.0618164
37	WT	F	-0.000151413	0.0316406	0.000314629	0.0500977	0.000283964	0.0389648	0.000258722	0.0477539	0.00017934	0.0612305	ND	ND
38	WT	F	-0.000166827	0.0298828	0.000444244	0.0717773	0.000320459	0.0319336	0.0002041	0.0404297	0.000302693	0.0500977	0.000116015	0.0641602
39	WT	M	-4.09851e-05	0.028125	0.000175128	0.0647461	0.000101738	0.0298828	8.1275e-05	0.0404297	9.05721e-05	0.0524414	2.92547e-05	0.0603516
40	WT	M	-7.13846e-05	0.0272461	0.000211538	0.0662109	0.00012158	0.028125	1.66115e-05	0.0316406	5.80593e-05	0.0375	0.000200068	0.0454102
41	WT	M	-0.000163064	0.028125	0.000307832	0.0486328	0.000187863	0.0307617	0.000174238	0.0383789	0.000337923	0.047168	0.000156707	0.0606586
42	WT	M	-0.000145669	0.028418	0.000290891	0.0678898	0.000196308	0.0304687	0.000129332	0.0389648	0.000217667	0.0489258	0.000112012	0.0624823
43	WT	M	-8.13513e-05	0.0348633	0.000255603	0.0706055	0.000170152	0.0418945	0.000159724	0.0521484	6.75448e-05	0.0667969	ND	ND
44	WT	M	-0.000150972	0.0316406	0.000352017	0.0708984	0.000222128	0.0325195	0.000173881	0.0421875	0.000285711	0.0524414	0.000109179	0.0665039
45	WT	M	-9.47176e-05	0.0369141	0.000179744	0.0861328	0.000144269	0.0398437	3.13606e-05	0.0457031	5.19196e-06	0.0495117	7.74516e-06	0.0550781
46	WT	M	-7.19583e-05	0.0295898	0.000191631	0.0665039	0.000146943	0.0316406	0.000115504	0.0413086	0.000127795	0.0518555	4.74233e-05	0.0670898
47	WT	M	-0.00012576	0.0292969	0.000326688	0.0708984	0.000227271	0.0322266	0.000110748	0.0413086	0.000140564	0.0521484	4.33431e-05	0.0665039
48	WT	M	-0.000132721	0.0304687	0.000169145	0.0530273	7.19021e-05	0.0313477	0.000114885	0.0407227	0.000174449	0.0518555	7.4864e-05	0.0667969
49	WT	M	-0.000161478	0.0292969	0.000285258	0.05625	0.000197461	0.0328125	0.000142615	0.0430664	0.000116494	0.055957	1.86205e-07	0.0618164
50	WT	M	-0.000139826	0.0307617	0.000238893	0.0802734	0.000149661	0.0345703	8.80788e-05	0.0457031	3.78589e-05	0.0571289	1.53774e-05	0.0629883
51	WT	M	-7.29356e-05	0.027832	0.000254165	0.065918	0.000119905	0.0307617	0.000166391	0.0395508	0.00023119	0.0486328	7.43988e-05	0.0635742
52	WT	M	-0.00010376	0.0398437	0.00023516	0.0720703	0.000221929	0.0433594	0.000157934	0.0544922	8.94301e-05	0.0624823	3.47414e-06	0.065918
53	WT	M	-0.000126018	0.0254883	0.000210056	0.0556641	0.000165035	0.0266602	3.86807e-07	0.0295898	0.000145471	0.0351562	0.000298206	0.0421875
54	WT	M	-7.4162e-05	0.0287109	0.000165127	0.0615234	7.94709e-05	0.0292969	4.41814e-06	0.0328125	5.15455e-05	0.0366211	0.000150877	0.0442383
55	WT	M	-0.000155224	0.0298828	0.0003897	0.0509766	0.00017819	0.0313477	0.000149098	0.0380859	0.000321892	0.046582	0.000140339	0.058867
56	WT	M	-0.000135792	0.027832	0.000239956	0.0498047	9.86851e-05	0.0313477	0.00011203	0.037793	0.000252706	0.0462891	0.000129633	0.0583008
57	WT	M	-5.36728e-05	0.028418	0.000116194	0.0679687	7.65309e-05	0.0316406	6.72149e-05	0.0413086	4.03536e-05	0.050781	1.86535e-05	0.0676758
58	WT	M	-5.92587e-05	0.0328125	0.000247978	0.0678898	0.000230439	0.037793	0.000198294	0.0459961	9.09879e-05	0.058867	3.34967e-08	0.0650391
59	WT	M	-0.000135452	0.028418	0.000202864	0.0462891	0.00010454	0.0313477	9.45493e-05	0.037207	0.000242964	0.0457031	0.000124393	0.0574219